

**DESIGN AND FABRICATION OF WIRELESS POWER
TRANSMISSION THROUGH RESONANT
COUPLING FOR CHARGING SMALL CPES**

**A PROJECT SUBMITTED TO
THE NIGERIAN COMMUNICATIONS
COMMISSION**

BY

**ENGR.DR.EVANS C. ASHIGWUIKE
DEPARTMENT OF ELECTRICAL/ELECTRONIC
ENGINEERING
FACULTY OF ENGINEERING
UNIVERSITY OF ABUJA**

JANUARY 2022

TABLE OF CONTENTS

TABLE OF CONTENTS	i
LIST OF FIGURES	iii
LIST OF TABLES	vi
LIST OF ABBREVIATIONS	vii
ABSTRACT	viii
1.0 INTRODUCTION	01
1.1 Background Information	01
1.2 Problem Statement	02
1.3 Aim and Objectives	03
1.4 Justification of the Project	03
2.0 REVIEW OF CONTEMPORARY LITERATURE	06
2.1 Review of Relevant Literature and Studies	06
2.2 Non-radiation WPT System	14
2.2.1 Capacitive Wireless Power Transfer System	16
2.2.2 Inductive Wireless Power Transfer System	18
3.0 SYSTEM OVERVIEW	26
3.1 Methodology	27
4.0 POWER SUPPLY	29
4.1 DC Power Supply Design	29
4.2 Section Summary	39
5.0 TRANSMITTER CIRCUIT DESIGN	41
5.1 Amplification and Oscillator	41
5.2 Oscillator Design	43
5.3 Inverting and Switching Stage	45

5.4	Section Summary	49
6.0	TRANSMITTER COIL DESIGN	50
6.1	Modelling and Simulation of Transmitter Coil Magnetic Field	52
6.1.1	Introduction	52
6.1.2	Numerical Simulation	53
6.2	Modelling	53
6.2.1	Model Implementation	54
6.2.2	Comparative Study of Transmission Coil Configurations	56
6.2.3	Finite Element Mesh:	58
6.2.4	Simulation and Analysis	60
6.2.4.1	Single Race-Track (SRT) Transmitter Coil configuration	60
6.2.4.2	Double Race-Track (DRT) Transmission Coil configuration	62
6.2.4.3	Triple Race Track Transmission (TRT) Coil configuration	63
6.2.5	Investigation of the Performance of TRT transmitter Coil Configuration	65
6.2.5.1	The Influence of Coil Internal Diameter (d_{in}) on the Magnetic Field Strength	66
6.2.5.2	The Effect of varying the Insulation Layer Thickness (T_{in}) on the Magnetic Field strength.	67
6.2.5.3	The Effect of varying the Coil Dimension on the Magnetic Field strength	68
6.3	Section Summary	71
7.0	RECEIVER CIRCUIT DESIGN	73
7.1	Receiver Circuitry	73
7.2	Receiver Coil Design	76
7.2.1	Calculation of Mutual Inductance	78
7.2.2	Inductance vs Excitation Current and Number of Coil Turns	80
7.3	Section Summary	84

8.0	EVALUATION OF OVERALL SYSTEM	86
8.1	Power Transfer Efficiency (PTE)	86
8.2	Power Transfer Calculations	88
8.3	Maximum Coverage Distance	91
8.4	Charging Time	92
8.5	Experimental Setup	98
8.6	Section Summary	101
9.0	CONCLUSION	103
10.0	PUBLICATION(S)	105
11.0	ACKNOWLEDGEMENTS	105
12.0	REFERENCES	106
13.0	APPENDIX	114
13.1	APPENDIX A	114
13.1.1	Circuit Diagram	114
13.2	APPENDIX B	116
13.2.1	8s003f3p6 Pin Descriptions	116
13.3	APPENDIX C	117
13.3.1	Assembly Program Listing	117
13.4	APPENDIX D	120
13.4.1	Prototype Testing	120

LIST OF FIGURES

Fig 1: Resonator	11
Fig 2: Equivalent Circuit of a Resonant Coupled System	11
Fig 3: Basic Concepts of Capacitive and Inductive WPT	15
Fig 4: Capacitive Wireless Charger Possible Plate Structures	16

Fig 5: Equivalent Circuit of capacitive WPT System	17
Fig 6: Six compensation topologies for a WPT system	21
Fig 7: A dynamic WPT system with parallel-connected transmitter coils	23
Fig 8: Equivalent circuit of RC-coupler a) with receiver pad b) without receiver pad	23
Fig 9: System architecture for a Multiple Transmitter Multiple Receiver WPT System	24
Fig 10: Simplified System Architecture of a multi-frequency WPT System	25
Fig 11: Power Supply Circuit	34
Fig 12: A diode full-bridge rectifier connected to voltage source	36
Fig 13: The waveform of the full-bridge diode rectifier	36
Fig 14: Block diagram of the transmitter section	39
Fig 15: LM324 connection to the 8s003f3p6 microcontroller	44
Fig 16: K27 pin configurations (PNP 2907A, NPN 2222A)	45
Fig 17: 9926A pin configurations (n-channel MOSFETs)	46
Fig 18: 4953 pin configurations (p-channel MOSFETs)	46
Fig 19: Connections between the K27 transistor ICs and the MOSFET ICs	48
Fig 20: Waveform of the transmitter coil voltage output	52
Fig 21: Block diagram showing the steps involved in FE modelling of the generation and Reception of Magnetic Flux by the Transmitter and Receiver Race-Track coil	55
Fig.22: Schematic of WPT Transmission coil configurations. (A) Single Race-Track coil, (B) Double Race-Track coil, (C) Proposed (B) Triple Race-Track coil configuration combining the current path and (C) magnetic fields of (A) and (B) .	56
Fig.23: The cross sectional view and the magnetic field interaction of coil configuration under investigation: (a) SRT coil, (b) DRT coil and (c) TRT.	57

Fig.24: FE mesh; (A) SRT coil, (B) DRT coil, (C) TRT coil.	59
Fig.25 Time history of the External current density for used to excite the SRT, DRT and TRT coils.	60
Fig.26: 3D surface plot showing the magnetic field line around the SRT coil.	61
Fig. 27: Shows the line graph of the magnetic field across the SRT coil.	61
Fig. 28: 3D surface plot showing the magnetic field line around the DRT coil.	62
Fig. 29: Show the line graph of the magnetic field across the DRT coil.	63
Fig. 30: 3D surface plot showing the magnetic field line around the TRT coil.	64
Fig. 31: show the line graph of the magnetic field across the TRT coil.	65
Fig. 32: The effect of Variation of coil internal diameter on the Magnetic Field Strength.	66
Fig. 33: The effect of variation of insulation layer thickness on the Magnetic Field Strength.	68
Fig. 34: The effect of variation of the K-factor on the Magnetic Field Strength.	69
Fig. 35: Cross-section of TRT Coil showing surface plot of magnetic flux density at K factor (A) 2, (B) 3 and (C) 4.	70
Fig. 36: Block Diagram of the Receiver Circuit Design	73
Fig. 37: bq51013b used as a wireless power receiver and power supply system	74
Fig. 38: Schematic of a dual resonant circuit	76
Fig. 39: Plot of Mutual Inductance against the coupling coefficient	80
Fig. 40: Plot of the Self-inductance against the excitation current	82
Fig. 41: Power Transfer Efficiency plotted against the Coupling Coefficient	88
Fig. 42: Simplified Inductive WPT circuit diagram	89
Fig. 43: Plot of coupling coefficient against the lift-off distance	92
Fig. 44: Comparison of charge time for some phone models using the WPT system	96

Fig. 45: Spatial diagram of the measurement Set-up to observe the effect of lift-off distance on induced voltage and current	98
Fig. 46: Set-up for measurement of distance of coverage.	99
Fig. 47: Measurement of the Receiver voltage at 2mm lift off.	100
Fig. 48: Measurement of the Receiver voltage at 8mm lift off.	101
Fig. 49: Measurement of coil direct mutual inductance.	101
Fig. 50: An Energised four (4) Compartment Transmitter prototype	120
Fig. 51: An Energised four (4) Compartment Transmitter prototype charging a phone with an inbuilt wireless receiver (iphone 11 promax) .	120
Fig 52: An Energised four (4) Compartment Transmitter prototype charging a phone with external wireless receiver (Normal Android phone).	121

LIST OF TABLES

Table 1: LM324 pin configurations	42
Table 2: Relationship between K27 IC and the MOSFET ICs	47
Table 3 Transmission coil parameters used for the simulation	57-58
Table 4: Coil Type Simulation Result	65
Table 5: Performance index of Z1258 anti rust silicone baffle paint	67- 68
Table 6: Ratio of coil width to coil thickness.	69
Table 7: Mutual inductance against coupling coefficient	79
Table 8: Comparison of charge time of some phone models	95
Table 9: Comparison of Magnetic Properties of some materials	97
Table 10: Receiver output reading in relation to the lift-off.	99-100

LIST OF ABBREVIATIONS

CPE	Consumer Premise Equipment
DRT	Double Race –Track
EMF	Electromotive Force
IPT	Inductive Power Transfer
MOSFET	Metallic Oxide Semi-Conductor Field Effect Transistor
PTE	Power Transfer Efficiency
RMS	Root-Mean-Square
SRT	Single Race-Track
DRT	Double Race-Track
TRT	Triple Race-Track
WPC	Wireless Power Consortium
WPT	Wireless Power Transfer
FEM	Finite Element Model
Mf	Magnetic Field
MVP	Magnetic Vector Potential
SCD	Source Current Density

Abstract

Wireless power transfer (WPT) is the transfer of power wirelessly from source to sink. The source is the primary or transmitter coil while the sink is the secondary or receiver coil. There are limitations to achieving this effectively no matter the design or set-up. The design seeks to eliminate the issue of dead-zone, which reduces the efficiency of power transfer. This can be achieved by incorporating an A6 transmitter coil type using three (3) partially overlapping coils and the receiver used incorporates a bq51013b IC that provides rectification and regulated output within a given voltage range.

Efficiency of power transfer depends primarily on the coupling coefficient of the primary and secondary coils which also depends on the distance between the two coils. The mutual inductance of the two coils is also an indication of the efficiency of the WPT system. As the magnetic field strength increases so does the mutual inductance. At 0.5 value of coupling coefficient, the mutual inductance of the primary and secondary coil is $15.3\mu\text{H}$. A simulation for three transmitter coil types – single race-track coil (SRT), double race-track coil (DRT) and triple race-track coil, is done on COMSOL Multiphysics using finite element method (FEM) to solve the resulting partial differential equations (PDEs). The results of the simulation showed that the TRT coil has the strongest magnetic field with a pulse width of 0.8 and eliminates the occurrence of a low field region or dead-zone. During the testing of the physical design set-up, it was observed that for a lift-off distance from 1mm up to 18mm, the power transfer efficiency of the system was 98.39%. This value was possible because a coupling coefficient of 0.5 was achieved for the system. The minimum value of efficiency for the system was observed to be 45% at 0.01 coupling coefficient. The design and experimental testing proved that using a TRT coil provides power transfer efficiency up to 98.39% between 1mm and 18mm lift-off distance.

1.0 INTRODUCTION

1.1 Background Information

The need for transfer of power from the source to the receiver is an important part of any electrical or electronic system. Power travels through a defined medium from the generating source or transmitter and arrives at the load point or receiver. The dominant mode of power transfer since its discovery has been through wires which can be high tension or low tension. In any city or town, wires run crisscross distributing power to the needed points. If you are using an electronic device perhaps a mobile phone and you need to recharge the battery then you will probably have to get a charger and connect the phone to the wire. But what if you could charge it without having to connect it to wire, power will be transferred wirelessly. This is possible through a concept called Wireless Power Transmission (WPT). Research and studies have been done ever since the 19th century but only recently has this concept begun to be implemented. WPT enables the wireless charging of various electronic devices such as mobile phones, game controllers, laptops, implantable devices [1, 2], trains, logistic robots, electronic vehicles. Wireless power transfer technologies have brought forth innovative vehicle energy solutions that utilize wireless sensor networks (WSNs). Currently engineers are trying to discover how to increase the efficiency of power transmitted wirelessly and also methods that are safe to human beings and the environment also. These methods should be cheaper and as such can be commercially implemented. Though, still in the early stages, several electronic companies are beginning to roll out devices that can wirelessly transmit power. Wireless Power Transmission (WPT) is based on the principle of electromagnetic induction. Electromagnetic induction works on the concept of a primary coil generating a predominantly magnetic field and a secondary coil being within that field so that a current is induced within its coils. This causes the relatively short range due to the amount of power required to produce an electromagnetic field.

Although WPT has been known for more than a century after Nikola Tesla discovered it, only now has the WPT industry started its rapid growth. Current solutions are having great success in the marketplace with diffusions of innovations from innovators to early adopters as of now.

The goal of this project is to evaluate and study the wireless power transfer technologies and the physics behind it. A wireless energy transmission system prototype will be designed and implemented for CPEs.

It is strongly believed that this project will provide potentials for extending the advantages of communication, easier approach to phone utilization, and providing revenue for technology developers and mobile network operators in Nigeria.

1.2 Problem Statement

In a wired power transfer system like the conventional use of cables for transfer of power from one point to another, efficiency is an issue. The amount of power generated and transferred never makes it to the desired destination. This is as a result of losses due to heat and I^2R losses across the length of the conducting wires. How to efficiently transfer power from one point to another became a problem that needed solving and led to the invention of wireless power transfer.

Wireless power transfer brought about an improvement in the efficiency in terms of power transferred in a conventional two-coil system consisting of a single transmitter coil and a single receiver coil. But a region of low-field operation or dead-zone is inherent in this system and presents an issue to this power transfer system over an operating distance or lift-off distance. This affects the efficiency of power transfer in the case of misalignment of the transmitter and receiver coils.

The project which is based on wireless power transfer seeks to eliminate the occurrence of dead-zone in the power transfer system arrangement, thereby improving power

transfer efficiency and also the maximum covering (lift-off) distance of the receiver coil from the primary coil. Elimination of the dead-zone will be achieved by incorporating multiple transmitter coils that are partially overlapping; this will result in a stronger magnetic field and allow for transmission of power over longer distances and improves the overall efficiency. The method of wireless power transfer to be used is based on resonant coupled inductive transfer.

1.3 Aim and Objectives

The main goal of this project is to improve the power transfer efficiency of a wireless power transfer system by improving the magnetic field strength and interaction in the transmitter coils and thus eliminating the occurrence of dead-zone which is a region of low-field operation. This will improve the maximum covering distance of the inductance and increase the efficiency of the wireless power transfer system in charging mobile devices. The following specific objectives will be met:

1. Design and assembly of a power supply unit and amplifier for the dc supply.
2. Design and assembly of an appropriate oscillator.
3. Develop the transmitter and receiver coils
4. Designing a battery charging circuit for multiple ports.
5. Design the receiver module and charging pads.
6. Experimental validation of the entire system.

1.4 Justification of the Project

The transfer of power from one point of supply (the source) to another point where it is utilised (the sink) is a very useful operation that a lot of activities in our everyday lives depends on. Wired power transfer which involves the use of conducting wires has been in existence and use since Thomas Edison and his invention and enjoys immense popularity.

But this method comes with its own set of problems or disadvantages. The disadvantages of a wired power transfer system include the following:

1. Cost of providing the needed wires to establish a connection between two points that is from the source of power to the sink.
2. Power is lost during the transmission in the form of heat and resistive losses and these losses increase over the distance of the wires and the duration of usage.
3. The possibility of becoming electrocuted when one comes into contact with any exposed part of the conducting wires.
4. Mobility and portability is limited. This is due to the fact that portability depends on the length of wires used to create a connection between the power supply source and where it is needed. To increase portability, more wire length is needed and this implies an increase in the cost of the installation which is generally expensive.

Wireless power transfer (WPT) system is an alternative to wired power system and is presented as a solution to the listed problems of the wired power transfer system. WPT reduces the number of circuit components in contact by eliminating the use of wires since the mode of power transfer is by induction and the use of magnetic fields which is wireless. This WPT system design also offers high values of efficiency up to 90%. Efficiency of a power transfer system is measured by the ratio of useful power to the amount of power actually generated. To ensure this, the design adopts three transmitter coils as the source, fed by the same dc supply meaning there will be no under-utilisation of dc power supply. The use of multiple transmitter coils ensures that regions of low field of operation are eliminated and it also allows for adequate power to reach the receiver coil (sink) for the required purposes. This translates to improved efficiency of the system design. This design is for small scale applications and specifically for charging of mobile

devices. It is designed in such a way to allow for simultaneous charging of mobile devices.

The benefits of this WPT system design includes portability, reduced chances of electric shocks, less expensive to build and also possible high levels of efficiency.

2.0 REVIEW OF CONTEMPORARY LITERATURE

2.1 Review of Relevant Literature and Studies

Wireless power transfer has been gaining recognition in recent years in terms of research and deployment in various fields. Wireless power transfer is employed in wearables, electric vehicles, ventricular assist device [1], consumer electronics etc. Due to its continuous deployment, there is need for research into ways in which the power transfer can be optimized.

In the beginning of 20th century, Nikola Tesla carried out his experiments on power transmission by radio waves instead of the wire grid. However, his typical embodiments involved undesirably large electric fields, which were radiating their power in every direction. To circumvent the energy loss, microwave power transmission using very short wavelengths and optical reflectors of practical dimensions was investigated. This technology led to the microwave-powered helicopter and the solar-power satellite concept [2]. However, such power transmission requires the existence of an uninterrupted line-of-sight and a complicated tracking system in the case of mobile objects.

The inductive coupling was a traditional way of power transmission. A surge in the use of autonomous electronic devices usually requires rechargeable batteries. These batteries sometimes show the failure during the power recharging from the mechanical contact. Energy transfer utilizing inductive coupling can overcome this contact failure problem and makes it convenient [3]. Electrical circulatory assist devices such as total artificial heart generally use a brushless dc motor as their pump. Since these devices are inside the body, it is desirable to transfer electrical energy to these circulatory assist devices transcutaneous without breaking the skin [4]. There is a demand for developing new power-transmission methods for a multitude of electronic devices such as sensor networks. Those ubiquitous sensing will be used in our daily life to enhance security, safety, and convenience. T. Sekitani et al., made the

large-area wireless power transmission system using inductive coupling and MEMS () technology [5]. However, inductive coupling is effective only for short distances. The efficiency of inductively coupled has been shown to be improved by using resonant circuits [1]. Also the use of more than one transmitter coil as shown in [1] where multiple transmitter coil formation was used, can improve efficiency levels.

The review of scientific achievements in the field of WPT is given in [6-8]. The main benefit from WPT implementation is that the use of wires is greatly reduced in the transfer of energy between the power source and load. This allows for the development of devices that are user friendly and easy in the exploitation. The elimination of the physical connection between the charging station and the energy consumer simplifies the charging process and removes safety concerns. The WPT system should comply with the wireless power consortium (WPC) standards. WPT technology finds its application in electrical vehicles [9-14], electronic gadgets charging [15], medical applications [16] and in many other applications. A promising WPT application is dynamic charging of electric vehicles [17] by placing WPT transceiver side under the road. Such approach allows increasing of the electric vehicle market, because in such a way the energy storage capacity requirement can be reduced and the range limit of electric vehicles extended. The WPT charging system of electric vehicles can be designed with high efficiency [18] comparable with traditional contact charging system efficiency [19-21].

WPT systems have also been used in communication. In [22], WPT based on magnetic resonant coupling technology was used with an in-band wireless communication. The proposed system used a loop antenna and a selectable capacitor array. This enabled the transmission distance to be increased and also compensate for the effective capacitance [1], [22]. S. Kim et al in [22], added a communication protocol operated at the same frequency band was added to manage the network and control power circuits. In [22], they were able to

show that the loop antenna achieved a high Q factor in power transfer mode and enough passband in communication mode. X. Chen et al in [23] also studied the effect of co-channel interference (CCI) generated by wireless power transfer on information delivery for three widely used setups a) Power Beacon (PB) b) Hybrid Access Point (HAP) c) Simultaneous Wireless Information and Power Transfer (SWIPT).

In [24], a unique WPT structure was proposed called a rail transformer used to drive multiple low-power devices such as electronic shelf label (ESL) devices. ESL device design comprises of a LCD for displaying the price, a wireless communication unit for receiving information from a POS database.

For commercial use of WPT technology, high efficiency and misalignment insensitivity are of a major significance [25]. And for certain transfer range, the quality factor ($Q - factor$) and the uniformity of the transmitter coil's magnetic field are critical factors for the optimal efficiency and tolerance of WPT systems [25]. When designing a WPT system, efficiency in the power transfer process is the most important goal. Achieving this efficiency takes many factors into consideration. These factors include coil geometry, Q-factor [1, 25], coupling parameters, operating frequency. In inductive coupled systems, the coupling is loose resulting in degradation of efficiency and power transmission being efficient for only short range applications. This efficiency degradation can be compensated by using coils with high quality factor. This is possible because the magnetic field strength of an inductor is a function of the coil's self-inductance which also plays a role in determining the quality factor of the coil. Increasing the coil inductance increases the coil quality factor and the magnetic field strength and allows for more power to be transferred by induction. In a resonant inductively coupled system, the drawback of high quality factor value is that the capacitor's peak voltage is too high.

In [26], inductive power transfer was used to feed traction to a train on a real time without battery charger at a frequency of 60 KHz and efficiency of transferred power at 82% for a 128m long transmitter. Using a long transmitter coil increases the area of conduction and minimizes the issue of misalignment. In smaller applications, the A6 transmitter coil has been shown to limit the misalignment issue and allow for free positioning of the receiver coil [1, 26].

The most common methods of wireless power transfers according to their modes of power transfer are:

a) Radio Frequency: Waves are propagated through a vacuum hence this is the most common method of transmitting data. The operating principle is based on the interactions of the electric and magnetic fields [1] and determined by Maxwell's equations.

b) Optical Link: This method uses light in the ultraviolet and infrared regions of the electromagnetic spectrum. The transmitter is a light-emitting source for high power delivery and data transmission [1]. The receiver is a light-sensitive device which could be solar cells or a photovoltaic converter while the optical link can be free space, air or fiber optics. This method is mostly used for data transmission and higher power in the form of laser or solar can also be transmitted [1].

c) Ultrasound Propagation: Ultrasound waves propagate in physical media such as air, water, human tissue etc., by interacting with the energies within the medium. Ultrasound frequency can range from 20 KHz and up to several megahertz. Power delivery in the ultrasound mode is usually applied to low power data transmission, non-destructive testing, navigating systems [1] though higher power transfer is also possible. One advantage is that ultrasound waves can travel long distances depending on the link's attenuation.

d) Capacitive Power Transfer (CPT): Power is transferred wirelessly using electric field between capacitive plates. The coupling capacitance inversely varies with the minimum distance between the plates. This method is mostly applied to low power and data transmission systems such as biomedical implants, bio-instruments, isolated power supply etc.

e) Inductive Power Transfer (IPT): Uses time-varying magnetic field between mutually coupled coils to transfer power wirelessly. The transmitter generates eddy currents which mutually induce current in the receiver coil connected to the load. IPT can be tightly or loosely coupled systems. In tightly coupled systems, the coupling factor or coefficient is closer to unity and as such transferred power efficiency is quite high [1]. This application can be found in power transformers. In loosely coupled IPT systems, the coupling factor is between 0.01 and 0.5, [5-6] and this is considered low. Low coupling coefficients are due to the large distance between the coupled coils when compared to the coil sizes and the absence of high permeable magnetic path connecting them [1]. Low coupling coefficient reduces the transferred power efficiency; therefore resonators need to be used to increase the efficiency. This means operating the receiver coil at the same frequency as the transmitter coil and this happens when the capacitive and inductive reactance are the same.

Wireless power transfer (WPT) systems can be classified into two concepts based on the technology, transmission and applications. They are

A) Near-Field WPT: It is a non-radiative method of power transfer. Also referred to as near-contact [27] and is based on the principle of Tesla using a) near-field inductive coupling and b) magnetic resonant coupling mechanism [28]. The former is for short range power transfer applications while the resonant coupling is for medium range power transfer. Resonant coupled WPT is based on the principle that two resonators tuned at the same resonant

frequency can effectively transmit energy between each other with greater efficiency [28] at a long operating distance compared to inductive coupling approaches. Resonant coupled WPT are often referred to as mid-range WPT.

In mid-range WPT, the transmission medium source and the load is separated by adaptors, which makes the power transmission more efficient [28]. With the use of a suitable coupling element, frequency converters can be used to match the switching frequency of the source or transmitter to that of the load for effective transmission.

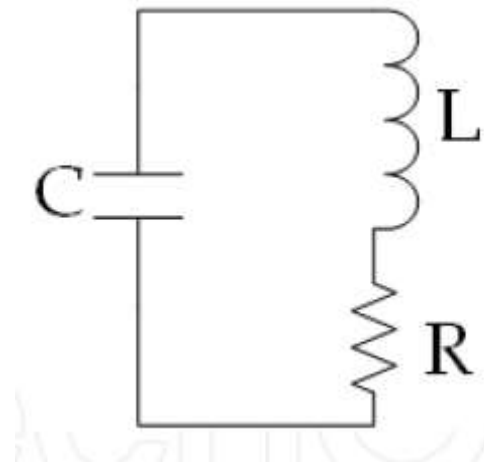


Fig. 1: Resonator

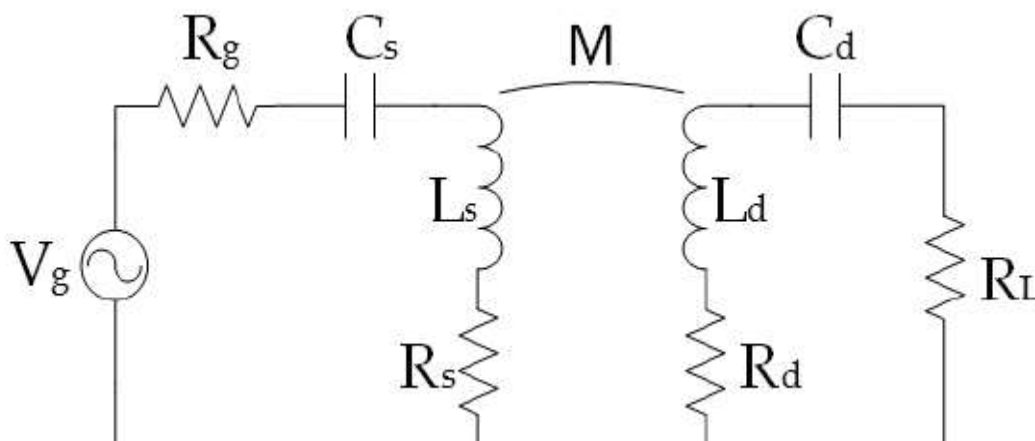


Fig. 2: Equivalent Circuit of a Resonant Coupled System [1]

The idea behind the resonant coupled WPT system is to transfer energy efficiently between two conductive materials that are tuned to resonate at the same frequency, by creating a strong magnetic coupling, between them. These materials are now referred to as resonators. For the current carrying coils, this occurs through their varying or oscillating magnetic fields. In the system of coupled resonators, a strongly coupled system is preferable for effective transfer of energy. Mid-range WPT using a strong coupling system is almost unidirectional and effective with minimum losses or interference [28]. In mid-range resonant coupled WPT system, there is one stable resonant frequency and both coils should tune in their self-resonance frequency in order to achieve maximum flux linkages for high efficiency. In a resonant coupled mechanism, the primary coil coupled with a capacitor and fed by the energy source, produces a magnetic field. When the secondary coil is tuned at the same frequency, it cuts enough of the induced field in primary coil resulting in the absorption of energy. A parameter, quality factor (Q) determines the rate at which the oscillation between the inductor and capacity in the primary side disappears. This Q factor can be defined by the lumped parameters (L, C, R), resonant frequency ω_0 and its intrinsic loss rate Γ as

$$Q = \frac{\omega_0}{2\Gamma} = \frac{1}{R} \sqrt{\frac{L}{C}} = \frac{\omega_0 L}{R} \quad (1)$$

where L represents the self-inductance of a circular coil having a cross-section a and radius r , given by

$$L_{self} \cong [In\left(\frac{8r}{a}\right) - 1.75]; \text{ assuming } \frac{a}{r} \ll 1 \quad (2)$$

The parasitic capacitance of the coil can be calculated as follows,

$$C_{self} = \frac{1}{\omega_0^2 L_{self}} = \frac{1}{4\pi^2 f_0^2 L_{self}} \quad (3)$$

For high performance, the coupling value of the field should be made small enough. This can be achieved by having a high Q factor of coils as well as low effective parasitic resistance of the coils. The parasitic resistance (R_p) of a circular coil can be determined from the length of conductive wire, l , conductive material resistivity ρ and wire radius a as

$$R_p = \frac{2l\rho}{\pi a \delta}; \delta = \sqrt{\frac{2\rho}{\omega\mu}}; \mu = \mu_0\mu_r \quad (4)$$

where δ is the skin depth

ρ is conductor resistivity

μ_0 is the magnetic permeability of free space

μ_r is the relative magnetic permeability of the coil's material

The following are some benefits of resonant coupled wireless power transfer system:

- 1) Flexibility: Flexible in terms of the orientation between the transmitter and receiver during operation. Though there might be a misalignment of coils issue.
- 2) There is a possibility of powering two or more loads using a single source even when they have different power requirements [28].
- 3) Magnetic repeaters or resonators can be used to increase the range of power transmission significantly.
- 4) Various sizes of resonators can be used in the WPT system

Resonant IPT is a fast-growing area of electromagnetic research originating with Tesla's first studies in wireless transfer of energy between a resonant transmitter and receiver [29].

B) Far-field WPT:

These are radiative methods of power transfer and uses electromagnetic induction. Power transfer is through microwave and light or LASER technology. The far field involves the use of electromagnetic radiation while the nearfield using a) near-field inductive coupling and b) magnetic resonant coupling mechanism [28] the use of electromagnetic induction.

Far field WPT makes use of antennas and suffers from trade-off between directionality and transmission efficiency [28]. With the use of high-gain antennas, some RF and microwave systems can transfer power at 90% efficiency over several kilometers.

With the advent of IoT (Internet of Things), far-field WPT technology might allow us find alternatives to energize the huge number of electronic devices that will be interconnected [30]. Design of localization and tracking methods is an essential for practical applications in order to focus the energy and to improve on end-to-end transfer efficiency.

2.2 Non-Radiation WPT System

Non-radiation based WPT technologies are two - inductive power transfer that is used very widely and capacitive power transfer [31]. The basic concept of both WPT systems is shown in Fig. 3, the inductive WPT coil leakage inductance should be compensated by capacitance-based resonance network and the resonance network also should also be designed for capacitive WPT. For the high frequency signal generation traditional power electronics topologies can be used and also developed more advanced new topologies [32-34]. A good comparison between both technologies is given in [35], the capacitive power transfer is more suitable for a smaller air gap and lower power in comparison with the inductive power transfer [35] although in several papers the WPT system for high power is reported [36-37]. The new wide band gap semiconductor devices allow increasing the

switching frequency [38], therefore, capacitive power transfer can be applicable for higher power transfer and larger air gap applications in the near future.

The inductive WPT system has its own drawbacks and the use of this technology is problematic in many fields. The inductive WPT system has the EMI issue, electromagnetic radiation is proven to have adverse effects on the environment and health [8] of the people exposed to the radiation, therefore shielding is required. The shielding and use of magnetics make the cost of such system extremely high [9]. This motivates researchers to find alternative forms of wireless energy transfer.

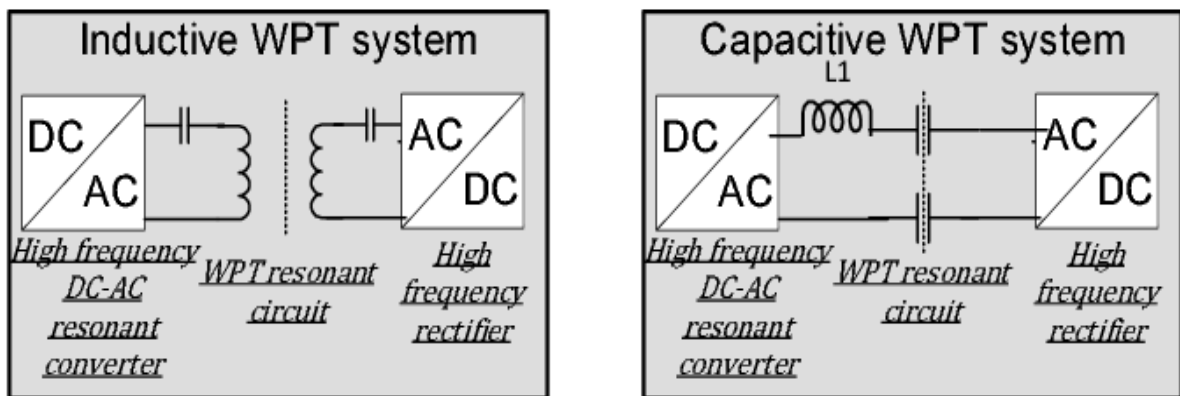


Fig. 3: Basic concepts of Capacitive and Inductive WPT

2.2.1 Capacitive Wireless Power Transfer System

Capacitive wireless power transfer is based on the concept of two surfaces separated by a small air gap [3] or a dielectric material forms capacitance, the basic equation to calculate the capacitance of two parallel plates is as follows:

$$C = \frac{\epsilon_r \epsilon_0 S}{d} \quad (5)$$

where C is the capacitance in farads (F),

S is the area of overlap of the two plates, m^2

ϵ_r is the relative static permittivity of the material between the plates (for a vacuum, $\epsilon_r = 1$)

ϵ_0 is the electric constant ($\cong 8.854 \times 10^{-12} Fm^{-1}$)

d is the separation between the plates, m

The capacitive wireless power transfer system is well proposed to transfer power through dielectric material with $\epsilon_r > 1$ (Fig. 2) as the capacitance value between the plates in this case is larger and power transfer is easier.

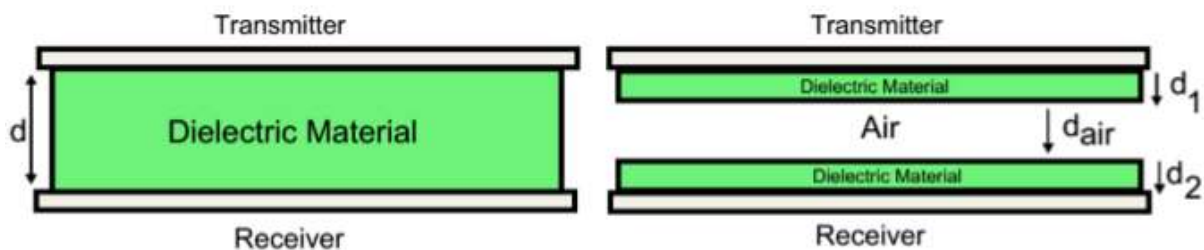


Fig. 4: Capacitive Wireless Charger Possible Plate Structures [39]

The operation of capacitive power transfer (CPT) is in the megahertz region and for capacitors the power transferred depends on the voltage across the plates with time.

According to [40] load together with the full-wave rectifier can be replaced by equivalent load R' load:

$$R' \text{ load} = \frac{8}{\pi^2} \frac{U_2^2}{P_2} \quad (5)$$

Equation 5 shows that for verification of wireless power transfer, the equivalent resistive load without rectifier can be used

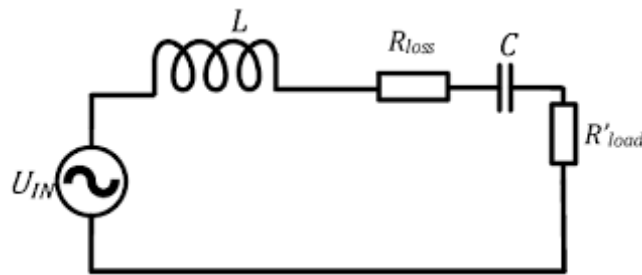


Fig. 5: Equivalent Circuit of capacitive WPT System

For a simplified analysis of the circuit, the input voltage can be replaced by a sinusoidal voltage source as the resonant network is tuned on fundamental frequency of the square shape voltage.

If only capacitances between the plates are considered, the WPT circuit with simple series inductance compensation can be described with a simple equivalent circuit presented in Fig. 5. For such compensation circuits, the resonant inductor can be chosen to compensate all capacitance of the plates:

$$L = \frac{1}{(2\pi f_{res})^2 C} \quad (6)$$

The voltage on wireless power plates can be calculated as follows:

$$U_c = \frac{1}{j(2\pi f_{res})^2 C} \quad (7)$$

As equation 6 shows, by increasing the switching frequency also the value of inductance needed to compensate, the challenge associated with the increase of frequency is increased switching losses of semiconductor devices and losses in the inductor. The larger air gap between the plates means smaller capacitance and following higher voltage to transfer large power in case of a significant air gap. From this follows that capacitive WPT has limitations to transfer large power through a large air gap or plates with a large surface area are required.

As equation 7 shows, to transfer larger power to the load (larger load current), the voltage on the capacitor plates should be increased (it is limited due to safety reasons and isolation of the dielectric material) or the resonance frequency (switching frequency) should be increased.

2.2.2 Inductive Wireless Power Transfer System

WPT through magnetic coupling is achieved by generating a flux linking between the primary and secondary coils. This system is also known as inductive power transfer [28]. This transfer takes place across a substantial airgap between primary and secondary coils. This differs from a transformer in the sense that while a transformer is considered to be strongly coupled (high coupling factor) [1], [28], the coils in the IPT system are loosely coupled [1], [28]. It is considered to be loosely coupled because while the separation between the coils is high, the reluctance of the mutual flux magnetic path length is higher relative to that of the leakage flux [28]. Consequentially, the leakage magnetic field in inductive WPT systems is high and can limit significantly, the transferred power levels. The low coupling factor leads to small values of impedance being reflected to the primary side thereby bringing the power supply close to unloaded operation at which most of the dissipated power from the

primary coil doesn't reach the secondary coil [1], [28]. In loosely coupled systems, optimization for the system's efficiency is necessary by including the power supply, magnetic link and also secondary side remote electronics.

Power is transmitted from source coil to load coil, using Faraday's laws of induction [1]. A magnetic core is used to shape the path, increase inductance and enhance coupling [1]. AC flows through transmitting coil, generating a magnetic field. The receiver coil picks up the field and generates a current to save power. The effective operating range is usually 30% of the diameter of the coils. IPT system can effectively transmit power from a source using the principle of electromagnetic induction but non-radiative as the system does not rely on the propagation of electromagnetic wave. Efficiency of the IPT system can be up to 70% for low power (about 5 watts) mobile phone charging. For low power industrial and domestic applications, the operating frequency range of the inductive coupling technique is usually from 20KHz to several megahertz. As the transmitter coil moves further away from the receiver coil, the efficiency begins to drop and misalignment issues arise. Metallic shields can be used to reduce the high frequency magnetic fields around the system and to reduce the electromagnetic interference. There will be losses in the form of eddy current inside the coil and metallic shield, and magnetic core losses which together make an efficient coil design important in a WPT system.

Misalignment issues arise when there is a misalignment between the transmitter and receiver coil or from change in airgap. When the coils are misaligned, there exists a dead angle and this drops the induced voltage while also changing the resonant frequencies on both coils [41 - 42]. In [42], a novel coil with high misalignment tolerance was proposed. This coil set up on COMSOL was referred to as Taichi coil due to its similar geometry and compared to the double-D (DD) coil and circular coil in misalignment tolerance [42]. In [43], Z. Yan et al proposed a rotation-free wireless power transfer system based on a new coil structure to

achieve stable power output and efficiency against rotational misalignments for charging autonomous underwater vehicles. The new coil structure has two decoupled receivers composed of two reversely wound receiver coils and the magnetic flux directions of the two receivers are perpendicular to each other. This enables a relatively constant mutual inductance and a decoupled characteristic under rotational misalignments. A high Q factor is important in maintaining high efficiency when the coupling coefficient is reduced due to misalignment or increased distance between transmitter and receiver [44].

Conventionally, a two coil approach is used [1, 28, 24, 29, 45]. That is a transmitter coil and a receiver coil. The major disadvantage is that one single device can be charged or powered at any point in time [1], [46]. A two coil system also suffers from unpredictable inductive link performance since the efficiency of the power transfer is highly dependent on the alignment of the coils as well as the operational distance between the source and receiver [1], [46].

This conventional two coil power transfer system provides a limited set of design parameters for example Q factor and the coupling factor k [1], [46], for tuning the currents in the magnetic coils. Optimization is also needed in order to maintain a sufficient efficiency in transferred power.

Recently, multi-coil approach has become increasingly popular for a wider range of wireless power transfer applications such as simultaneous charging of multiple devices. Based on the above, the following are the possible WPT conventions using magnetic coupling:

1. Single Transmitter and Single Receiver: this is the conventional system. One transmitter coil and one receiver coil for power transfer. This system is very limited and doesn't allow for the charging of more than one device. Two coil inductive WPT systems in its basic

configuration can have six different compensation topologies as shown in the figures below [1].

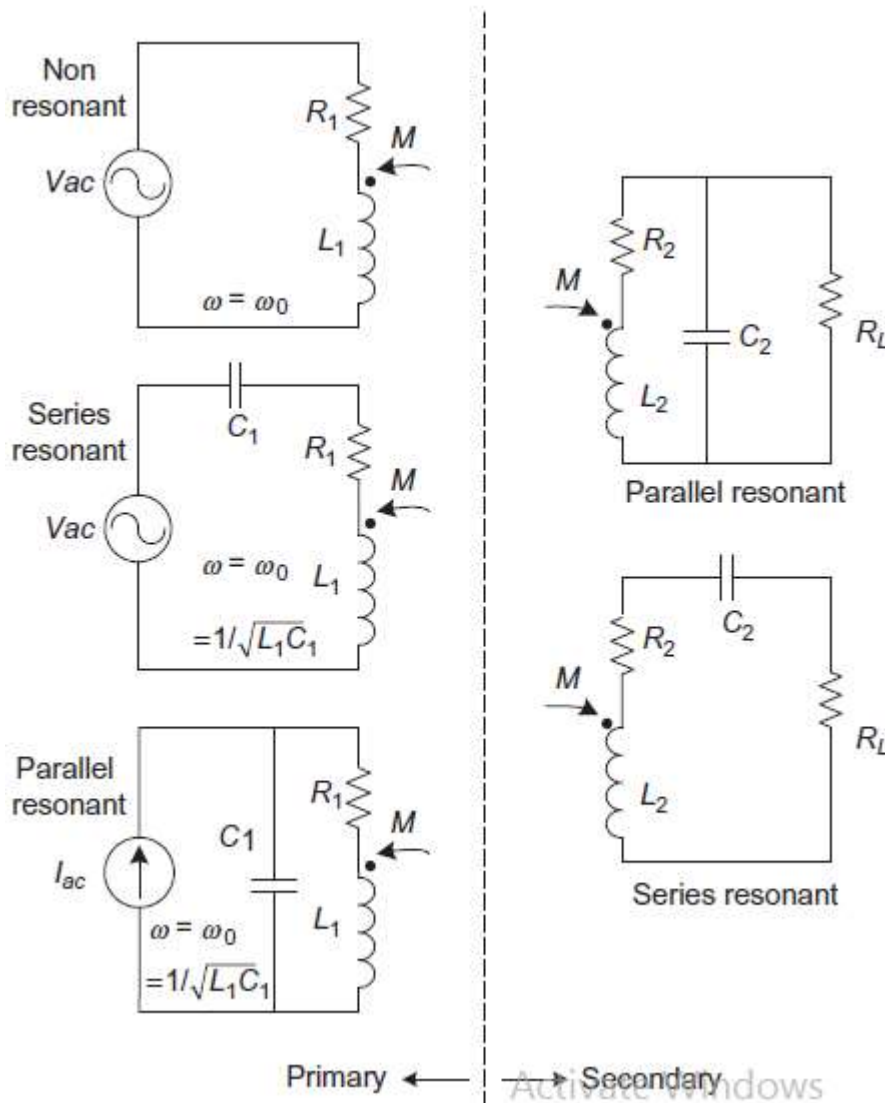


Fig 6: Six compensation topologies for a WPT system [1]

In the figure above, V_{ac} represents the AC voltage source and I_{ac} the AC current source, ω_0 is the resonant frequency. R_L is the load resistor while R_1, L_1, C_1 and R_2, L_2, C_2 are the resistors, inductors and capacitors on the primary coil side and secondary coil side respectively.

2. Single Transmitter, Multiple Receivers: In some WPT systems it is possible for multiple receivers to get power simultaneously from a single transmitter pad. The amount of power transferred to each receiver is linearly related to the resistance it reflects to the transmitter. A challenge here is the magnetic cross coupling between the receivers when they are close to each other. Cross coupling imposes problems to the system performance [1]. One method to reduce the cross-coupling is to make each receiver resonant to one of the transmitter carrier frequencies. In [47], K. Lee et al proposed a multi-coil approach using a transmitter and two receiver coils. The transmitter coil is placed in between the two receiver coils. A compensating reactance is found and is used to eliminate cross coupling between receivers. The paper showed that the transmission efficiency can be improved by locating the first receiver at a further distance from the transmitting coil when the first receiving coil has a higher quality factor or the distance between the transmitting coil and the second receiver is shorter [47].

In [48], a method to control power was proposed. This was due to the issue of selective power flow among the loads in a WPT system with multiple receivers. Efficiency was shown to peak at the resonant frequency of the receiving loop regardless of the resonant frequency of the sending loop.

3. Multiple Transmitter, Single Receiver: In this convention, there are multiple transmitter coils along the path of a receiver. For power transfer, the receiver coil just needs to align with any of the transmitter coils. It is grouped into two areas of application a) Dynamic WPT and b) Misalignment Tolerant Systems

In dynamic WPT systems, power transfer is done wirelessly while the receiver is in motion [1]. For instance, in the dynamic charging of an electric vehicle, multiple coils are placed along the driving path of the vehicle with the receiver coil in it. The problem here is amount of dissipated power that might be lost. The multiple transmitters can be connected to

one power supply and current flows in the transmitter coil aligned with the receiver coil using reflected impedance [1, 28, 41] while there is no current flowing in the other transmitter coils. Implementing multiple transmitter coils increases the tolerance of two mutually coupled coils. Multiple transmitter coils also provides a freedom of movement to the receiver in that area.

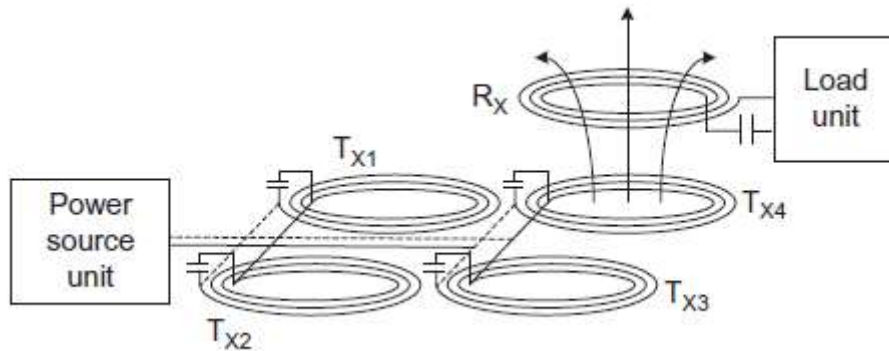


Fig 7: A dynamic WPT system with parallel-connected transmitter coils [1]

4. Multiple Transmitter, Multiple Receiver: In this approach, the transmitter contains multiple coils which can be arranged as a coil array. A multiple output WPT system can be used in applications where multiple receivers need to be charged simultaneously [49]. To avoid non-load losses and avoid leakage magnetic fields, it is desirable to switch on those transmitter coils that are currently needed by a receiver and switch off the rest [49]. X. Chen et al in [49] proposed a novel receiver-controlled coupler (RC-coupler) that can realize switching on or off transmitter coils without using bidirectional switches or sensors. The switch is designed in series with each transmitter coil and only activates when a receiver is put on top.

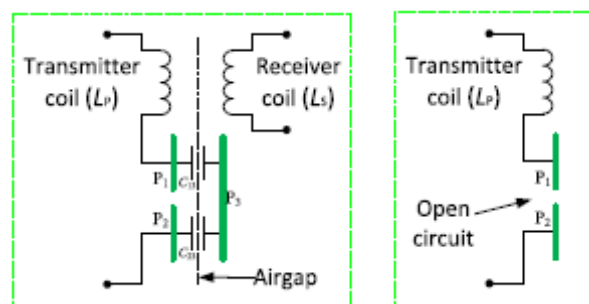


Fig 8: Equivalent circuit of RC-coupler a) with receiver pad b) without receiver pad [49]

A common topology is the single inductor multiple output (SIMO) approach proposed in [46]. A. T. L. Lee et al proposed a hardware prototype of a single-inductor three-output (SITO) which uses a buck-boost inverter delivery medium. The topology proposed enables a DC-AC power conversion from a DC power source into multiple independently controlled sinusoidal AC voltages with a wide load range. The advantages of this approach are:

1. increased likelihood of proper coil alignment
- 2) improvement in freedom of positioning of the device without affecting power transfer efficiency
- 3) concurrent charging of multiple electronic devices since there are multiple transmitter coils
- 4) allows for scalability and flexibility of the wireless chargers catering for multiple devices rated at different power levels and speed

Despite the above merits, the topology increases design complexity substantially. This project is based on the multiple transmitter multiple receiver convention.

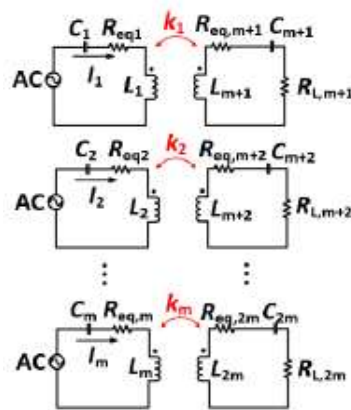


Fig 9: System architecture for a Multiple Transmitter Multiple Receiver WPT System [46]

In [50], a Gallium Nitride (GaN) inverter was used to achieve a multiple transmitter multiple receiver system. The use of GaN inverters simplifies the system by eliminating the need for blocking diodes or transistors which are required when using a Silicon MOSFET (Metallic Oxide Semiconductor Field Effect Transistor). This proposed GaN based SIMO

(Single Inverter Multiple Output) inverter has the advantages of a simplified structure, reduced component count, smaller form factor, higher power density and improved power efficiency.

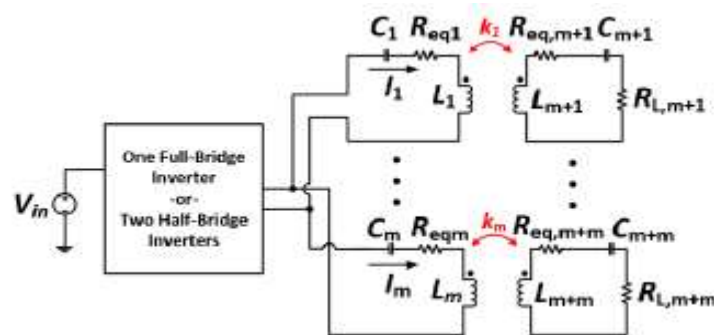


Fig 10: Simplified System Architecture of a multi-frequency WPT System [46]

The most popularly used standard for WPT transmission is the Qi standard which utilizes magnetic inductive WPT in the low frequency range from 100 to 300KHz [47], [48]. Other standards are PMA (Power Matters Alliance, which uses the same technology as Qi with operating range from 277 to 357KHz) [47], [50] and A4WP (Alliance for Wireless Power) which offers more spatial freedom of position and operates at a high frequency of $6.78\text{MHz} \pm 15\text{KHz}$ over a long range [47], [50]. A4WP also allows for multiple charging of device since the charging power can go up to 50W.

3.0 SYSTEM OVERVIEW

In building a wireless power transfer network, a transmitter and receiver sections are required. Wireless Power Transfer relies on the coupling between planar coils using magnetic induction. The devices involved are either a base station or a mobile device. Power moves from the base station to the mobile device meaning the base station generates the power while the mobile device sinks it. The base station contains the power transmitter which comprises a primary coil (transmitter coil) while the mobile device has a power receiver which comprises a secondary coil (receiver coil). The system of two coils is in fact, a coreless resonant transformer with the coils acting as either halves of the transformer [1]. The transmitter section receives power from a source, amplifies it and sends it by induction to the receiver section. This is done inductively since both sections are coupled through inductor coils and in this case by a resonant circuit (RLC network). Resonance improves the efficiency of the system [2]. The receiver section now rectifies and regulates it to the desired output value for DC usage. The process can be made more efficient by using multiple transmitter coils partially placed on each other for each receiver coil. This design is the A6 transmitter type design [1]. This design reduces the inherent dead-zone in the middle of each coil. The dead-zone is the space in the middle of the coil where no power is produced. This design allows for free positioning. Hence, for power reception the receiver coil in the mobile device needs to be aligned completely on any region of the transmitter coils. The advantages of this design include the following

1. Improvement in efficiency: This is due to multiple coils that works as a single, increases the area of transmission and reduces dead-zone and misalignment issues. The dead-zone is inherent in a single coil system [3-6].

2. Improvement in magnetic field strength for better depth penetration. This is validated by the experimental testing of the system.

Shielding is also an important part since shielding protects electronic components from undesired magnetic flux. Shielding is placed under the primary coil and on the top face of the secondary coil. Shielding and the close proximity of the coils ensure that the magnetic field is kept within the required area of operation and thereby enhancing efficiency.

3.1 METHODOLOGY

The design process involved simulation and experimental validation. The simulation and modelling was done using COMSOL Multiphysics. Then a physical experimental setup was used to validate the simulation results.

The WPT system designed in this project was done with the aim of achieving high level of efficiency. The factors that affect the efficiency of a WPT system include:

1. Coil size and geometry: This translates to the number of coil turns, the shape of the coil turns and how they affect the coil inductance and the generated magnetic field. Generally, a racetrack coil is favoured in comparison to a circular due to stronger magnetic field and area of operation. This research used a racetrack coil during the course of the study both in the simulation and testing.

2. Q-factor: This is the quality factor of the coil and at high values it affects the efficiency of the inductor coil positively. During the design care was taken to ensure that the quality factor value of the coil was high enough and above the minimum value as specified in the WPC standards. The Q-factor is dependent on the coil inductance and switching or resonant frequency. Therefore, the frequency was kept in the kilohertz region which is high and the selected coil was chosen with an inductance value that would give a high Q-factor value.

3. Lift-off Distance: The coupling distance between the primary and secondary coil affects the coupling coefficient inversely. Reduce the lift-off distance, the coupling coefficient increases and this directly increases the efficiency of the system. The magnetic field strength limits the maximum covering distance allowable by the system. Beyond the maximum covering distance, there is no induction. Improving the magnetic field strength of the transmitting coil helps increase the maximum covering distance. This is shown by the triple-race track coil configuration (TRT) simulation in COMSOL. COMSOL is used to compare the magnetic field strengths and the pulse width of the SRT coil (single race-track coil), the DRT coil (double race-track coil) and the TRT coil.

These three factors were considered in the design of the WPT system and the inductor coils so as to maximize efficiency.

The COMSOL simulation was modelled in such a way to test the characteristics and factors that affect the power transfer efficiency through the magnetic field strength of the transmitter coil. The simulation is used to make a comparative study of several coil configurations and how they affect the magnetic field strength and the elimination of dead-zone which is a region of low field operation. The modelling calculates for the peak-to-peak amplitude of the magnetic field, the magnetic pulse width and its relation to the occurrence of dead-zone. It was also expected that the use of the TRT coils will increase magnetic field interaction and distribution which would eliminate dead-zone. Further development of the system and prototyping was based on the results of the simulation.

The experiment was used to test the designed system and the power transfer efficiency in terms of the maximum coverage distance (lift-off) and current induced in the receiver coil from the transmitter coil. Hence the experiment was to validate the simulation results and to show working of the designed system.

4.0 POWER SUPPLY

The power supply is based on switch mode power supply. In comparison to the linear mode power supply, it is more efficient. This setup provides the power to the transmitter circuitry which includes the quad amplifier, an oscillator and the power MOSFET inverter ICs. The output of the power supply is 5 volts which will be amplified by the op-amp.

4.1 DC Power Supply Design

The DC power supply circuit diagram is shown in fig 11. It is designed to power the four charging pads of the transmitter. Each pad has three partially overlapping coils which can supply a maximum of 12 volts, 22 watts for each coil. This gives us about 2 amps for each coil. The dc power supply was designed to handle 150 watts and a maximum of 12 volts and 12 amps dc current when all the pads are in use.

In the design of a dc power supply, some important sections are considered. These are,

1. Voltage Step-Down (Input)
2. AC Rectification
3. Filtering and Smoothing
4. Controller
5. Pass Transistor
6. Feedback
7. Voltage Step-Down (Output)

The power supply design specifications are given as below:

V_{in} (Input Voltage): 110V – 220V (after regulation)

V_o (Output Voltage): 5V

$I_{o,max}$ (Maximum Output Current): 20A

P_{max} (Maximum Power): 100A

f_s (Switching Frequency): 500KHz

Minimum Load: 10%

The transformer has three windings n_1 , n_2 and n_3 . The winding ratio between the primary winding n_1 and the reset winding n_2 is chosen as 1. This ratio defines the maximum duty ratio (D) which is 50% to ensure proper reset.

The winding ratio between the primary winding n_1 and the secondary winding n_3 is made small enough so as to ensure that the required output voltage is achievable at maximum D and minimum input voltage, but large enough to use the entire range of D.

The gain is based on the standard buck gain modified by the winding ratio n_3/n_1 . That gives us,

$$\frac{V_o}{V_{in}} = \frac{n_3 \times D}{n_1} \quad (8)$$

Where V_o is 6V (the extra 1V takes care of forward voltage drop and voltage drop across the output inductor), V_{in} is minimum at 110 Volts, D is 0.5

$$\frac{6}{110} = \frac{n_3 \times 0.5}{n_1}$$

$$\frac{n_1}{n_3} \leq 9.17$$

The choice of core size is ETD34 by TDK Corporations which requires a minimum primary turns count in order to guarantee non-saturation.

$$n_1 > \frac{V_{in,max} \times D_{max} \times \frac{1}{f_s}}{B_{sat} \times A_e} \quad (9)$$

Where $V_{in,max}$ is 220 Volts, D_{max} is 0.5, f_s is 500KHz, B_{sat} is 0.3T (allowed maximum core flux density for ferrites to guarantee non-saturation), A_e is $97.1 \times 10^{-6} m^2$ for ETD34.

$$n_1 > \frac{220 \times 0.5 \times \frac{1}{500000}}{0.3 \times 97.1 \times 10^{-6}}$$

$$n_1 > \frac{220 \times 0.5 \times \frac{1}{500000}}{0.3 \times 97.1 \times 10^{-6}}$$

$$n_1 > \frac{220 \times 0.5 \times \frac{1}{500000}}{0.3 \times 97.1 \times 10^{-6}}$$

$$n_1 > 7.55 \text{ turns}$$

Since the winding ratio which is,

$$\frac{n_1}{n_3} \leq 9$$

is needed and a minimum of 8 turns for n_1 in order to avoid saturation, we can choose n_3 as 3 turns, then $n_1 = n_2 = 27$ turns, for a turns ratio of 9.

The output inductor value must have an inductance value large enough to ensure continuous conduction mode at the minimum load though larger values of inductance means more and larger turns and this increases the dc resistance and thus copper losses [7]. The peak to peak current ripple must be less than twice the minimum dc current through the inductor. This minimum dc current value is given by,

$$I_{L,min} = 10\% \times 20A = 2 \text{ Amps}$$

Therefore, the peak-to-peak ripple current should be , $\Delta i_L < 4$ amps. This peak-peak ripple current for the output inductor can be calculated for rising current during the ON time of the MOSFET (t_{on}) or OFF time during decaying current,

$$\Delta i_{L_o} = \left(\frac{n_3}{n_1} \times V_{in} - V_o\right) \times \frac{1}{L_o} \times t_{on} \quad (10)$$

From,

$$\frac{V_o}{V_{in}} = \frac{n_3 \times D}{n_1}$$

But,

$$D = t_{on} \times f_s \quad (11)$$

Substituting equation (4) into equation (3),

$$t_{on} = \frac{V_o}{V_{in}} \times \frac{n_1}{n_3} \times \frac{1}{f_s} \quad (12)$$

Hence,

$$\Delta i_{L_o} = \left(\frac{n_3}{n_1} \times V_{in} - V_o\right) \times \frac{1}{L_o} \times \frac{V_o}{V_{in}} \times \frac{n_1}{n_3} \times \frac{1}{f_s} \quad (13)$$

Rearranging, making L_o subject of the equation and substituting 4 amps for Δi_{L_o} ,

$$L_o = \left(1 - \frac{n_1}{n_3} \times \frac{1}{V_{in}} \times V_o\right) \times \frac{1}{\Delta i_{L_o}} \times V_o \times \frac{1}{f_s} \quad (14)$$

Where V_{in} is 220 volts and V_o is 5 volts

$$L_o = \left(1 - 9 \times \frac{1}{220} \times 5\right) \times \frac{1}{4} \times 5 \times \frac{1}{500000}$$

$$L_o > 1.99\mu\text{H}$$

An inductance value of $3\mu H$ is chosen in order to account for tolerance. Therefore, $L_1 =$

$$L_2 = L_3 = 3\mu H$$

The highest primary side current occurs when the full output power is delivered at lowest input voltage. Designing for an efficiency of at least 75%, the power in the primary side can be calculated from

$$\eta = \frac{P_o}{P_{in}} \quad (15)$$

where P_o is 100 W and η is 0.75

$$P_{in} = 133.33 \text{ W}$$

The mean primary side current during t_{on} when D is 0.5 is calculated from,

$$I_{pri,mean} = \frac{P_{in}}{V_{in} \times D} \quad (16)$$

$$I_{pri,mean} = \frac{133.33}{110 \times 0.5}$$

$$I_{pri,mean} = 2.42 \text{ amps}$$

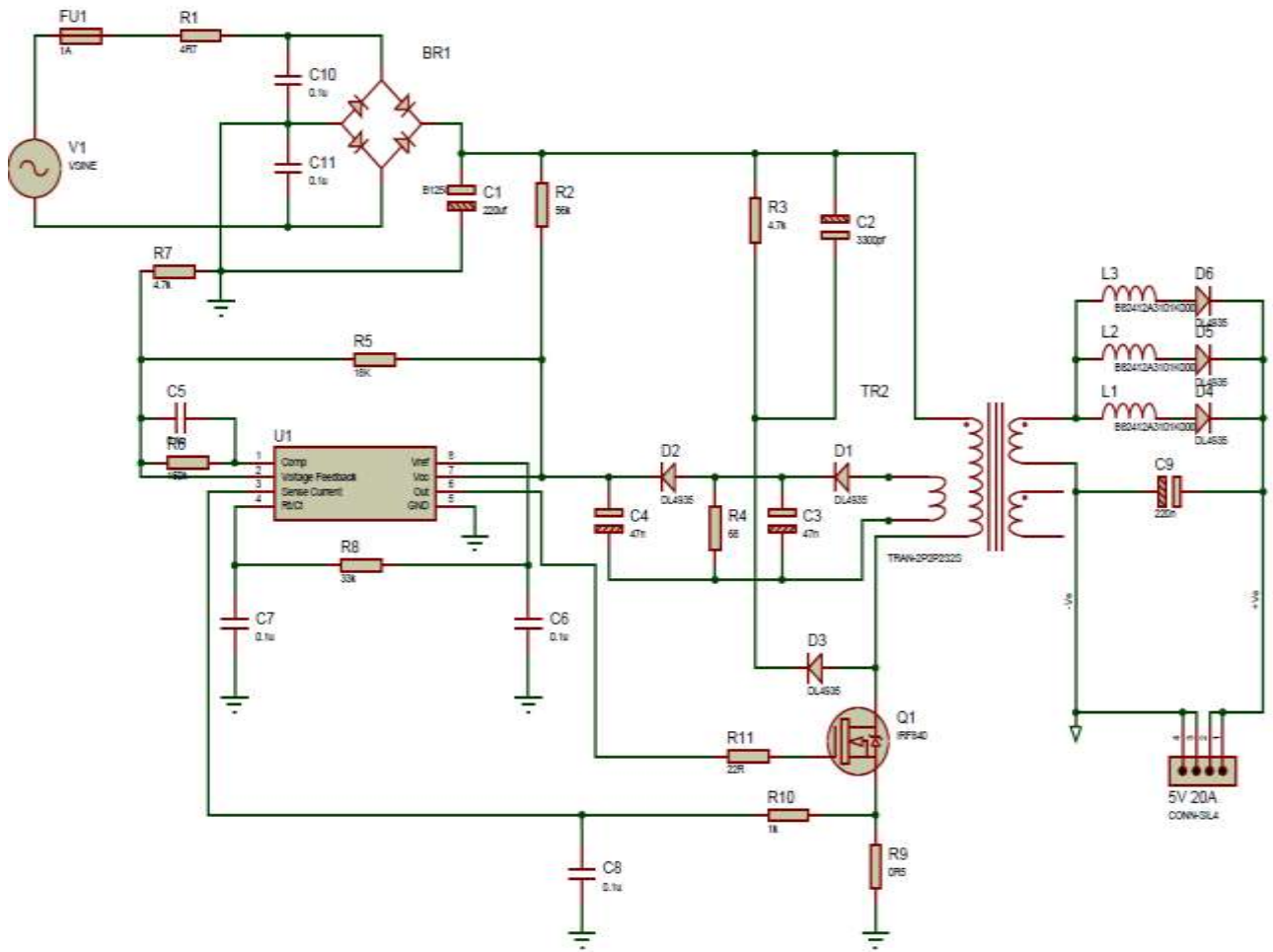


Fig 11: Power Supply Circuit

The expected voltage input coming to the rectifier is between 110 volts and 230 volts. This enables enough voltage to be in the secondary to handle voltage drops and required output voltage.

Figure (11) shows the power supply circuit connections and it consists typically of an input step-down transformer, a rectifier, an output step-down transformer, the output inductor, the pass MOSFET transistor and the current controller IC which switches the MOSFET on or off depending on the feedback. The controller IC and the MOSFET are part of a feedback loop mechanism.

The next stage involves the rectification or the conversion of the A.C. to D.C. The rectification can be achieved using a half-wave or a full-wave rectifier. The full wave rectifier is more power efficient and also makes more DC voltage available on the output side for the regulator. This difference in voltage output is shown by the calculation for the DC output voltage (measured value) of a rectifier. The full wave rectifier provides twice the DC output the half-wave rectifier would as can be seen from the equations (17) and (18) below.

$$\text{For a half-wave rectifier, } V_{DC} = V_m * 0.3185 \quad (17)$$

$$\text{For a full-wave rectifier, } V_{DC} = 2 * V_m * 0.3185 \quad (18)$$

where V_m is the peak voltage and is given by,

$$V_m = V_{RMS} * 1.414 \quad (19)$$

Where V_{RMS} is the voltage on the secondary side or AC side of the rectifier which is at 115 volts,

$$V_m = 115 * 1.414$$

$$V_m = 162.61V$$

. The output voltage wave form from using a full-bridge rectifier is bidirectional since it accounts for both positive and negative swings while the half-bridge rectifier is unidirectional. This means that for the half-bridge rectifier, there is no output during the negative half cycle and the dc voltage output is at approximately zero volts during this negative swing. For the WPT system there needs to be output at both half-cycles of the AC supply.

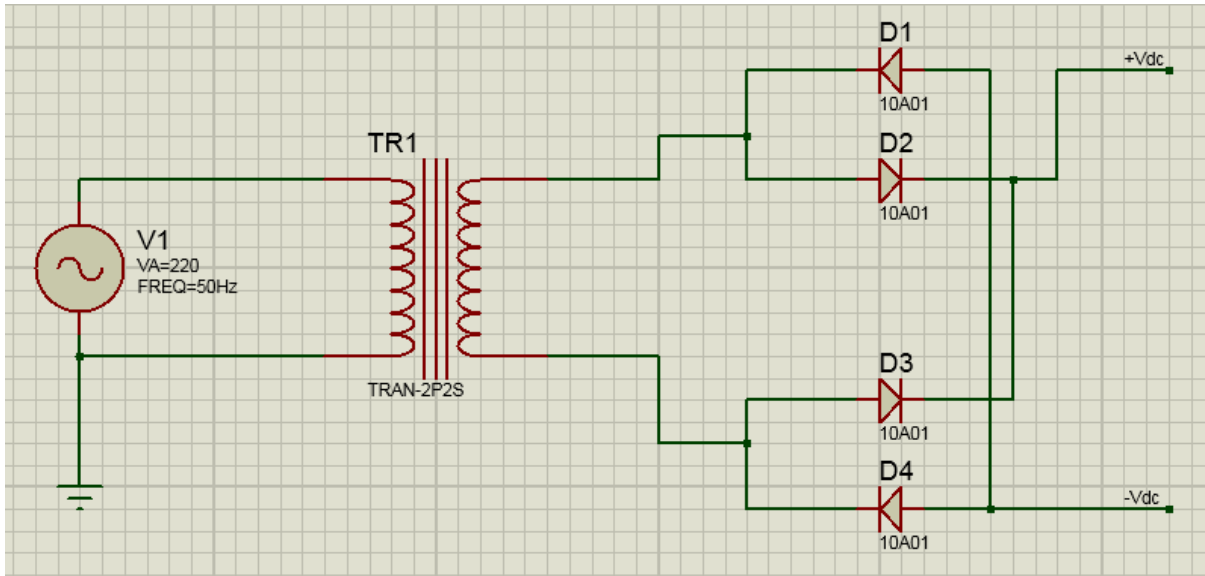


Fig 12: A diode full-wave rectifier connected to a voltage source

In figure (12) above the full-wave rectifier makes use of four power diodes to rectify the AC input from the secondary side of the transformer. Two diodes are used per half-cycle. The output waveform of the full-wave rectifier is shown below in figure (13).

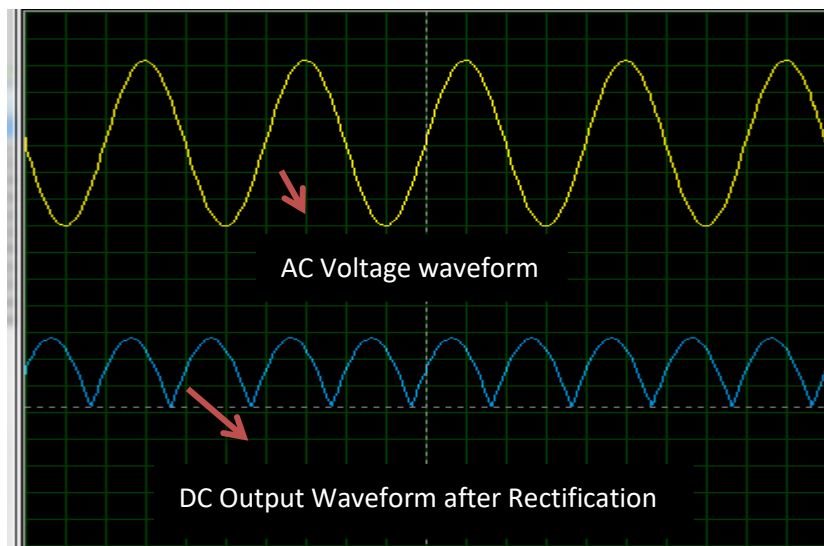


Fig 13: The waveform of the full-bridge diode rectifier

The rms value of the rectified voltage is attenuated by the value 0.9 as shown by equations (12 - 14). This is shown in figure (13), the dc output waveform after rectification is smaller in amplitude than the AC voltage waveform on the transformer secondary side.

The only advantage in using a half-wave rectifier is that the voltage drop is just 0.7V (diode voltage drop for a Silicon diode) while for a full wave rectifier it is twice, that is 1.4V. Though, in using a centre-tapped transformer, the voltage drop across a full-wave rectifier is just 0.7V. Taking into account the voltage drops across the two diodes and the conversion from RMS voltage to DC voltage, the input voltage to the next stage being the voltage regulator becomes,

$$V_{IN} = (V_{DC} - 2V_D) \quad (20)$$

$$V_{IN} = ((2 * V_m * 0.3185) - 2V_D) \quad (21)$$

$$V_{IN} = ((2 * 162.61 * 0.3185) - 1.4)$$

$$V_{IN} \cong 102.18V$$

That leaves us with approximately 102 Volts for the input side of the voltage regulator, just after filtering.

The rectified voltage has ripples towards its peak amplitude. These ripples are undesirable and need to be filtered off or smoothened. A suitable capacitor is used for this filtering purpose. The value of the capacitor used is $220\mu F$. The process of using a suitable capacitor to eliminate the ripples from rectification is referred to as smoothening. This process “smoothen” the DC output voltage from the bridge rectifier and gives a constant voltage.

The circuit uses a current mode controller to provide the necessary control circuitry for off-Line and DC-to-DC converter applications. This controller which is a UC3844 IC features an

oscillator, a temperature compensated reference, high gain error amplifier, current sensing comparator, and a high current totem pole output ideally suited for driving a MOSFET.

The comparator (pin 1) is connected to the voltage feedback (pin 2). The comparator outputs a low impedance signal based on the difference between the set and current voltage then supplies this difference to the feedback pin. The current sense (pin 3) monitors the current through the circuit and the voltage across this resistor is provided as a feedback to the current sense pin. The Rt/Ct (pin 4) which stands for timing resistor/timing capacitor is used to set an internal oscillator IC by connecting an external resistor and capacitor this pin. Ground (pin 5) is connected to the ground of the circuit. The output (pin 6) is used to switch the MOSFET by using PWM (pulse width modulated) signals which are based on the feedback. And the reference voltage based on which the PWM signals are produced is from pin 8. Pin 7 is supply voltage (Vcc) of the IC. The output of this controller drives the power MOSFET switch in the primary leg of the output transformer. The switch is always turned OFF at a time corresponding to the falling edge of the internal system clock of the controller with a switching frequency of 500KHz.

To calculate the total output voltage from the power supply circuit, the equation (22) below is used,

$$V_o = V_{rms} \times \frac{n_3}{n_1} \times \frac{t_{on}}{T} - V_f \quad (22)$$

Where V_o is the required output voltage,

V_{rms} is the secondary side voltage after step-down = 115 volts

$\frac{n_3}{n_1}$ is the turns ratio of the output transformer which is chosen to be $\frac{1}{9}$

$\frac{t_{on}}{T}$ is the value of the duty cycle which is a maximum of 0.5. t_{on} is the on time of the cycle while T is the period of the pulses. The period is $\frac{1}{f}$ and f which is the internal clock frequency of the controller is 500 KHz hence the period T is $2\mu s$.

V_f is the forward diode voltage and the value is 0.7 volts.

$$V_o = 115 \times \frac{1}{9} \times 0.5 - 0.7$$

$$V_o = 5.68 \text{ volts}$$

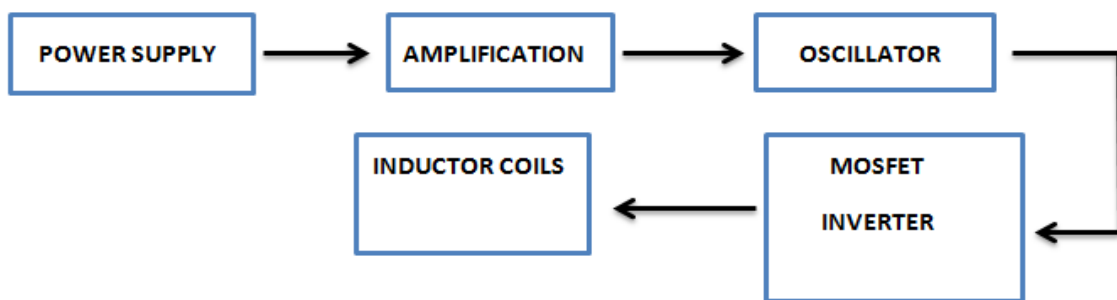


Fig 14: Block diagram of the transmitter section

Figure (14) shows the order of process of the transmitter section. The power supply from the switching-mode power supply provides voltage that are amplified by an LM324 amplifier IC. The amplifier provides analogue inputs which triggers oscillations as an output from a microcontroller. These oscillations are used to drive the MOSFET inverters which in turn drive the inductor coils.

4.2 Section Summary

In designing the power supply for the system, it was imperative that weight, size and efficiency were considered. The linear mode power supply would provide clean regulated dc

output without any feedback. The switch-mode power supply incorporates feedback using a pass transistor and a controller while using the energy stored in the output inductor, during the on periods of the transistor to maintain an output during the off periods of the transistor. This circuit uses a flywheel circuit which includes the inductor, a diode and a capacitor. During the MOSFET on period, it supplies current to the load, while the field of the output inductor expands and the output capacitor charges. During the MOSFET off period, the inductor returns its stored energy to the circuit and after this has been done, the output capacitor now provides the current within the circuit and to the load until another on period. By this process, a rippled waveform appears across the load rather than a square waveform. The peak-to-peak ripple amplitude is smaller than the current in the inductor as shown by calculations to be less than 4 amps where the current in the inductor is 2 amps.

5.0 TRANSMITTER CIRCUIT DESIGN

The transmitter circuitry involves the design of the amplification stage for the power from the supply and the oscillator stage which provides pulses for the inverter MOSFET gates. The amplification is achieved using an LM324 IC while a microcontroller is used to implement the oscillator.

5.1 Amplification and Oscillator

Amplification is an important stage of the circuit. Amplification is used to improve on the voltage output and subsequently power within the system. Amplification is used to raise the voltage level. The 5 volts output from the power supply is the input for the operational amplifier used as an amplifier. The LM324 IC is used for amplification purpose. LM324 which is a quad operational amplifier consists of four independent high gain with internal frequency compensation for operational amplifiers designed to operate from a single power supply over a wide voltage range. The LM324 has 14 pins and the pin configurations are listed below as given in the datasheet.

The LM324 provides two inputs into the microcontroller 8S003F3P6. The pin 1 output is the analog input 4 of the microcontroller. This pin 1 also serves as the ADC (Analog Digital Conversion) external trigger. It triggers the microcontroller to convert the analog signal in pin 5, pin 6, pin 19 and pin 20 of the microcontroller. The output from pin 14 of the LM324 is connected to the pin 11 (port B5) of the microcontroller which has an alternate function of being the I²C or break input.

Table 1: LM324 pin configurations

Pin 1	OUT1	Pin 8	OUT3
Pin 2	IN1(-)	Pin 9	IN3(-)
Pin 3	IN1(+)	Pin 10	IN3(+)
Pin 4	Vcc	Pin 11	GND
Pin 5	IN2(+)	Pin 12	IN4(+)
Pin 6	IN2(-)	Pin 13	IN4(+)
Pin 7	OUT2	Pin 14	

The inverting input (pin 3) of the op amp is used to provide voltage feedback with the aid of the two resistors R_1 and R_2 as voltage dividers. The voltage gain is dependent on the values of these resistors where,

$$V_{OP} = A_v \times V_{IP} \quad (23)$$

$$A_v = 1 + \frac{R_1}{R_2} \quad (24)$$

where V_{OP} is the voltage output from the operational amplifier, V_{IP} is the input to the non-inverting terminal of the operational amplifier and A_v represents the voltage gain of the operational amplifier as set by the resistance ratio.

Since, the required output from the op-amp is 9 volts, V_{OP} has to be 9 volts while V_{IP} is 5 volts which is the output voltage V_s of the supply already calculated.

$$A_v = \frac{V_{OP}}{V_{IP}} \quad (25)$$

$$A_v = 1.8$$

$$A_v = 1 + \frac{R_1}{R_2}$$

Therefore, $\frac{R_1}{R_2} = 0.8$ and $R_1 = 0.8R_2$ is the required ratio for precise amplification. The selected standard resistor value for R_2 is 2200Ω hence R_1 is 1760Ω which is a standard resistor value.

5.2 Oscillator Design

Oscillation stage is the next after amplification. The required oscillator should be able to provide pulses at a high rate so as to provide efficiency. The frequency of the pulses therefore, has to be very high. The microcontroller 8s003f3p6 is used to control the oscillation and switching. This microcontroller is an 8 bit microcontroller that belongs to STM8 family of microcontrollers. It has 20 pins and an internal clock frequency of up to 16 MHz. The pins of the microcontroller, how they are programmed and the program written in assembly language are in the appendix.

The pins of ports A, B, C and D are configurable as either input or output ports. The port pins B5, D2, D3, D5, D6 are configured as input pins while pins D4, C3, C4, C5, C6 and C7 are used as output pins. Four output pins of port C are used to provide pulsed inputs to the inverting K27 ICs. K27 is a dual transistor IC and is used in the inverting stage to drive inverter MOSFETs. The pins used as output are C3, C4, C6 and C7. These pins are all timer 1 pins and hence have the same oscillation frequency. The port C5 is also an output but for timer 2.

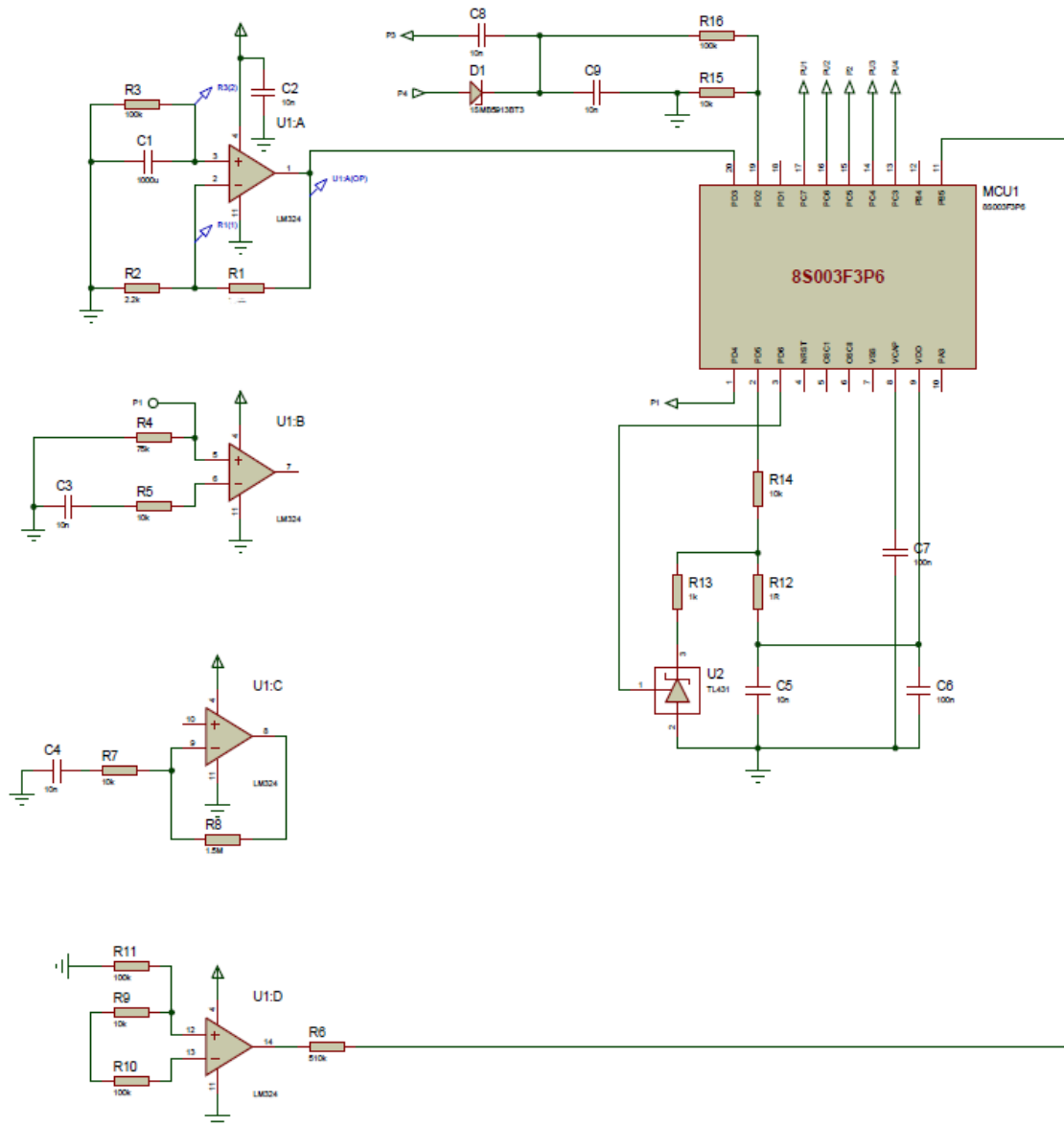


Fig 15: LM324 connection to the 8S003F3P6 microcontroller

Figure (15) shows the LM324 quad operational amplifier internal connections and how they provide analog input to the microcontroller which it processes and provides oscillations to the inverting stage. The absolute maximum voltage input to the 8s003f3p6 microcontroller is 6.5 volts according to the datasheet. The amplifier is configured to provide 9 volts to the microcontroller. The extra 2.5 volts is for tolerance and voltage drops along the linear components connected to the microcontroller.

The timer or the oscillator provides the control for the switching by setting the duty cycle of the oscillation.

5.3 Inverting and Switching Stage

The inversion uses MOSFETS and transistor IC packages. The MOSFET ICs used are 9926A which is a dual n-channel MOSFET and 4953 which is a dual p-channel MOSFET. The two ICs have 8 pins each with different pin configurations as shown in the diagrams below in figure (17) and figure (18) .

The transistor IC is a K27 which is a dual transistor IC. The first transistor in the package according to the datasheet is a 2907A PNP transistor and the second transistor is a 2222A NPN transistor. The K27 ICs receive pulses from the microcontroller and then drive the gates of the MOSFET ICs.

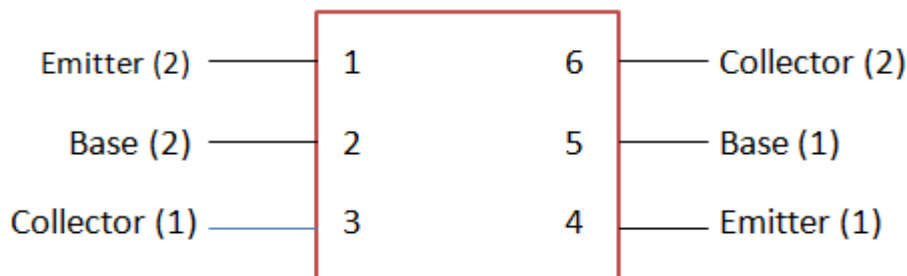


Fig 16: K27 pin configurations (PNP 2907A, NPN 2222A)

As shown in figure (16) above, the first transistor in the IC according to the datasheet is the PNP 2907A transistor while the second one is the NPN 2222A transistor. Their collector terminals drive the next stage of MOSFET ICs as explained.

In figure (17) below, the 9926A four source terminals are connected together in twos. According to the datasheet the two source (2) terminals are connected together internally while the same is for the two source (1) terminals.

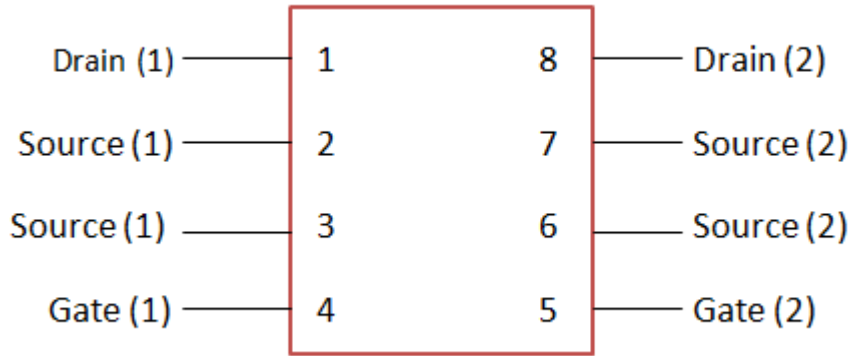


Fig 17: 9926A pin configurations (n-channel MOSFETs)

In figure (18) below, the two drain (1) terminals of the 4953 are connected together while the two drain (2) terminals are connected together.

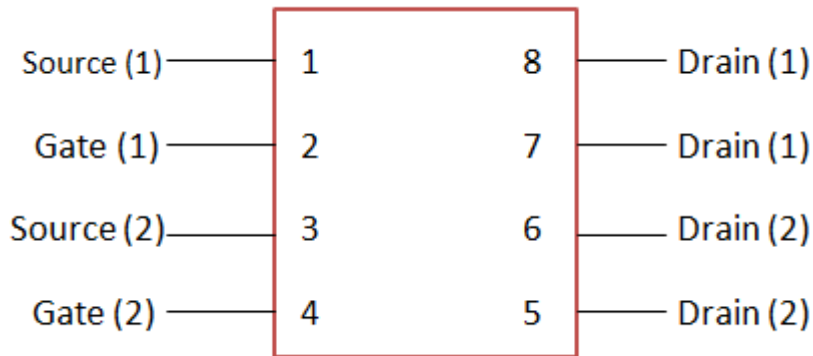


Fig 18: 4953 pin configurations (p-channel MOSFETs)

The two collector terminals of the K27 are connected together while the two base terminals are driven by the same channel input from the microcontroller. The first K27 is fed from the channel 2 (timer 1) output of the microcontroller (port C7) while the inverted channel 2 which is channel 4 (timer 1) output of the microcontroller (port C4) provides the base input of the second K27 IC. The microcontroller channel 1 output (port C6) provides the base terminal input for the fourth K27 IC and the inversion of channel 1 which is channel 3 (timer 1) from the microcontroller port C3 feeds the base of the third K27 IC. The inversion of the

channel or pulses is in order to ensure that all the K27 ICs are not switching ON at the same time but rather in pairs. K27(1) and K27(4) that is the first and fourth K27 IC switch ON at the same time and then are OFF when the other pair K27(2) and K27(3) are ON and vice versa. The switching ON and OFF of each pair of K27 ICs also controls the MOSFET ICs. Only one 9926A IC and 4953 IC is ON at any point in time. From the table below, how the K27 controls the MOSFET ICs is seen.

Table 2: Relationship between K27 IC and the MOSFET ICs

K27	MOSFET IC
1	9926A(1)
2	4953(1)
3	9926A(2)
4	4953(2)

This represents the switching stage of the transmitter circuit since only two MOSFET ICs are switched ON during each point of the pulse. For a duty cycle of 50%, each MOSFET pair that is one 9926 and one 4953 will be ON for half the period of oscillation. The diagram of the switching stage circuit is shown in Fig.19.

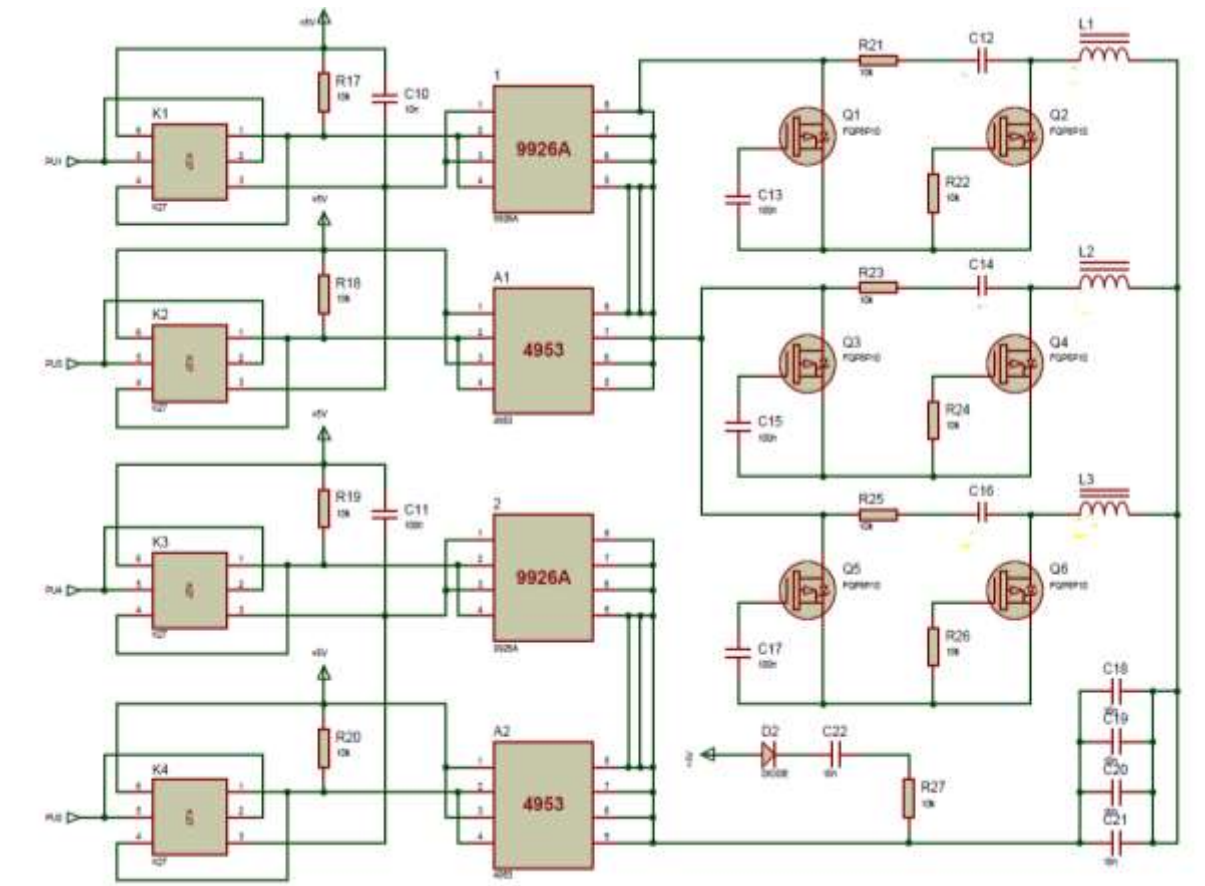


Fig 19: Connections between the K27 transistor ICs and the MOSFET ICs

The outputs from the MOSFET ICs drive the three transmitter coils as shown in the circuit in figure (19). The ICs output are in two groups of four. Group one includes K27(1), K27(2), 9926A(1) and 4953(1). The second group consists of K27(3), K27(4), 9926A(2) and 4953(2). Pins (5 – 8) of the individual MOSFET ICs are connected together, then the pins (5 -8) of the MOSFET ICs in the same group are looped together to provide output for the transmitter coils. During each half-cycle, one K27 in each group is conducting and driving one MOSFET IC. But since the pins 5 – 8 are tied together as shown in figure (19), there will always be an input to the transmitter coils. Each output provides the drain voltage V_D for a half-bridge MOSFET inverter. The voltage output of a half-bridge MOSFET inverter is calculated using the equation (19),

$$V_{om,rms} = 0.45 \times V_d \quad (19)$$

For there to be at least 2 amps in the output the value of the resistor in the network should not be greater than 10 ohms.

5.4 Section Summary

The output voltage from the dc power supply is not sufficient to the required voltage at the transmitter coil. This voltage is therefore to a sufficient voltage level for the oscillator and the inverting/switching stages.

A suitable oscillator is required to provide and handle the high switching frequency required for high efficiency levels in the WPT system. The oscillation is achieved using a microcontroller with switching frequency up to 16 MHz. It also provides the control required in the transmitter module by providing the timer channels used to switch on or off the inverter MOSFETs. Switching means that not all the MOSFETs are on at the same time. The switching frequency is at a high frequency and also the resonant circuit is designed with a resonant frequency in hundreds of kilohertz in order to enable compliance with the Qi standards. This design is in such a way that while not all the inverting transistors are conducting at the same time, current still gets to the three transmitter coils and hence induction is possible. Achieving high frequency levels in the resonant circuit is dependent on the choice of inductor coil inductance and the parallel capacitor in the resonant circuit during the transmitter coil design.

6.0 TRANSMITTER COIL DESIGN

The Qi standard operates at frequencies between 105 KHz and 300 KHz [1, 8, 9, 10]. At resonance, the output waveform becomes more sinusoidal and purely resistive. This resonant can be achieved by using an LC network. The values of the components of this LC network are selected bearing in mind the operating frequencies of the Qi standard on which the design is based. This frequency is referred to as resonant frequency. The resonant frequency of this design is chosen to be 120 KHz. The relationship between the resonant frequency f_R and LC components is given by,

$$f_R = \frac{1}{2\pi\sqrt{LC}} \quad (27)$$

Resonance is achieved when the inductive reactance is equal to capacitive reactance. That is to say at resonance,

Inductive reactance = Capacitive reactive

$$X_L = X_C \quad (28)$$

$$2\pi fL = \frac{1}{2\pi fC} \quad (29)$$

$$f_R = \frac{1}{2\pi\sqrt{LC}}$$

The selected values for the inductor and capacitor are 12.5 μ H and 140nF respectively. The resonant or operating frequency is calculated to be approximately 120 KHz. This is value is within the WPC (Wireless Power Consortium) specified standards.

At resonance the imaginary components of the circuit impedance cancel each other out and act like an open circuit with infinite resistance. At this point, the impedance is at a minimum

and the current through this circuit is the resistance of the resistor which presents a pure resistive load.

The voltage in the inductor can be calculated using,

$$V_L = I_{output} \times X_L \quad (30)$$

where X_L is the reactance of the inductor coil,

$$X_L = 2\pi \times f_R \times L \quad (31)$$

Therefore,

$$V_L = I_{output} \times 2\pi \times f_R \times L \quad (32)$$

$$V_L = 2 \times 2\pi \times 120 \times 1000 \times 12.5 \times 10^{-6}$$

$$V_L \cong 18.85 \text{ volts}$$

This voltage is within the specifications for the receiver stage IC which states a range of -0.8 to 20 volts for the AC input.

The quality factor is an important factor when equating the voltage of the real to that of the imaginary part. A high value of Q (quality factor) is desirable. For a series RLC circuit, the quality factor is given by,

$$Q = \frac{X_L}{R_{dc}} = \frac{9.4286}{0.065} \quad (33)$$

$$Q \cong 145.06$$

Where R_{dc} is the DC resistance of the inductor coils in the transmitter and the maximum specified value is $65m\Omega$ as used in the calculation of the Q factor. Also the Q factor is above 90 which is the minimum specified value according to WPC Qi standards.

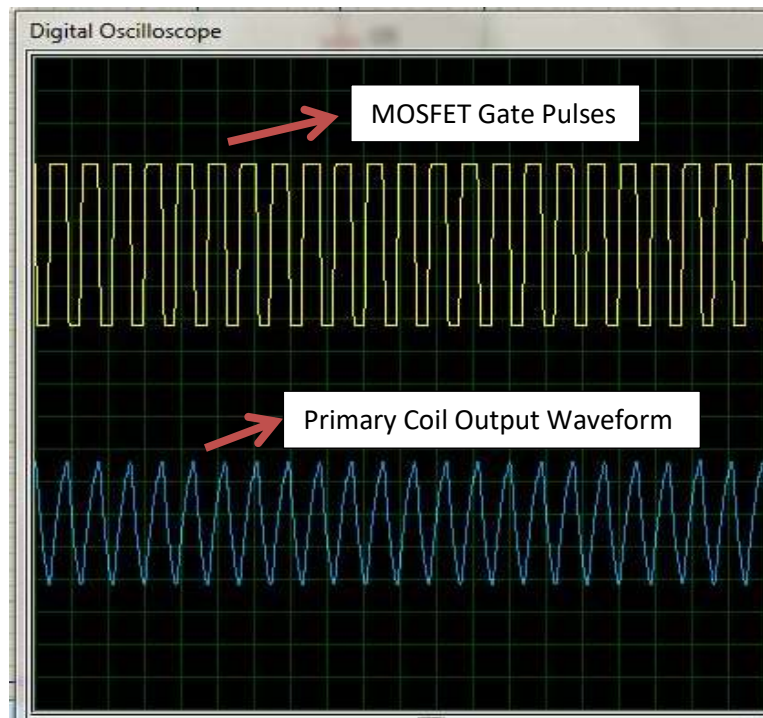


Fig 20: Waveform of the transmitter coil voltage output

Fig.20 shows that the transmitter output waveform is sinusoidal in nature. This is due to the inductive resonant circuit incorporated into the circuit. The resonant frequency is close to the oscillating frequency which is calculated as 120KHz.

6.1 Modelling and Simulation of Transmitter Coil Magnetic Field

6.1.1 Introduction

The purpose of this section is to develop a finite element model using a commercial software (Comsol Multiphysics®) to study and compare the magnetic flux density generated by both the WPT Transmitter and Receiver coil configurations. The aim is to investigate the strength of Magnetic flux density generated in order to understand and visualise the process of transmission and reception under any given condition. The finite element model is also used to investigate the performance of the Coil system by studying how some coil design parameters affects the density of magnetic flux generated.

6.1.2 Numerical Simulation

The core of inductive WPT operational mechanisms consist of electromagnetic fields created within the coil based on Maxwell's law of electromagnetic induction. As described in section (3.0), the Magnetic flux is produced by the time varying excitation current. The electrodynamic body forces cause the coupling of Transmitter and the Receiver coils for maximum power transfer. Therefore, the modelling process of inductive WPT involves the resolution of the electrodynamic problems.

The most accurate method to solve the electrodynamic problem is to invoke the differential form of Maxwell's equations (Ampere's law and Faraday's law of induction) with the appropriate boundary conditions taken into account. The most suitable solution to these problems is to use numerical techniques to find an approximate solution to the partial differential equations (PDE). The three commonly used techniques to solve PDE's are: the finite element method (FEM), the finite volume method (FVM) and the finite difference method (FDM) [54]. Amongst the three methods, FEM is often regarded as the most common and most accurate approximation technique employed in solid based simulations and structural mechanics. FVM and FDM employs slightly different method of finding solutions to PDE's, by discretising the problem to large number of grids and are widely used in computational fluid dynamics (CFD). In FEM, the geometry and the domains are discretised into a set of finite elements (mesh generation) and the final solution is the sum of the discrete solutions in each discrete element, hence the accuracy of the solution can be increased by increasing the number of discrete elements in the domain.

6.2 Modelling

For a 3D geometry the subdomains are partitioned into hexahedral or prism and tetrahedral elements. The geometry edges are partitioned into edge elements [54]. There is several

commercial simulation software based on FEM modelling techniques for solution of PDE's such as Comsol multiphysics, ANSYS, Abacus, ADINA and ALGOR. Comsol multiphysics is used in this research because of the following features:

- (i) Comsol multiphysics is very robust and versatile in the coupling of different physics which gives room for modelling of the actual phenomenon that take place in the operation of WPT (i.e. the conversion of electromagnetic energy into electrical energy and vice versa).
- (ii) The software makes use of Maxwell's equation in FE approximation method to solve electrodynamic problems. A unique feature of Comsol multiphysics is that the underlying equations for electromagnetics are automatically available in all other application modes, making coupling of different physics much easier between different application modes.
- (iii) The software has predefined physics interfaces which gives room for the control over the definition of constants, the use of the material properties and the boundary conditions.
- (iv) Comsol Multiphysics give room for models to take advantage of symmetry where possible to reduce computation time and exploit available memory.

6.2.1 Model Implementation

The design of the coil configurations model in Comsol Multiphysics started with the selection of appropriate modules related to the physics involved in WPT operation. The AC/DC module is used to solve the electrodynamics. Fig.21 shows the block diagram of the processes involved in modelling WPT coil configuration for the generation of Magnetic flux.

The simulation carried out in this section involves the generation of magnetic flux by the Transmitter coil (Race Track coil configuration) and the reception of the magnetic flux by the

receiver coil. The coils were simulated in 3D mode. The application mode used for the simulation is the magnetic field (mf). The mf describes the quasi-static magnetic field system for conducting, magnetic and dielectric materials. This feature is used for easy excitation of coils and other conducting structures. The dependent variable in this application mode is the vector magnetic potential in the Cartesian coordinate (A_x , A_y and A_z) and electric current can be used as input in the model subdomain setting. The Magnetic flux density and other magnetic parameters are calculated from the vector magnetic potential.

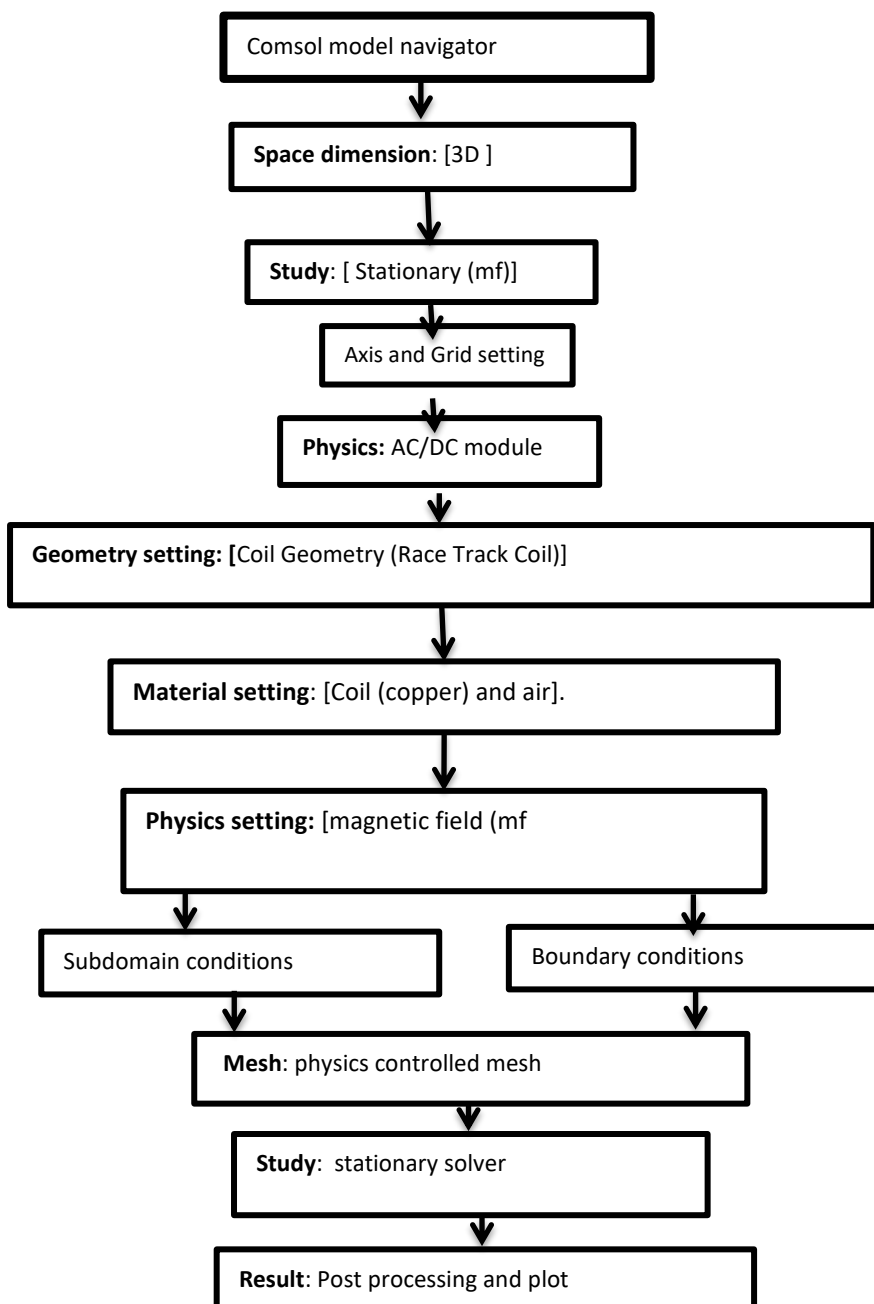


Fig 21: Block diagram showing the steps involved in FE modelling of the generation and Reception of Magnetic Flux by the Transmitter and Receiver Race-Track coil *configuration*. **55**

6.2.2 Comparative Study of Transmission Coil Configurations

The schematic diagram and cross sectional view of the Transmission coils under investigation is given in Fig.22 (A, B and C) and Fig. 13 (A, B and C) respectively. It consists of a transient magnetic field and a coil. The positive (+ve) section of the coil represent the in-plane current while the negative (-ve) section represent the out-plane current. The transient magnetic field for the transmitting coil is expressed in terms of magnetic vector potential (MVP) A , and source current density (SCD). If we assume that the coil material is infinitely long, the current densities j_{sk} and MVP have only longitudinal, and z-component [55-57]. Table 3 depicts the structural parameters in modelling the transmission coils.

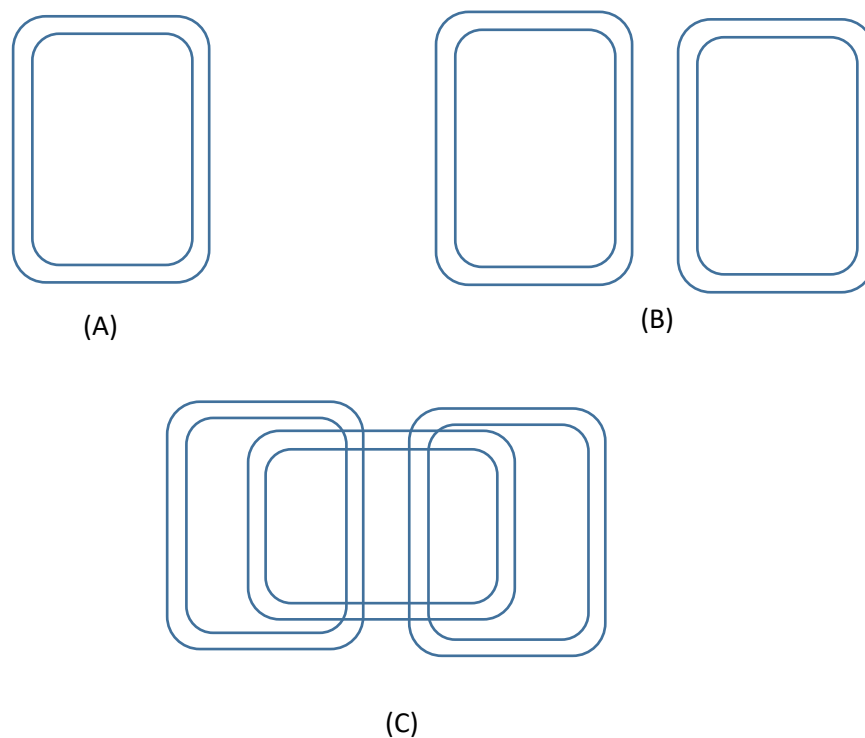


Fig. 22: Schematic of WPT Transmission coil configurations. (A) Single Race-Track coil (SRT), (B) Double Race-Track coil(DRT), (C) Proposed Triple Race-Track coil (TRT) configuration combining the current path and magnetic fields of (A) and (B) .

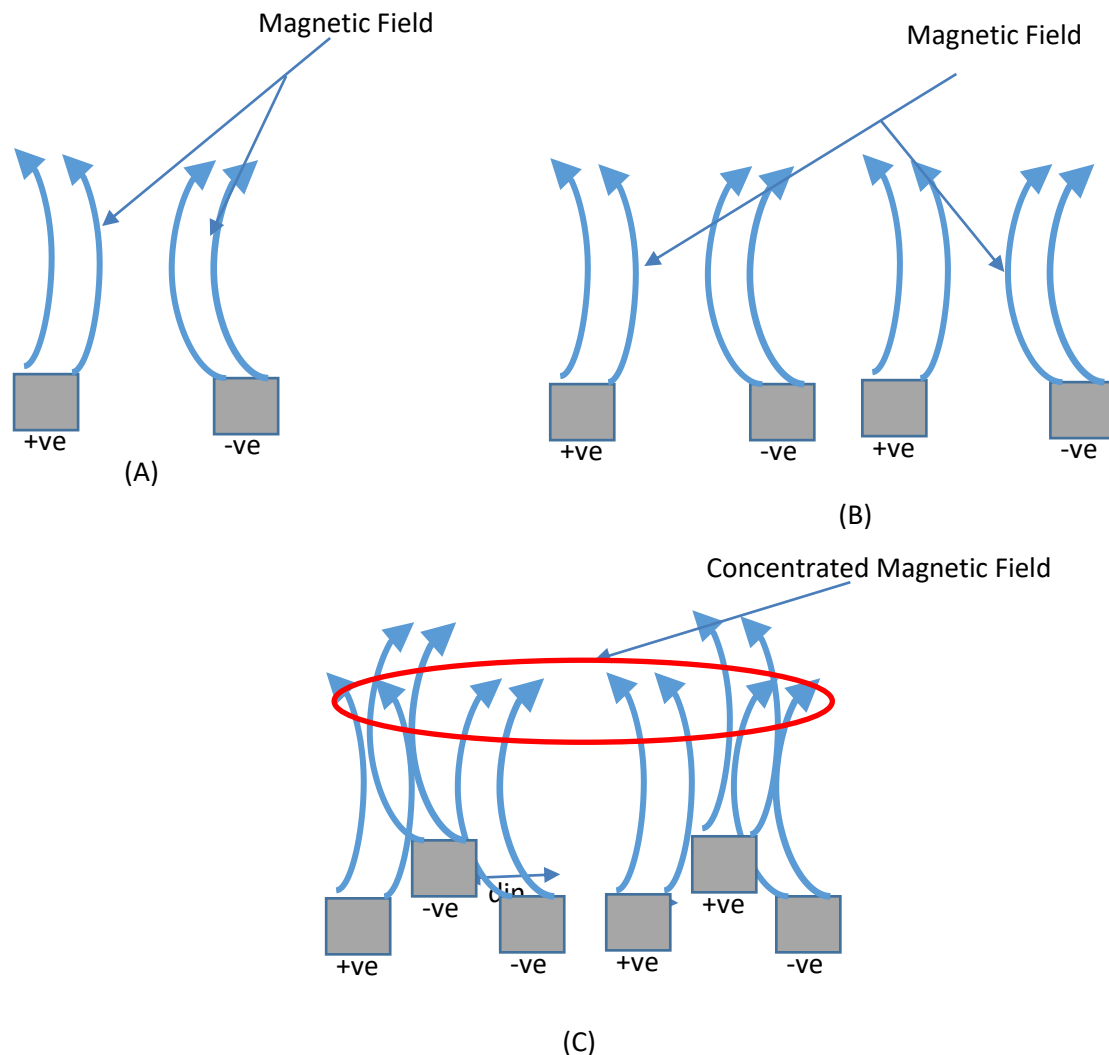


Fig. 23: The cross sectional view and the magnetic field interaction of coil configuration under investigation: (a) SRT coil, (b) DRT coil and (c) TRT.

Table 3: Transmission coil parameters used for the simulation

s/n	Parameter name	Abbreviation	size
1	Coil thickness	t_c	0.2mm
2	Coil width	Cw	1.5mm
3	Distance between Coils	Cs	1mm
4	Lift off distance	H	0.5mm

5	Internal Diameter	Din	4mm
6	Excitation Current	I0	2A
7	Excitation frequency	F0	50Hz

6.2.3: Finite Element Mesh:

The finite element mesh in Fig.24 (A, B and C) was obtained by discretising the physical model in to numerous second order quadratic triangular elements consisting of elements consisting of 55,872, 66765 and 78454 elements for the SRT, DRT and TRT coils respectively. The mesh element was refined at about 0.1mm around the skin depth surface of the copper coil. This refinement of the model significantly improves its accuracy, though the number of elements as well as the solution time was greatly increased. The refinement is achieved by continuously comparing the calculated result at different degree of refinement until the result hardly changes with refinement.

The time steps, relative tolerance and the absolute tolerance were adjusted for a more accurate calculation.

To obtain an accurate record of the variation of the extracted data from the simulation, the cut-line 3D probe was placed just above the coil cutting across the diameter.

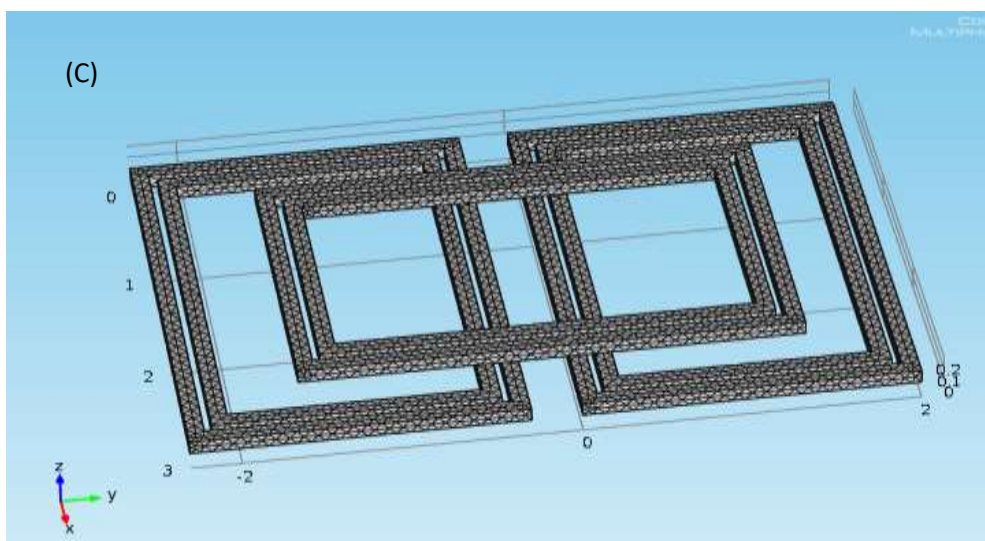
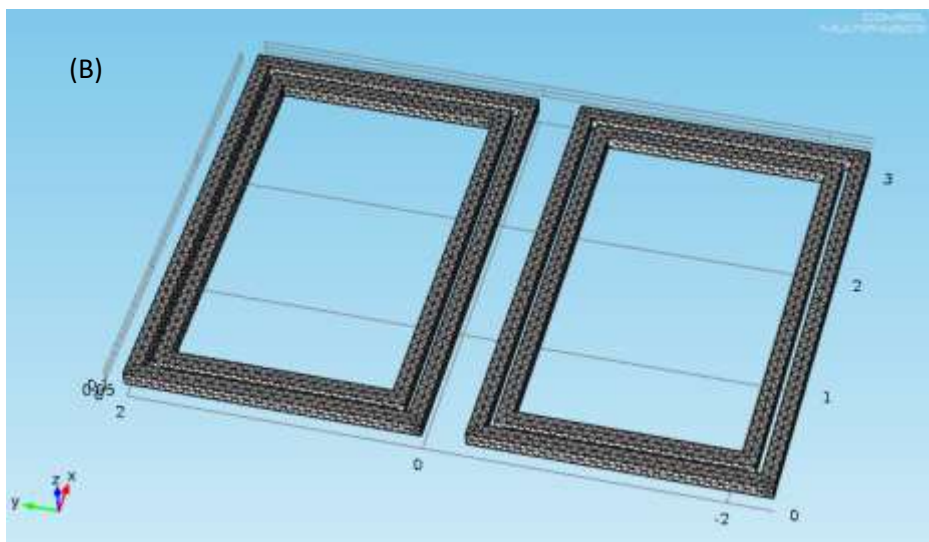
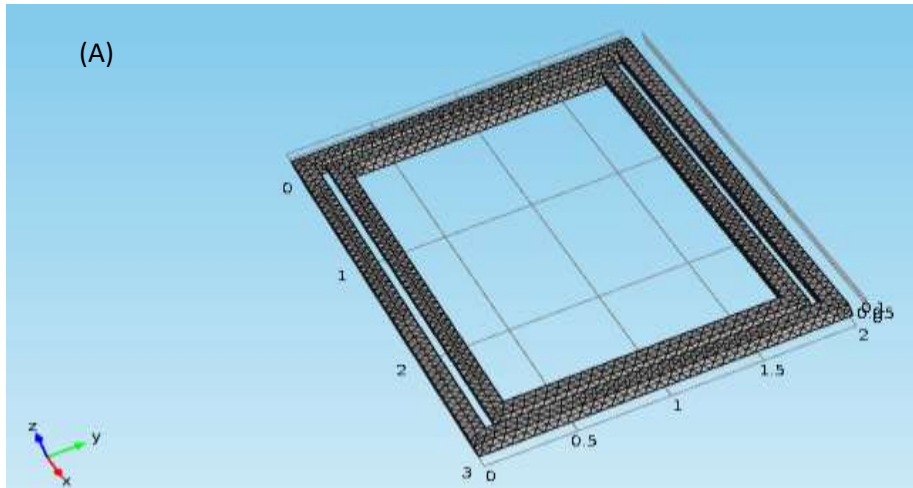


Fig.24: FE mesh; (A) SRT coil, (B) DRT coil, (C) TRT coil.

6.2.4 Simulation and Analysis

The driving current applied to the Transmitter coil is a two cycle continuous pulse signal. The driving current is converted to current density by dividing the magnitude of the current by the cross sectional area of the coil (i.e. $\frac{I_0}{A}$). The plot of the external source current density employed in the simulation is given in Fig.25.

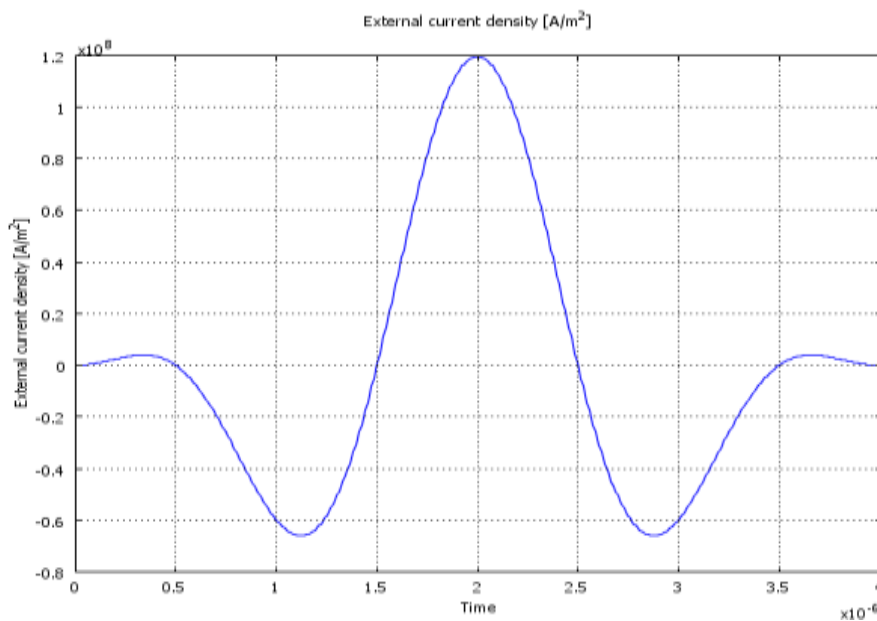


Fig.25 Time history of the External current density for used to excite the SRT, DRT and TRT coils.

Applying the external source current in the finite element model, the Electromagnetic equations are solved to obtain the magnetic flux density within the surface of the coil. A cut-line 3D plot of the magnetic flux density is obtained close to the surface of the copper coil for the SRT, DRT and TRT coils respectively.

6.2.4.1 Single Race-Track (SRT) Transmitter Coil configuration

Fig.26 shows the surface plot of dynamic magnetic fields in the coil material when a two turn SRT configuration is employed. The first two turns represent the in-plane current while second two turns represent the out-plane current as described in section 4.2.2. The result of the surface plot and the line graph in figs 26 and 27 respectively shows an uneven distribution

of magnetic flux around the coil with the weakest point found around the centre of the coil. This uneven distribution of the magnetic field gives rise to a small magnetic pulse width of 0.2, and a zone of low field referred to in this research as the DEAD ZONE. The peak to peak value of the magnetic field measured for this coil configuration is $35 \times 10^{-7} A/M$.

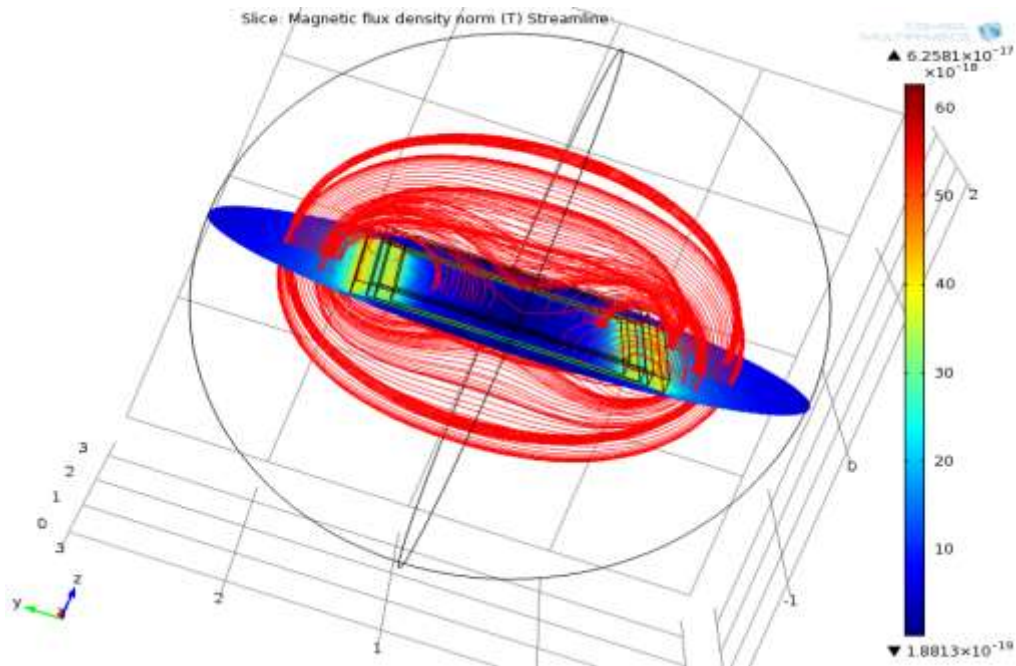


Fig.26: 3D surface plot showing the magnetic field line around the SRT coil.

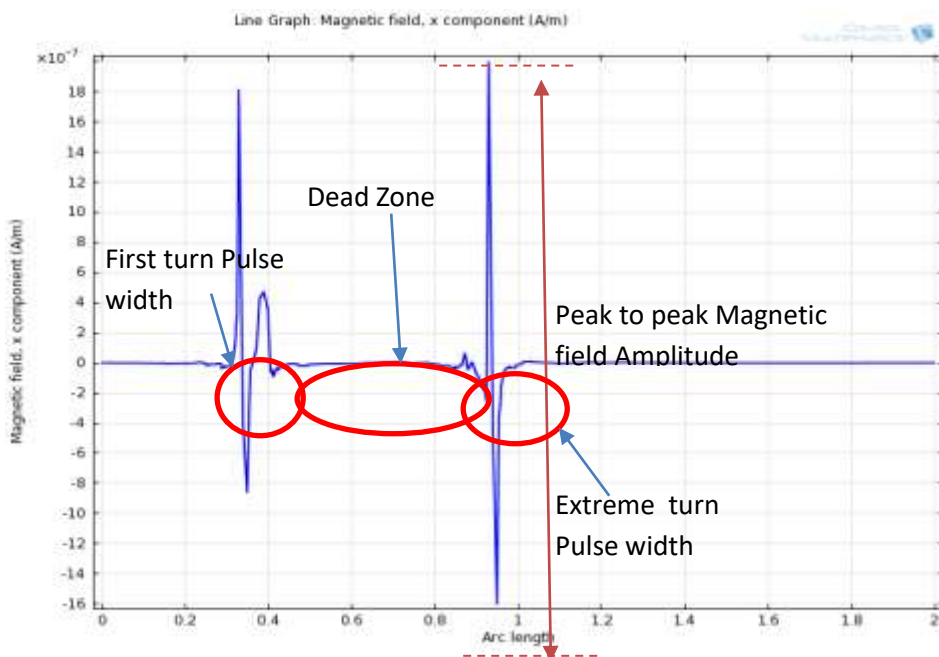


Fig. 27: Shows the line graph of the magnetic field across the SRT coil.

6.2.4.2 Double Race-Track (DRT) Transmission Coil configuration

The Double Race Tract coil configuration is formed when two SRT coils are placed side by side as shown in the figs 22 and 23 (A) above. Fig.28 shows the surface plot of dynamic magnetic fields in the coil material when a two turn DRT configuration is employed. The first and third turns represent the in-plane current, while the second and fourth turns represent the out-plane current as described in section 4.2.2 above. The result of the surface plot and the line graph in figs 28 and 29 respectively shows a more even distribution of magnetic flux around the coil with the strongest point found around the centre of the coil with more turns. The distribution of the magnetic field around the central turn minimises the occurrence of the low field region (DEAD ZONE), improves the magnetic pulse width to 0.4 and magnetic field strength. The peak to peak value of the magnetic field measured for this coil configuration is $95 \times 10^{-7} A/M$

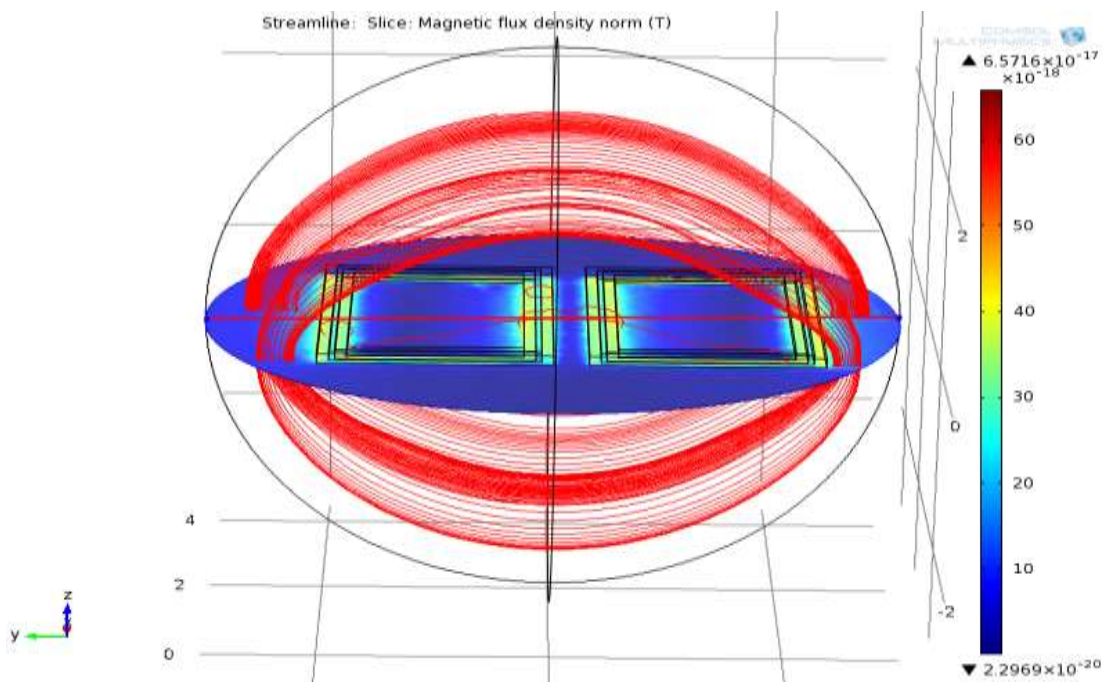


Fig.28: 3D surface plot showing the magnetic field line around the DRT coil.

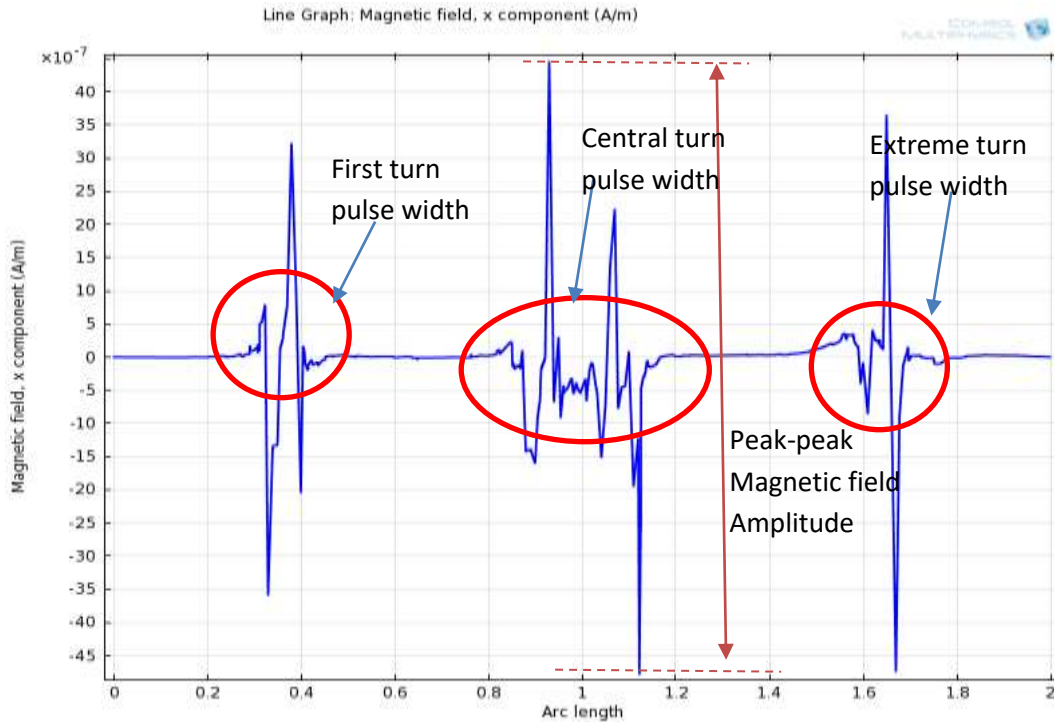


Fig. 29: Shows the line graph of the magnetic field across the DRT coil.

6.2.4.3 Triple Race Track Transmission (TRT) Coil configuration

The Triple Race Tract coil configuration is formed by combining a DRT and an SRT coils. In this configuration an SRT is Placed in a reverse order, but adjacently on top of a DRT as shown in fig (29) above. This configuration increases coil to coil surface area and magnetic field interaction as seen in fig.22 (c) above. Fig.30 shows the surface plot of dynamic magnetic fields in the coil material when a two turn TRT configuration is employed. The first and third turns represent the in-plane current, the second and fourth turns represent the out-plane current while another coil with both an in-plane and an out-plane current lie adjacent to the coils underneath it, as described in section 4.2.2 above. The result of the surface plot and the line graph in figs 30 and 31 respectively shows a more even distribution of magnetic flux around the coil with the strongest point found around the centre of the coil with more turns. The distribution of the magnetic field around the central turn eliminates the occurrence of the low field region (DEAD ZONE), improves the magnetic pulse width to 0.8 and magnetic

field strength. The peak to peak value of the magnetic field measured for this coil configuration is $27 \times 10^{-6} A/M$.

The result further shows that there is a correlation between, the peak to peak magnetic field amplitude, pulse width and occurrence of dead zone. The higher the pulse width, the higher the magnetic field strength and the lower the dead zone as shown in table 4. The result in Table 4 clearly shows that of all the coil configurations studied, the TRT coils exhibited a better response in mitigating the problem of dead zone whilst improving the magnetic field strength. Hence, further WPT development in this work was pursued using the TRT coil configuration.

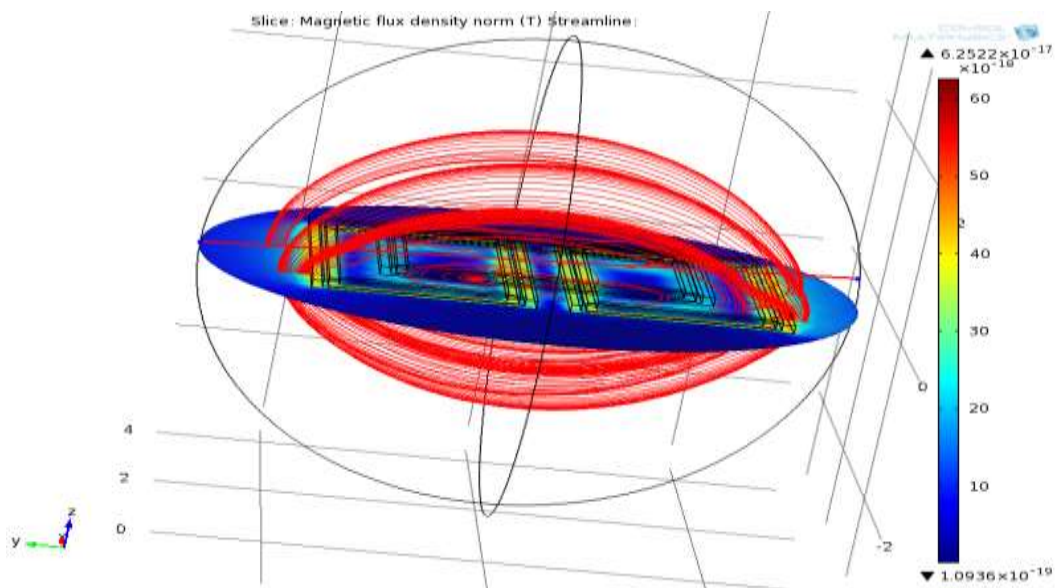


Fig. 30: 3D surface plot showing the magnetic field line around the TRT coil.

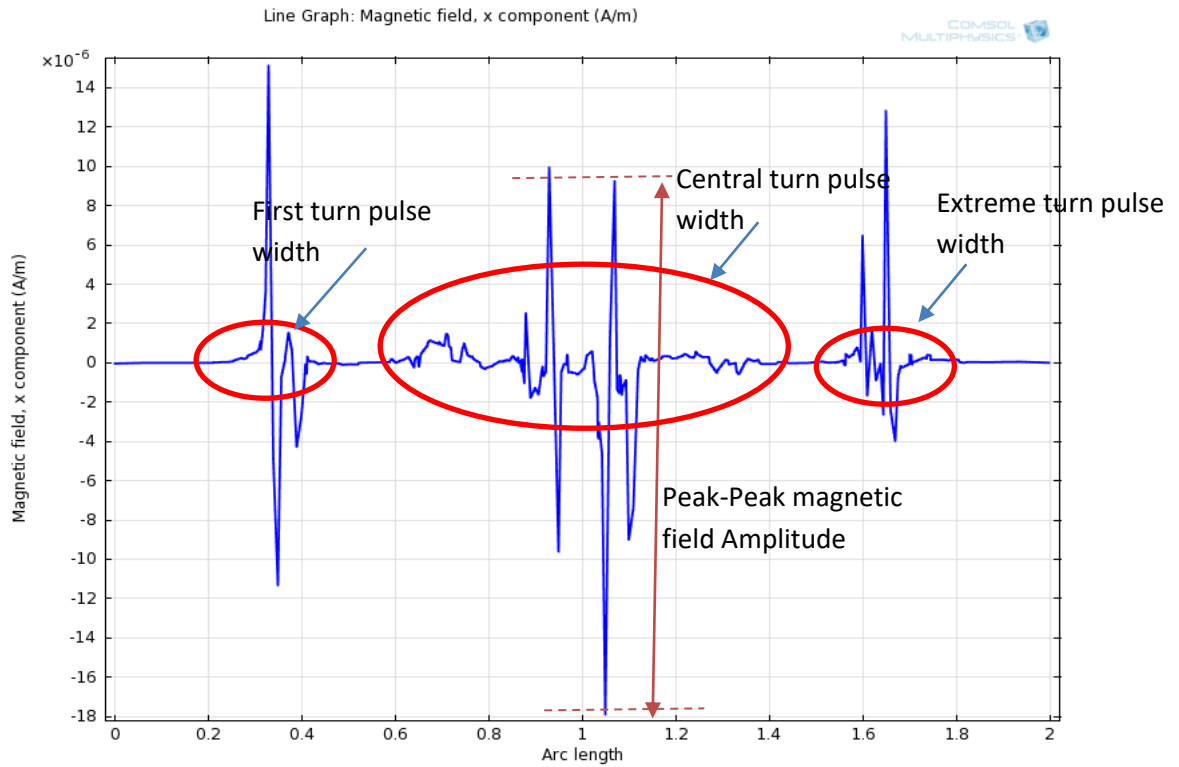


Fig. 31: Shows the line graph of the magnetic field across the TRT coil.

Table 4: Coil Type Simulation Result

COIL TYPE	Peak-Peak Magnetic Field Strength (A/M)	Pulse Width (Arc length)	Occurrence of Dead Zone
SRT	35×10^{-7}	0.2	Very High
DRT	95×10^{-7}	0.4	Low
TRT	27×10^{-6}	0.8	Very Low

6.2.5 Investigation of the Performance of TRT transmitter Coil Configuration

Having thus determined to focus on TRT coils for excitation, the coil parameters studied are Coil Internal diameter, Coil Insulation Layer Thickness and Coil Dimension. Several methods of optimising the performance of WPT system have been proposed by various researchers [58-62] . One of the methods used to improve the efficiency of any WPT system

is by improving the density and strength of magnetic flux generated, which translate to higher induced current density on the receiver coil.

6.2.5.1 The Influence of Coil Internal Diameter (d_{in}) on the Magnetic Field Strength

Fig. 32 shows a relationship between the internal diameter and Magnetic field strength generated by a TRT coil configuration. As the internal diameter is increased the Magnetic field strength also increases up to about 16mm, where any further increment has a negligible effect on the Strength of the field. This is due to the fact that as the internal diameter is increased, the interaction between opposing dynamic magnetic field created by the opposing current direction in the inner coil turns is reduced. This continues up to a point where there will be little or no effect of the opposing field. Therefore, for optimal performance of this coil configuration, the internal diameter must not be less than 15mm.

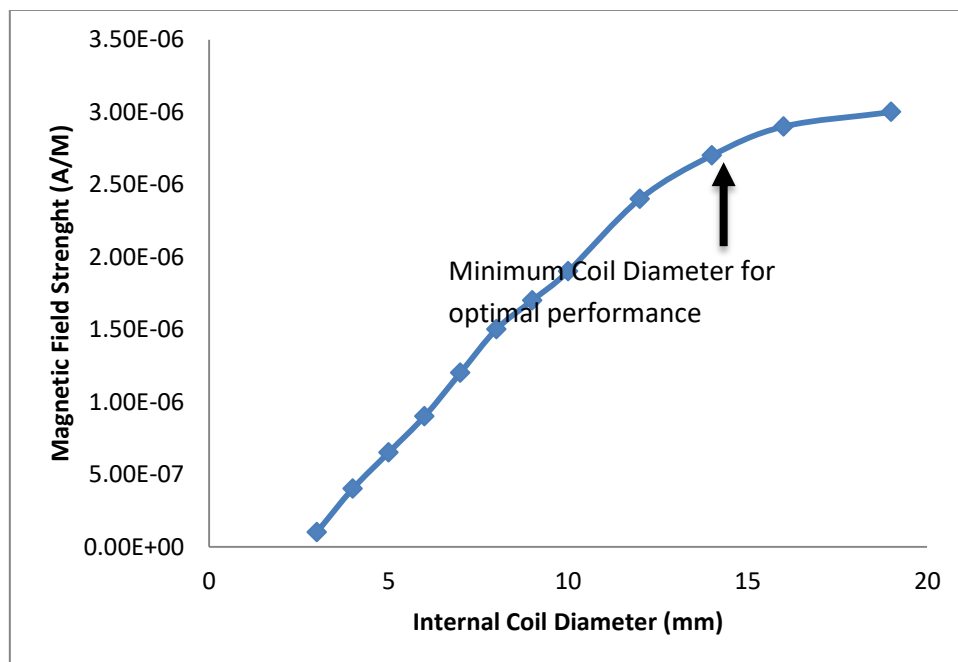


Fig. 32: The effect of Variation of coil internal diameter on the Magnetic Field Strength.

6.2.5.2 The Effect of varying the Insulation Layer Thickness (T_{in}) on the Magnetic Field Strength.

In the manufacture of the TRT coil, the copper conductor is wound tightly together for better concentration of magnetic flux. To prevent short circuiting and increase adhesion, the coils are bathed in an insulation material. The insulation material used in this simulation is Z1258 anti-rust silicone baffle paint. The performance index of Z1258 insulation material is listed in Table 5 and has the following properties [63];

- (i) Good heat resistance
- (ii) Firm adhesion
- (iii) Short drying period
- (iv) High dielectric strength of $30 \times 10^6 \text{ Vm}^{-1}$.

Fig.33 shows the result of the simulation. The result implies that, the magnetic field decreases exponentially with increasing insulation thickness. The highest value of magnetic field strength of $2.7 \times 10^{-6} \text{ A/M}$ was obtained at insulation thickness of 0.1 mm while the least value of $0.5 \times 10^{-7} \text{ A/M}$ was obtained at a thickness of 1.7 mm. Therefore, for optimal performance of the TRT coil, the insulation thickness must be between 0.1mm-0.6 mm.

Table 5: Performance index of Z1258 anti rust silicone baffle paint [63]

No	Index name	Unit	Index
1	Appearance		The film becomes bright after drying
2	Viscosity	cP	≥ 40
3	Content of solid paint, ($23 \pm 2^\circ \text{C/h}$)	(10g %)	55 ± 5
4	Drying time under room temperature	H	≤ 24
5	Dielectric strength	MVm^{-1}	≥ 30

6	Volume resistivity	$\Omega\text{-m}$	$\geq 1 \times 10^8$
7	Fineness(scraper fineness meter)	μm	≤ 45
8	Adhesion coil	grade	1~2

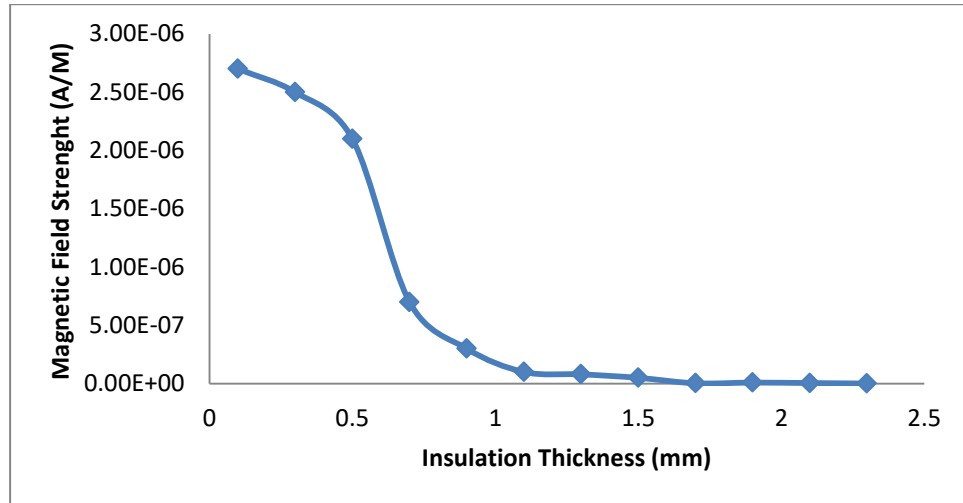


Fig. 33: The effect of variation of insulation layer thickness on the Magnetic Field Strength.

6.2.5.3 The Effect of varying the Coil Dimension on the Magnetic Field Strength

The effect of coil width on the magnetic field strength generated by Triple Race-Track (TRT) coil configuration was investigated. The Magnetic field strength was calculated at fixed current amplitude of 2A, coil thickness of t_c of 0.5mm and an excitation frequency of 50Hz. The value of K-factor which is the ratio of coil width (C_w) to coil thickness (t_c) was calculated and given in Table 6.

Different simulations were carried out by varying the coil width using the K-factor and the result obtained is shown in Figs. (34) and (35).

Table 6: Ratio of coil width to coil thickness.

Coil width (w_c)	Coil Thickness (t_c)	K-factor ($\frac{w_c}{t_c}$)
1mm	0.5mm	2
1.5mm	0.5mm	3
2mm	0.5mm	4
2.5mm	0.5mm	5
3mm	0.5mm	6
3.5mm	0.5mm	7
4mm	0.5mm	8
4.5mm	0.5mm	9
5mm	0.5mm	10

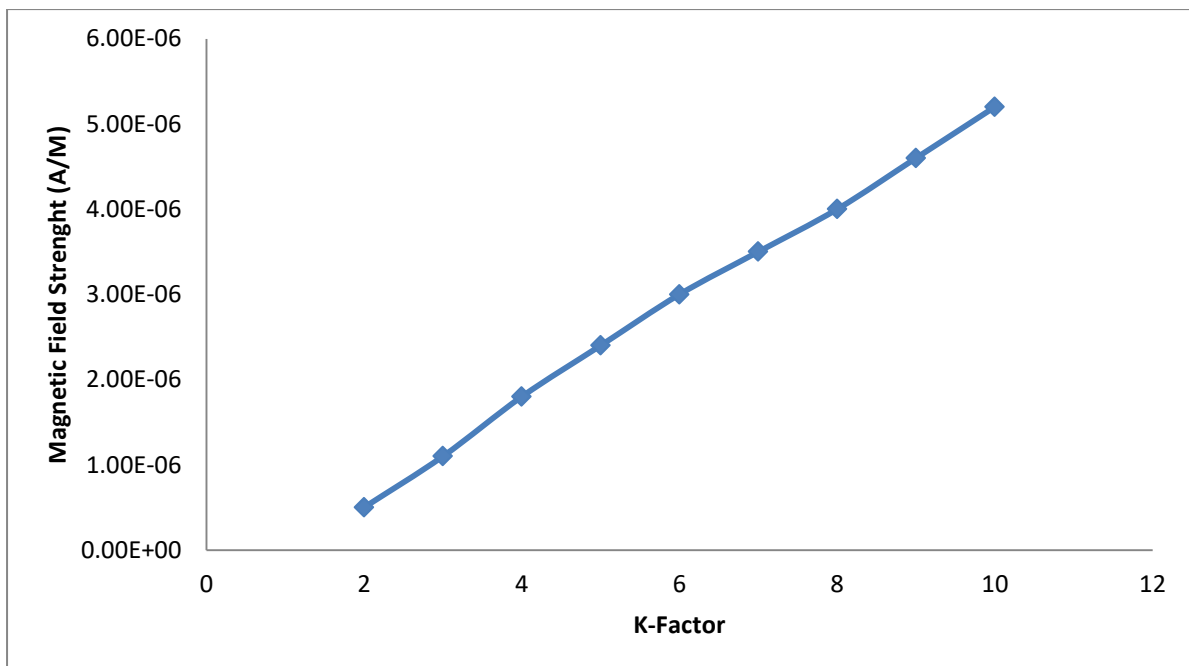


Fig.34: The effect of variation of the K-factor on the Magnetic Field Strength.

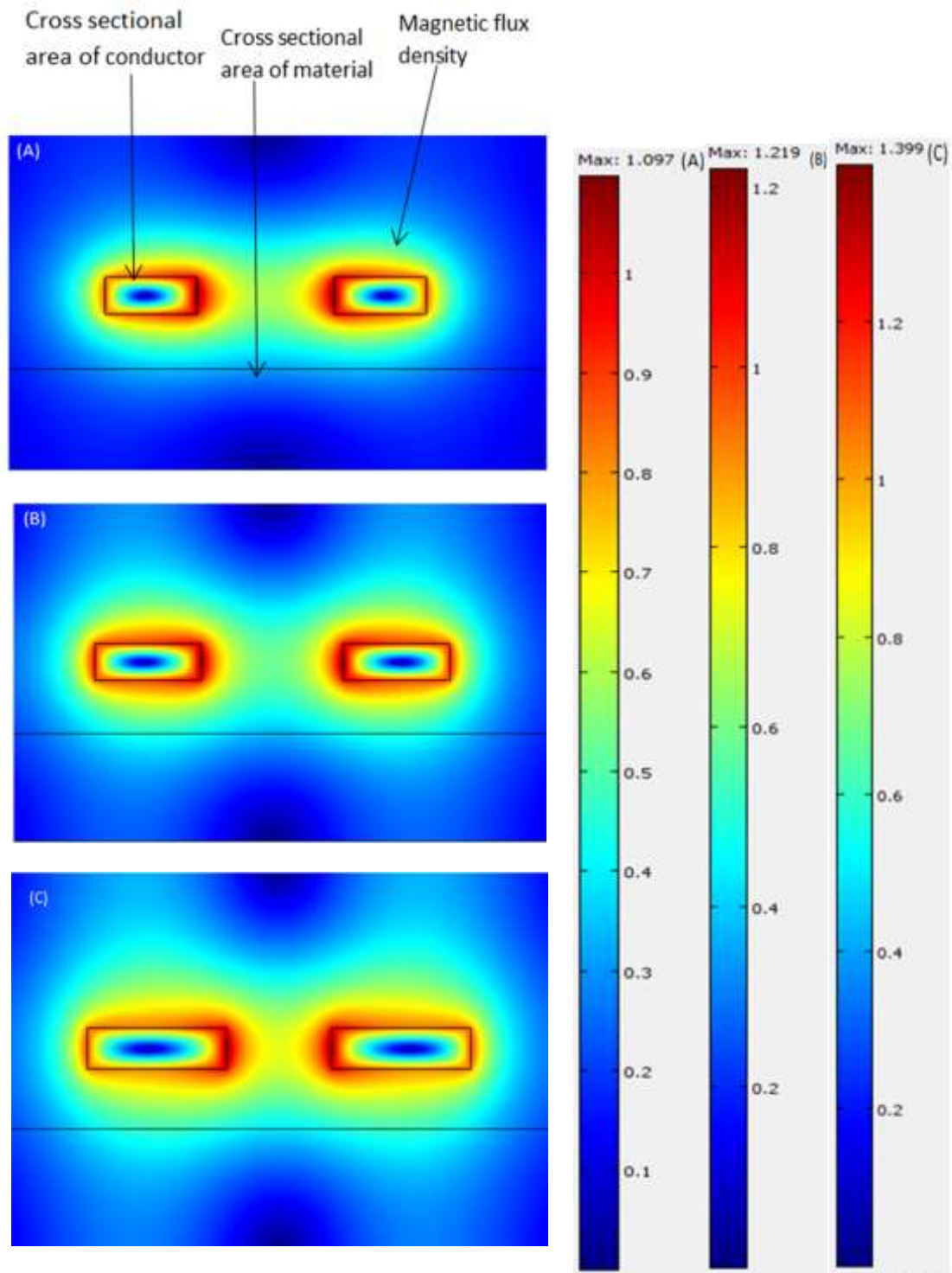


Fig.35: Cross-section of TRT Coil showing magnetic flux density at K factor (A) 2, (B) 3 and (C) 4.

The result in Fig. (34) shows that as the value of the K-factor is increased, the Magnetic Field Strength and magnetic flux density also increases. This is expected because when the coil

dimension is increased while the current density is fixed, the total current is increased and this gives rise to a stronger magnetic flux within and around the surface of the coil.

6.3 Section Summary

In designing the inductor coil and resonant circuit, the amount of voltage needed as output is considered. Also, the choice of capacitor value affected the output waveform by chipping off some of it at both peaks. Increasing the capacitor value increased the chipping off increased. The inductor on the hand produced a more amplified voltage across it when the inductance value is increased. Since the design resonant frequency is for 120KHz according to Qi standard, the choice of the inductor and capacitor value had to produce a resonant frequency of 120KHz. Several choices for capacitor and inductor values were tested in a Proteus 8 simulation and the output waveform observed for several values. It showed that an inductor value of about $12.5\mu\text{h}$ and capacitor values between 140nF and 141nF gave an acceptable waveform with a frequency of approximately 120KHz.

The quality factor was already a considered factor in inductance value choice. The acceptable value is 90 and the inductance value chosen at a high resonant frequency of 120KHz.

The coil type geometry used is a racetrack coil type because it provides greater operation region and hence magnetic field strength when compared to a circular coil. The modelling of the coil configurations done using COMSOL Multiphysics for single racetrack coil configuration (SRT), double racetrack coil configuration (DRT) or triple racetrack coil configuration (TRT) indicates that the TRT configuration has more magnetic field strength due to the interaction between the fields of each of the three racetrack coils. The TRT has the best pulse width value of 0.8 which is directly related to the occurrence of dead-zone. The TRT coil eliminated any dead-zone unlike the SRT and DRT coil configurations where dead-zone existed.

By using the TRT coil configuration and choosing a good value for the inductor coil which is $12.5\mu\text{H}$ and thereby eliminating regions of low field operation also known as dead-zone, the design allows for free alignment of the charging device since once the receiver coil aligned with any of the coils of the TRT configuration, induction happens.

7.0 RECEIVER CIRCUIT DESIGN

Designing the receiver section involves designing the receiver circuitry and the receiver coil. The specifications are according to the Wireless Power Consortium (WPC) 1.1 standard. The receiver section design consists of:

- A dual resonant circuit consisting of a secondary (receiver) coil, a series capacitance to enhance power transfer efficiency and a parallel capacitance to enable resonant detection.
- A bq51013b wireless receiver IC as a controller that interfaces between the receiver coil and the load which is the mobile device to be charged.

7.1 Receiver Circuitry

A receiver or secondary coil is inductively coupled to the transmitter or primary coil. The receiver coil and its base station or circuitry makes up the receiver section or system. Basically the receiver section comprises of the resonant circuit which includes the coil, a AC-DC rectifier, a filtering circuit and a voltage regulator where necessary as shown in fig (36).

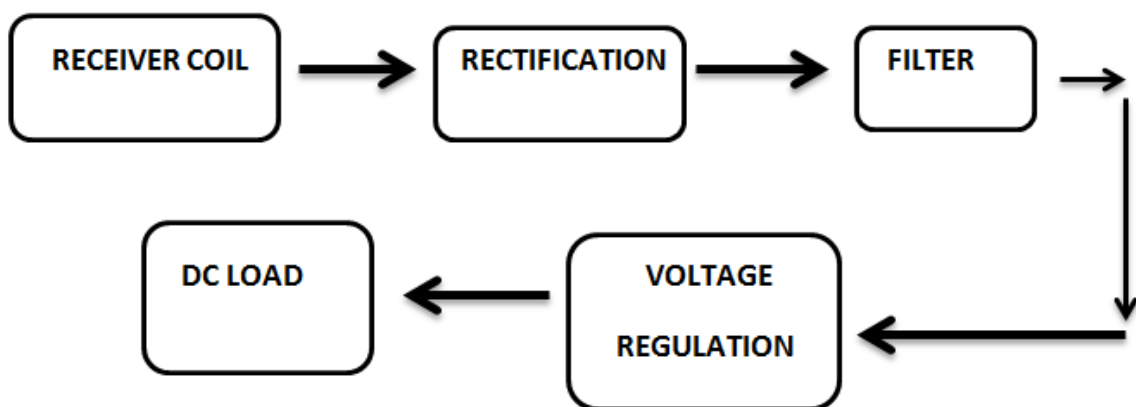


Fig 36: Block Diagram of the Receiver Circuit Design

The bq51013b is a charging IC that can be used in several applications but it is configured as a wireless power receiver and power supply for system loads. The bq51013b provides the receiver with AC-to-DC conversion and regulation while integrating the digital control required complying with the Wireless Power Consortium (WPC) Qi communication protocol. This IC is capable of delivering at the output 5 watts of power at 1000mA. This IC configuration is shown in the fig. 37 below.

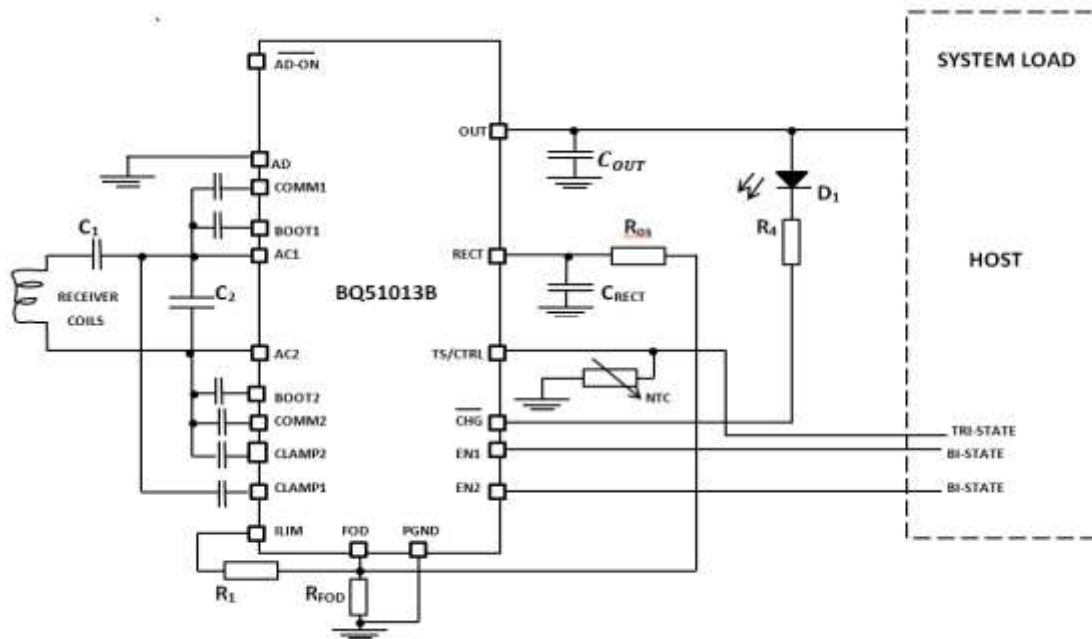


Fig. 37: BQ51013B used as a wireless power receiver and power supply system

When the above system in figure (37) is placed on the charging pad, the coil is coupled inductively to the magnetic flux generated by the coil in the charging pad which consequently induces a voltage in the receiver coil. When this voltage is induced through the receiver coil, it is fed to the RECT pin through a synchronous rectifier and then filtered using the capacitor C3. Hence, the bq51013b provides the functions of a bridge rectifier and a filter.

The bq51013b uses several capacitors to enhance its performance. These are the boot capacitors (C_{BOOT1} , C_{BOOT2}), clamp capacitors (C_{CLAMP1} , C_{CLAMP2}), communication capacitors

(C_{COMM1}, C_{COMM2}). The boot capacitors are used to make the internal rectifier FETs. The capacitors are chosen to be 10nF with a 25V. The clamp capacitors are used in the clamping process to protect against over-voltage. The clamp capacitors are connected from AC1 to CLAMP1 and then from AC2 to CLAMP2. The clamp capacitors are chosen to be 0.47 μ F and a rating of 25 V. The communication capacitors are used to enhance communication between the receiver and the transmitter and their values are chosen to be 22 μ F.

The current limit and foreign object detection functions are related. The sum $R_1 + R_{FOD}$ sets the current limit. Hence,

$$R_{ILIM} = R_1 + R_{FOD} \quad (34)$$

Where R_{ILIM} is the current limiting resistance value, R_{FOD} is the resistance connected across the foreign object detection pin, and R_1 is connected across the I_{LIM} pin. Under normal conditions the maximum current I_{MAX} is 1 amp and to calculate R_{ILIM} , we use the equation,

$$I_{LIM} = 1.2 \times I_{MAX} = \frac{K_{LIM}}{R_{ILIM}} \quad (35)$$

Where K_{LIM} the current programming is factor for hardware protection and is typically 314 A Ω .

Hence,

$$I_{LIM} = 1.2 \times 1 = 1.2A$$

Therefore,

$$1.2A = \frac{K_{LIM}}{R_{ILIM}}$$

$$1.2A = \frac{314}{R_{ILIM}}$$

$$R_{ILIM} \cong 262\Omega$$

Selecting R_{FOD} to be 166Ω ,

$$R_1 = 262 - 166 = 66\Omega$$

The RECT capacitance smoothens the AC to DC conversion to prevent minor current transients from passing to OUT pin. The OUT capacitance is used to reduce any ripple from minor load transients. Their values are chosen as $10\mu\text{F}$ each.

7.2 Receiver Coil Design

The receiver coil is connected to the AC1 and AC2 ports of the bq51013b charging IC through two resonant capacitors, C_1 and C_2 . The first capacitor $C_1(C_s)$ which is a series capacitance is used to enhance power transfer efficiency and the shunt capacitance $C_2(C_d)$ enables a resonant detection method. The combination of the receiver coil and the capacitors forms a dual resonant circuit as depicted in fig (38).

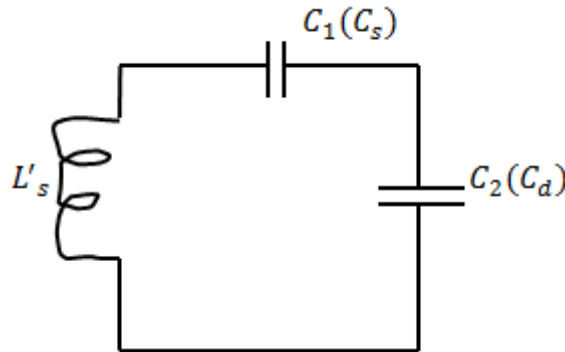


Fig 38: schematic of a Dual resonant circuit

The dual resonant circuits have the following resonant frequencies,

$$f_s = \frac{1}{2\pi\sqrt{(L'_s \times C_s)}} = 100 \text{ kHz } +5/-10\% \quad (36)$$

$$f_d = \frac{1}{2\pi \sqrt{L_s \times (\frac{1}{C_s} + \frac{1}{C_d})^{-1}}} = 1 \text{ MHz} \pm 10\% \quad (37)$$

Where L'_s is the self-inductance of the secondary coil in the presence of the transmitter that is the mutual inductance, L_s is the inductance of the secondary coil in free space, f_s is the secondary resonance frequency while f_d is the resonance frequency when the series when the shunt capacitor is taken into account.

The value of the capacitors are found using the following equations,

$$C_s = [(f_s \times 2\pi)^2 \times L'_s]^{-1} \quad (38)$$

$$C_d = [((f_d \times 2\pi)^2 \times L_s) - \frac{1}{C_s}]^{-1} \quad (39)$$

The value of C_s is chosen before calculating the value of C_d . The value of the inductances L_s and L'_s of the secondary coil depends on the coil chosen. The quality factor Q which is calculated with the formula given below must be greater than 77 [1],

$$Q_s = \frac{2\pi \times f_d \times L_s}{R} \quad (40)$$

Where R is the DC resistance of the receiver coil and is a few hundred milli-ohms.

For a typical material which is WPC compliant and made by TDX Corporation has a L_s value of $13.3\mu\text{H}$ and a L'_s value of $18.8\mu\text{H}$ and a DC resistance of 0.2Ω at 25°C . Therefore, the values of C_s and C_d can be calculated.

Let $f_s = 100\text{KHz}$, $f_d = 1\text{MHz}$, $L'_s = 18.8\mu\text{H}$ and $L_s = 13.3\mu\text{H}$,

$$C_s = [(f_s \times 2\pi)^2 \times L'_s]^{-1}$$

$$C_s = 134.7\text{nF}$$

$$C_d = [((f_d \times 2\pi)^2 \times L_s) - \frac{1}{C_s}]^{-1}$$

$$C_d = 1.93 \text{ nF}$$

Calculating the quality factor by using the formula in equation (38) above, Q will be 417.83.

This value is high enough and desirable indicating compliance to WPC standards.

7.2.1 Calculation of Mutual Inductance

Mutual inductance is as a result of the interaction of an inductor coil's magnetic field on another coil while also inducing a voltage in the coil. In an inductor coil an emf (electromotive force) is induced as a result of the changing magnetic field around its turns. Self-inductance is when this emf is induced in the same circuit in which the current is changing. But when this emf is induced in a nearby coil, within the same magnetic field, this induced emf is said to be inductive or by mutual induction (M). Mutual inductance is a property of two or more coils that are magnetically linked together by a common magnetic flux.

The strength of induced magnetic flux induced into an adjacent coil or coil coupled magnetically with the inducing coil depends largely on the spacing between the two coils. As the spacing between the two coils increases the strength of the flux weakens. That is to say the mutual inductance depends largely on the coupling coefficient k . The formula to calculate mutual inductance for two coils is given below from [64],

$$M = 2 \times k \times \sqrt{L_1 L_2} \quad (41)$$

Where L_1 the self-inductance of the transmitter coil is $12.5\mu H$ and L_2 is the self-inductance of the secondary coil in the presence of the transmitter coil, $18.8\mu H$.

$$M = 2 \times k \times \sqrt{12.5 \times 18.8}$$

$$M = 2 \times k \times \sqrt{235}$$

$$M = 2 \times k \times \sqrt{L_1 L_2}$$

$$M \cong 30.66k$$

The value of k is typically between 0.01 and 0.5 for a resonant inductive coupled WPT system, so the value of M is computed as k varies and shown in the table 7 below.

Table 7: Mutual inductance against coupling coefficient

Coupling Coefficient (k)	Mutual Inductance (M)
0.01	0.3066 μH
0.05	1.5330 μH
0.10	3.0660 μH
0.14	4.2924 μH
0.18	5.5188 μH
0.2	6.1320 μH
0.25	7.6650 μH
0.30	9.1980 μH
0.4	12.2640 μH
0.5	15.3300 μH

Table (7) above and figure (39) below shows that with less spacing between the coils, the coupling coefficient is increased and consequentially, the mutual inductance is increased. The maximum value of the inductance is 30.66 μH but this is obtainable in tightly coupled systems like a transformer. The mutual inductance value is an important value when calculating the output current from the transmitter to the receiver.

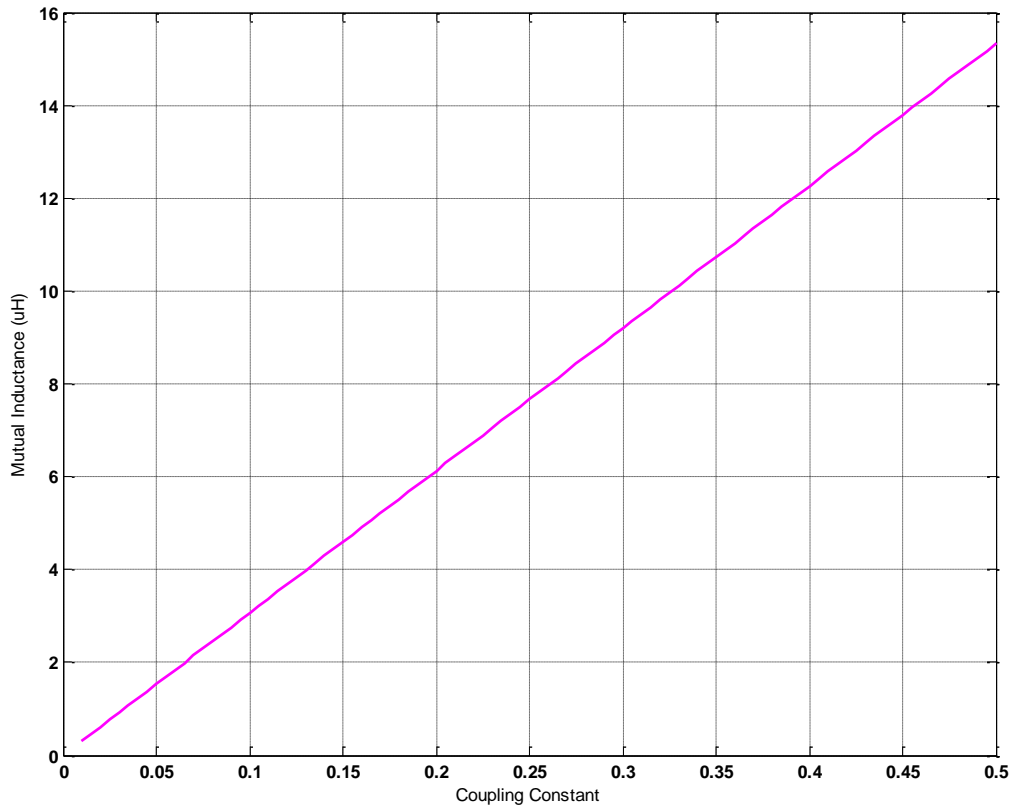


Fig. 39: Plot of Mutual Inductance against the coupling coefficient

The plot in figure (39) above shows that the mutual inductance varies linearly with the coupling coefficient or constant. For better mutual inductance, the coupling coefficient has to be higher and to achieve that, the distance or spacing between the two coils to be coupled should be very small.

7.2.2 Inductance vs Excitation Current and Number of Coil Turns

The inductance of the inductor coil depends on several parameters like the coil size or geometry, the number of coil turns, the excitation current, and permeability of coil material. Inductor stores energy in its magnetic field just like the capacitor stores energy in the electric field between its plates. This energy can be found by integrating the magnetic energy density,

$$u_m = \frac{B^2}{2\mu} \tag{42}$$

over an appropriate volume. To understand the effect of these parameters on the inductance, the coil is assumed to be a cylindrical solenoid with a constant magnetic field given by $B = \mu_0 nI$ everywhere within the solenoid. Thus the energy stored in a solenoid is given as,

$$W = u_m \times V \quad (43)$$

$$W = \frac{B^2}{2\mu} \times Al \quad (44)$$

$$W = \frac{(\mu_0 nI)^2 \times Al}{2\mu_0} \quad (45)$$

$$W = \frac{1}{2}(\mu_0 n^2 Al)I^2 \quad (46)$$

But,

$$L = \mu_0 \left(\frac{N}{l}\right)^2 Al = \mu_0 n^2 Al = \mu_0 n^2 V \quad (47)$$

Therefore,

$$W = \frac{1}{2}LI^2 \quad (48)$$

where, W is the magnetic energy stored in the field, V is the volume of the solenoid which is equal to the product Al , A is the cross-sectional area of the solenoid, μ_0 is the permeability in free space, $n = \frac{N}{l}$ is the turns per unit length of the coil, N is the number of coil turns, I is the excitation current and L is the self-inductance of the coil.

From equation (48) above,

$$L = \frac{2W}{I^2} \quad (49)$$

This equation shows that the self-inductance of the coil varies inversely with the square of the excitation current. Hence, an increase in the excitation means a decrease in the inductance of the coil if the magnetic field is non-varying. Mathematically,

$$L \propto \frac{1}{I^2} \quad (50)$$

$$L = \frac{K}{I^2} \quad (51)$$

where K represents a constant of proportionality and from calculations for transmitter coil design $L = 12.5\mu H$ and the excitation current $I = 2$ Amps,

$$K = 12.5 \times 10^{-6} \times 2^2$$

$$K = 0.00005$$

The effect of varying the excitation current can be seen from the plot in figure (40) below. From equation (51), increase in excitation current causes an increase in the magnetic energy within the magnetic field of the coil. But the increased excitation current brings about a decrease in the inductance at the same value of magnetic field energy.

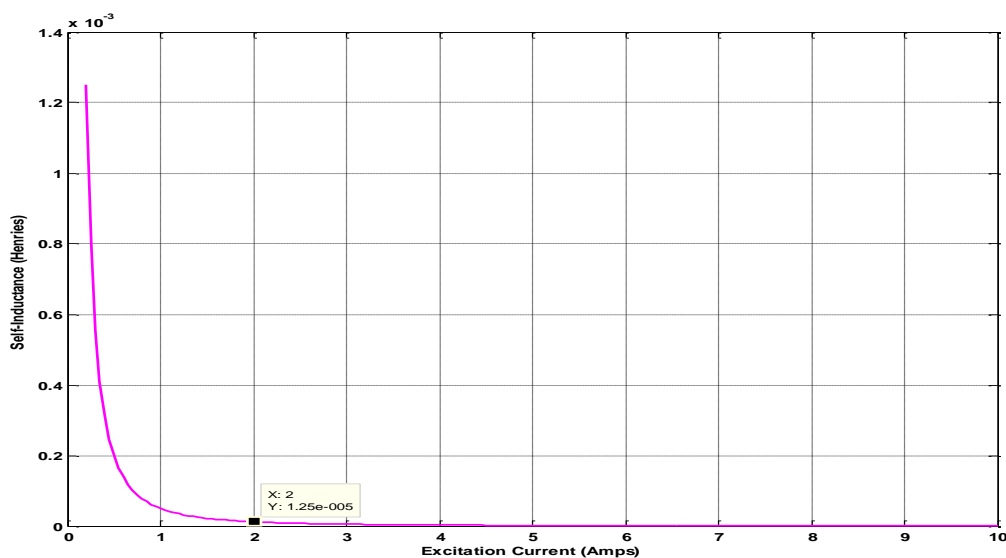


Fig 40: Plot of the Self-inductance against the excitation current

From the plot in figure (40) above it can be seen that while the excitation is increased, the self-inductance decreases from left to right and as the excitation current is increased further beyond 4 amps, the inductance value began to converge to zero. At 10 amps excitation current, the inductance value is now approximately zero. The inductance of the coil used is indicated on the plot as $12.5\mu\text{H}$ at the value of 2 amps.

The relationship between the inductance of the coil and the number of turns per length of coil is directly proportional. The more length of coil means more turns and a larger inductance value.

From equation (47) above,

$$L = \mu_o n^2 Al = \mu_o n^2 V$$

It can be seen that the permeability μ_o and cross-sectional area A of the coil are constant while the value of L depends on the value of n which is the turns per unit length. For a coil length l of 200mm and cross-sectional area $A = \pi(r_{ext}^2 - r_{int}^2)$

Where r_{ext} is 26 mm and r_{int} is 14mm, $A = 4525\text{mm}^2$

$$L = \mu_o n^2 Al = \mu_o \frac{N^2}{l} A \quad (52)$$

Substituting for μ_o , A and l ,

$$L = 0.000028N^2$$

Clearly,

$$L \propto N^2 \quad (53)$$

which also means that,

$$L \propto n^2 \quad (54)$$

The number of turns or turns per unit length varies directly with coil's inductance. As either quantity increases, so does the coil's inductance. Two coils of the length and material but different number of coils, their inductance will vary. The downside of this is that during continuous conduction mode, the dc resistance increases too leading to resistive losses.

7.3 Section Summary

The receiver module is directly coupled to the receiver coil. The receiver circuit basic process includes:

1. to received voltage by induction through its receiver coil when aligned properly with the transmitter coil.
2. Rectify and filter the induced voltage since it is AC and the required output is DC
3. Regulate the output voltage to a desired level. This regulation is a linear regulation.

The use of a charging IC, the bq51013b handled the rectification and regulation aspects of the receiver module or section. It also incorporates a control loop that ensures that the output voltage remains at a minimum of 4.93 volts and a maximum of 5.06V provided the induced voltage is within the range of -0.8 volts to 20 volts as stated in the datasheet. During the design of the transmitter coil, the voltage in the inductor coil is about 18 volts. This value is within the range for input into the bq51013b IC.

In designing the receiver coil, its characteristics like number of turns, coil geometry, spacing between turns etc., an operating condition like the excitation current to be used also plays a role and affects the inductance of the coil.

The number of turns or turns per unit length of the inductor has a direct proportional relationship with the coil inductance. As stated and shown in section 2.1, the larger the number of coil turns, the greater the inductance value of the coil. The analysis in this section

proved that. The only consequence being that the resistive losses increases with the coil turns and coil inductance value.

The excitation current on the other hand varies inversely with the coil inductance. The excitation current, the coil inductance and the magnetic field strength are related by an equation. Increasing either the coil inductance or its excitation current increases the magnetic field strength. The analysis and plot assumed a constant magnetic field strength and the relationship between the excitation current and coil inductance explored. And it is seen that increasing the excitation current reduces the self-inductance of the coil though not linearly and at higher values of excitation current beyond the required point of operation, the inductance value begins to converge towards zero.

The mutual inductance between the receiver and transmitter coil helps determine the efficiency of power transferred from the transmitter to the receiver. Besides being dependent on the values of the self-inductances of the receiver and transmitter coil, it also depends on the coupling coefficient or the distance between the two coils. The smaller the distance between the two coils, the stronger the mutual inductance value and consequentially, the induction from the primary (transmitter) coil to the secondary (receiver) coil.

8.0 EVALUATION OF OVERALL SYSTEM

The goal of the WPT system is to efficiently transfer power from the primary coil (transmitter) to the secondary coil (receiver) for charging of small CPEs for example mobile phones. The efficiency of the system depends on several factors like number of coil turns, coupling coefficient, quality factor of the coils and system etc.

8.1 Power Transfer Efficiency (PTE)

The amount of power transferred in a WPT system depends on a couple of factors like, the coupling coefficient, the quality factor of the coils, the lift off distance and the frequency of operation. The ratio of the power transferred to the power generated is the efficiency of the system.

For increased efficiency of the system, the frequency of operation of both resonant circuits should be high and matched. Hence, the resonant frequency values are in the few kilohertz region.

From calculations made earlier it shows that the quality factor value depends on the frequency of resonance, the dc resistance of the coil and the coil inductance value. The dc resistance is in few hundred milli-ohms and constant while the coil inductance is also not varying. This implies that the quality factor depends largely on resonant frequency and as such it needs to be very high for higher quality factor value. A high quality factor, improves the efficiency of the system.

The coupling coefficient k and the lift off distance are related. The coupling coefficient indicates how tightly coupled the two coils are. The value of k goes from unity for strongly coupled systems like a transformer to 0.5 for loosely coupled systems like the wireless power transfer system which is inductively coupled. The lift-off distance is the distance between the transmitter coil and the receiver coil. Increasing the distance between the two coils reduces

the value of k . Consequently, as the coupling coefficient reduces so does the power transfer efficiency of the system.

Power transmission efficiency of a WPT system is the ratio of the output power to the input and is largely dependent on the values of k and Q which must be as high as possible. The efficiency is calculated from equation (55) in [22, 52],

$$\eta_{max} \approx 1 - \frac{2}{kQ} \quad (55)$$

For better accuracy when the WPT topology of transmission is either series or parallel, the maximum efficiency value can be calculated using the equation (56) from [22, 52],

$$\eta_{max} = \frac{(kQ)^2}{(1 + \sqrt{1 + (kQ)^2})^2} \quad (56)$$

where the quality factor Q is the geometric average of the quality factors of the two coils.

This can be calculated from the formula below [22],

$$Q = \sqrt{Q_p Q_s} \quad (57)$$

Where Q_p is the quality factor of the primary coil which was calculated as 145.06. Q_s is the quality factor of the secondary coil which was calculated as 417.83. Hence,

$$\begin{aligned} Q &= \sqrt{145.06 \times 417.83} \\ &= \sqrt{60610.4198} \\ Q &\cong 246.192 \end{aligned}$$

The coupling coefficient k in inductive wireless power transfer systems is small and ranges from 0.01 – 0.5 [22]. A high Q factor is important in maintaining high efficiency when the coupling coefficient reduces due to coil misalignment or increased distance between the

transmitter coil and receiver coil [1, 41]. For a value of about 0.025 for k , the power transfer efficiency value is approximately 70% when calculated using equation (56) above. At 0.5 value for k , the efficiency of the system is 98%. It can be seen that the coupling coefficient plays an important part on the efficiency of transfer for the WPT system. Factors like coil size and geometry also affect the efficiency of transfer.

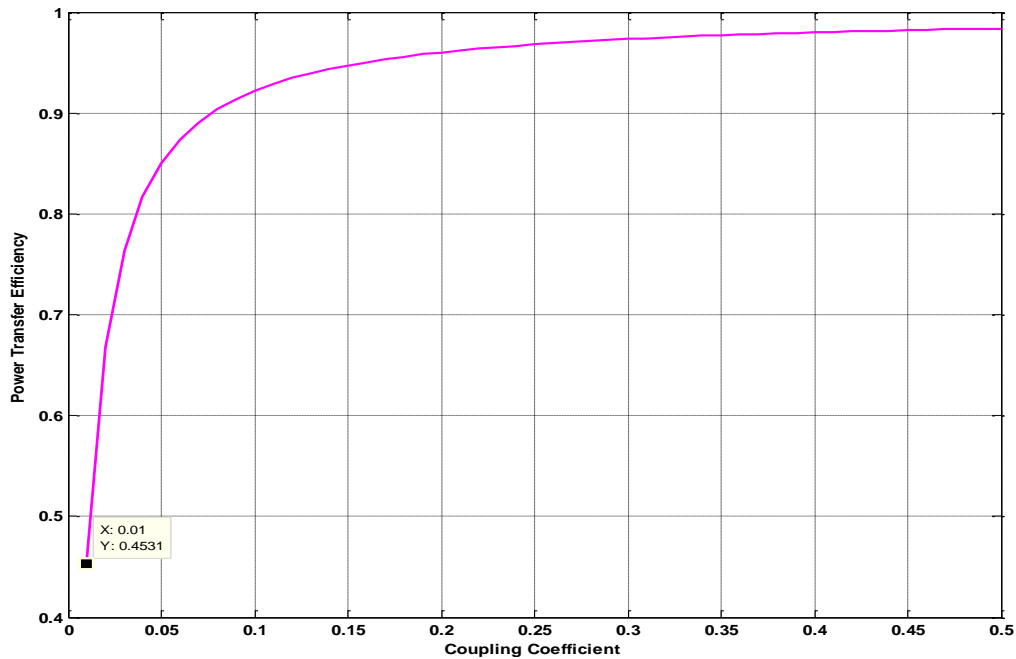


Fig 41: Power Transfer Efficiency plotted against the Coupling Coefficient

The relationship between the power transfer efficiency and the coupling constant is shown in fig.41. As the coupling coefficient the efficiency of the system at a given value of Q also increases. Beyond 0.25 for value of coupling coefficient, the efficiency value starts to converge. For higher efficiency values, the coupling coefficient must be increased.

8.2 Power Transfer Calculations

The WPT system designed in this project is modelled as simple two coil system with one transmitter coil and one receiver coil. The output voltage and the current of the transmitter coil have been calculated earlier in section 4.0. The mutual inductance of the two coils have

also been calculated for varying values of coupling coefficient and for simplicity the maximum possible value of coupling coefficient is used and this resulted in a mutual inductance value of $15.33\mu H$ (see section 7.2). To calculate the voltage and current fed induced in the transmitter coil, the system is simplified as shown in Fig 42.

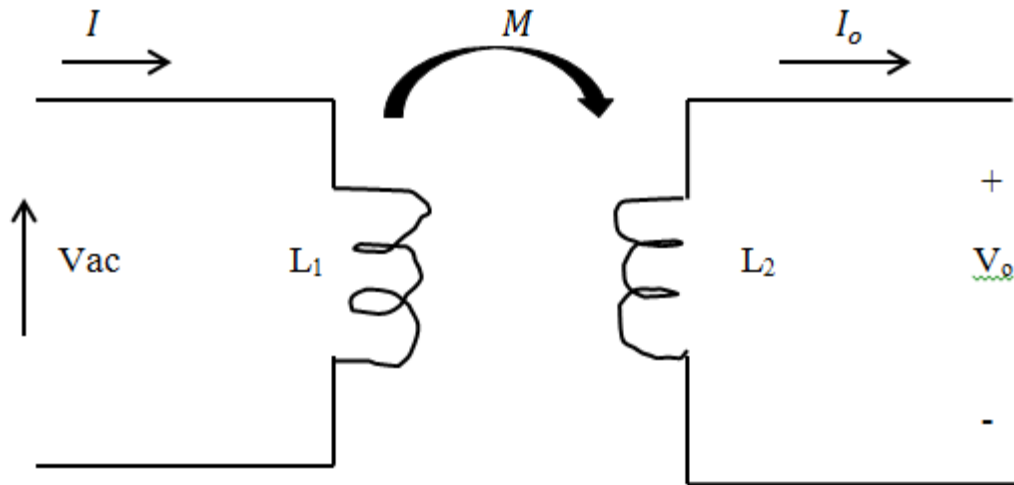


Fig 42: Simplified Inductive WPT circuit diagram

The equations for calculating the voltage and current induced in the receiver coil are given by [2],

$$V_o = j\omega MI \quad (58)$$

$$M = V_o / \omega I \quad (59)$$

$$I_o = MI / L_2 \quad (60)$$

Where M (mutual inductance) = $15.33\mu H$, I (current in transmitter coil) = 2 amps and L_2 (secondary coil inductance) = $18.8\mu H$. I_o current induced in the receiver coil can be calculated as,

$$I_o = \frac{15.33 \times 2}{18.8}$$

$$I_o = 1.63 \text{ amps}$$

The value 1.63 amps is the absolute maximum current that can be induced in the receiver coil.

The maximum power that can be delivered to the receiver when you find the product of equations (58) and (60) is then,

$$P_{output,max} = \frac{\omega I^2 M^2}{L_2} \quad (61)$$

$$P_{output,max} = \frac{2 \times \pi \times 120 \times 1000 \times 2^2 \times (15.33 \times 10^{-6})^2}{18.8 \times 10^{-6}}$$

$$P_{output,max} = 37.716 \text{ W}$$

Therefore, the maximum voltage that can be induced in the receiver is calculated from equation (62),

$$V_{o,max} = \frac{P_{output,max}}{I_o} \quad (62)$$

$$V_{o,max} = \frac{37.716}{1.63}$$

$$V_{o,max} \cong 23.14 \text{ volts}$$

The maximum input voltage specified in the datasheet of the bq51013b IC is 20 volts. Factoring in tolerance, temperature conditions and voltage drop across the inductor, this value of 23 volts is acceptable.

Based on the calculated output voltage and current, the maximum induced voltage from the transmitter would be,

$$V_{tx} = V_{o,max} \div 0.9839 \quad (63)$$

Where the maximum efficiency at 0.5 coupling constant is 98.39%,

$$V_{tx} = 23.14 \div 0.9839$$

$$V_{tx} \cong 22.77 \text{ volts}$$

From earlier calculations, the calculated voltage across the inductor coil was approximately 19 volts. This value is within the acceptable range for the required input voltage for the bq51013b receiver IC as stated in the datasheet.

8.3 Maximum Coverage Distance

The maximum coverage distance is the maximum spacing allowable between the transmitter and receiver coil for efficient transfer of power. That is to say the maximum lift-off distance beyond which the power transfer efficiency drops to less than 50%. From the plot in figure (43), it is seen that between 0.01 and 0.02 values of coupling coefficient, the efficiency of the system moves from 45% to 66.8%. This indicates that the value of k for 50% efficiency lies between these two values. By interpolation, the value of k required for approximately 50% efficiency is 0.0115. Then applying equation (64) obtained from [64],

$$k = \frac{N^2}{(AX^3 + BX^2 + CX + D) \times (1.67N^2 - 5.84N + 65) \times 0.64} \quad (64)$$

Where the values of A, B, C, D are inductor turns and gotten from [64] are 0.184, -0.525, 1.038, 1.001 respectively. N is the number of turns for both the primary and secondary coil and X is the distance between the two coils and our variable of interest.

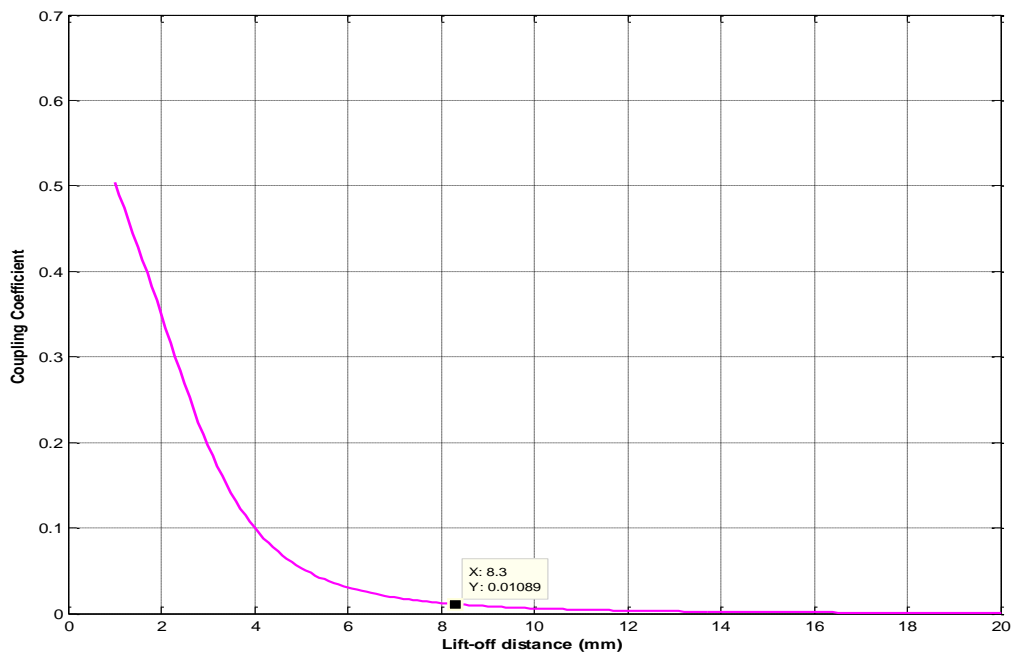


Fig 43: Plot of coupling coefficient against the lift-off distance

The plot is generated for various values of X, from 1mm to 20mm at 9 turns of coil for both primary and secondary coils. At 8.1mm of lift-off, the coupling coefficient is 0.01178 and at 8.3 mm, the coupling coefficient is 0.01089. By interpolating between the two values, the lift-off distance that will give a coupling coefficient of 0.0115 is 8.15mm. If the lift-off distance is increased further, the efficiency of transfer drops below 50% and 20mm of lift-off distance, the coupling coefficient is approximately zero; barely any current would be induced at this point. This is validated by the experimental testing.

8.4 CHARGING TIME

The time taken to completely charge a phone's battery is dependent on the battery capacity of the phone. And since, various phone models exist from Android to iOS, so will their charge time vary.

For a wired charger, the time taken to fully charge a battery from zero percent level to 100 percent level depends on the output of the charger in watts (i.e. volts x amperes) and the battery's wattage hour (volts x amperes hour). Mathematically,

$$\text{Charging time (hours)} = \frac{\text{Battery Wattage Hour (Wh)}}{\text{Charger Power Output (W)}} \quad (65)$$

But practically, there is a 40% loss in power when charging a phone and this has to be factored in the calculation above using a factor of 1.4 hence,

$$\text{Charging time (hours)} = \frac{1.4 \times \text{Battery Wattage Hour (Wh)}}{\text{Charger Power Output (W)}} \quad (66)$$

Battery wattage-hour is a product of the battery's nominal voltage and the capacity of the battery in mAh (milli-amperes hours). Milli-amperes hour indicates how long a particular battery can power a phone depending on the consumption. For instance, a 5000mAh battery would power a phone consuming 100mA for 50 hours. This depends of intensity of usage for the said device as activities like internet surfing draws more power than calls and texting. Rechargeable phone batteries are lithium based and they have a nominal voltage between 3.7V and 4.2 V at full charge. Therefore, using a nominal voltage of 3.8 volts for a battery of 5000mAh, its wattage-hour (Wh) would be,

$$\text{Wattage - hour} = \frac{1.4 \times 3.8 \times 5000}{1000}$$

$$\text{Wattage - hour} = 26.6 \text{ Wh}$$

The charger output power is already pre-designed usually at 5V, 1A or 5V, 2A. The latter is obtainable for chargers for most Android and iOS phones providing power ranging from 7.5W to 10W. Faster chargers providing 20 W exist like the turbo chargers.

If we use a wired charger with a 10 W output to charge our 5000mAh battery, the charging time would be,

$$\text{Charge time} = \frac{26.6}{10}$$

$$\text{Charge time} = 2.66 \text{ hours}$$

That is approximately three hours theoretically. Practically beyond 80-90% full charge, phones go into the trickle charging mode [65, 66]. The trickle charging mode implies a drop in power and consequentially, the last 10-20% takes more than the estimated time to charge. Therefore, the charge time calculations would account for 85% of charging from 1%.

From calculations and plots during design of the WPT system, the transmitter output is 5V, 2A and the lift-off is estimated to be 6mm due to the casing and covering as well as allowance for the phone's back cover. This 6mm lift-off implies a coupling coefficient of 0.024 which means that the power transfer efficiency of the system is 71.40% using equation 56. Using this WPT, the charge time for a 3.8V, 5000mAh battery is,

$$\text{Charge time} = \frac{26.6}{10 \times 0.7140}$$

$$\text{Charge time} = 3.72 \text{ hours}$$

This value which is slightly higher than that obtained using a wired charger at the same power output. This is one of the trade-offs using a wireless charging since the coupling is between 15 and 50%, energy transfer takes more time. The highest efficiency possible with this WPT system is 98.39% and the charge time at this efficiency is 2.70 hours which is approximately the same as what is obtainable with the wired charger.

The table below presents several phone models and their charge time based on the WPT system. The nominal voltage for each battery being 3.8 Volts.

Table 8: Comparison of charge time of some phone models

Phone Model	Battery Capacity (Ah)	Charge Time (Calculated, hours)	Charge Time (Actual, hours)
Gionee Marathon M5 Lite	4	2.98	3.20
Iphone 8	2.691	2.01	2.20
Iphone X	2.716	2.02	2.25
Iphone XR	2.942	2.19	2.35
Iphone 11	3.110	2.32	2.50
Samsung Galaxy S9	3	2.24	2.40
Samsung Galaxy S10	3.4	2.53	2.65
Samsung Galaxy S10+	4.1	3.06	3.35
Samsung Galaxy S10e	3.1	2.31	2.40
Tecno Camon X Pro	4	2.98	3.15

An Iphone 7.5W wireless charger takes approximately 3.2 hours to charge a 3110mAh battery [67] which implies about a 69% efficiency in terms of power transfer. Comparing this with the transfer efficiency of this WPT system at 71%, shows an improvement of 2% thereby making this system more efficient.

From the table (8) above and figure 44 below, it is evident that the charge time is highly dependent on the battery capacity. Also the phone brand specifications affect the charge time as shown by the Tecno Camon X pro and Gionee Marathon M5 Lite, both with capacity of 400mAh but different charging time at 3.15 hours and 3.20 hours respectively.

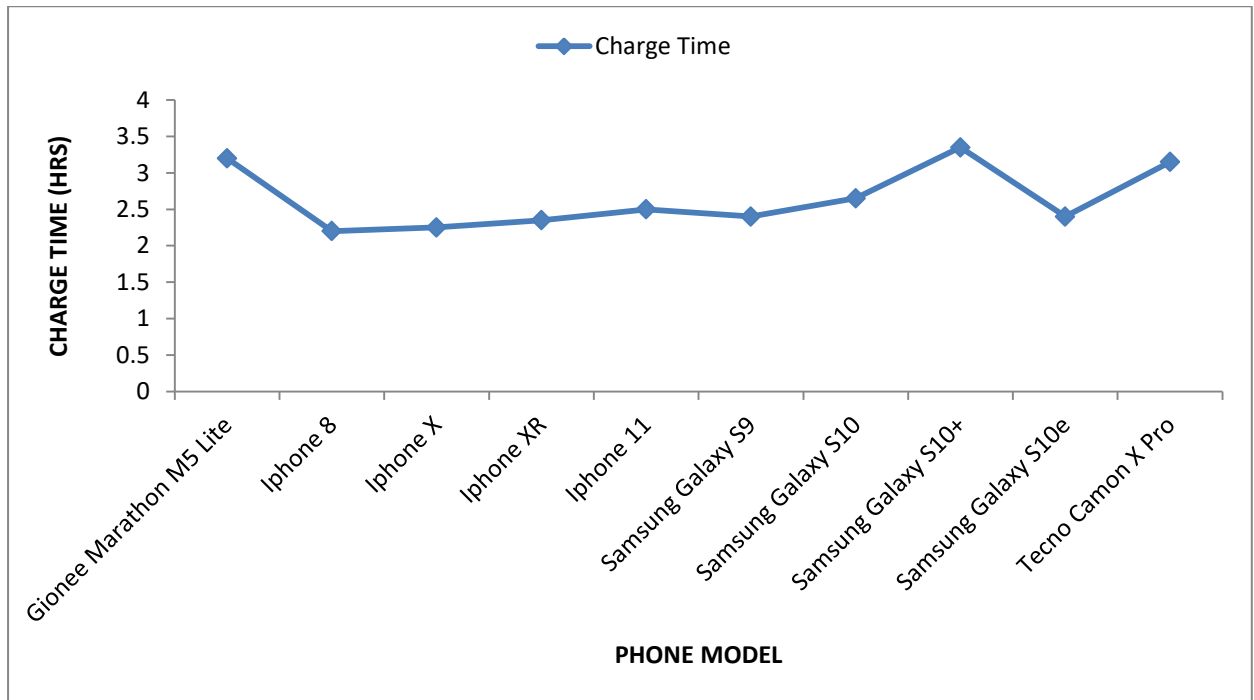


Fig. 44: Comparison of charge time for some models using the WPT system

8.5 CASING MATERIAL

Choosing a proper covering or casing for the transmitter coils is important and as such magnetic properties of some materials were considered. The materials selected were compared based of their relative magnetic permeability. Permeability indicates the ability of a material to support the formation of magnetic fields within the material and is measured in H/m (henries/meter). Relative permeability μ_r is the ratio of the permeability of a specific medium or material μ to the permeability of free space μ_o .

$$\mu_r = \frac{\mu}{\mu_o} \quad (67)$$

The most desirable materials are the materials with a relative magnetic permeability closer to 1.0 which is to say that the magnetic response of the material is the same as free space or vacuum. The possible media are air, aluminum, austenitic stainless steel, bismuth, copper, neodymium magnet, platinum, Teflon, wood, PMMA (polymethyl-methacrylate, acrylic or plexiglass). A comparison of the magnetic properties of some of the materials is in table 9 below.

Table 9: Comparison of magnetic properties of some materials

Medium	Permeability, μ (H/m)	Relative permeability, $\frac{\mu}{\mu_0}$
Air	$1.25663753 \times 10^{-6}$	1.00000037
Aluminum	1.256665×10^{-6}	1.000022
Austenitic Stainless Steel	1.260×10^{-6}	1.003
Bismuth	1.25643×10^{-6}	0.999834
Copper	1.256629×10^{-6}	0.999994
Neodymium Magnet	1.32×10^{-6}	1.05
Platinum	1.25697×10^{-6}	1.000265
Teflon	1.2567×10^{-6}	1
Wood	$1.25663760 \times 10^{-6}$	1.00000043
Acrylic (PMMA)	1.256865×10^{-6}	0.999893

Acrylic is readily available in the market and the surface provides the WPT system with a beautiful finish. The value of its relative magnetic permeability is less than one as well as it having a volume resistivity of $10^{13} \Omega m$. This implies that while acting as a “free space” to the

induced magnetic field, it is highly resistive to current flow within it. Thus acrylic is chosen as the most suitable casing for the transmitter coils.

8.6 EXPERIMENTAL SETUP

After the prototype has been built, a testing environment is set up to observe the DC output of the receiver when coupled with a transmitter in the WPT system. The block diagram of the experimental setup is shown in fig. 45. The transmitter used in testing has a 5 volts, 2 amps output. The DC output off load on the receiver side is measured using a DC voltmeter at various lift off distances. Lift indicates the distance between the transmitter coil and the receiver coil. Pieces of acrylic material cut to a uniform thickness of 1mm were used to measure the lift off distances as shown in figs 46, 47 and 48. The receiver coil is placed on these acrylic and since the magnetic flux can penetrate the material, the output voltage or current measured would not be affected.

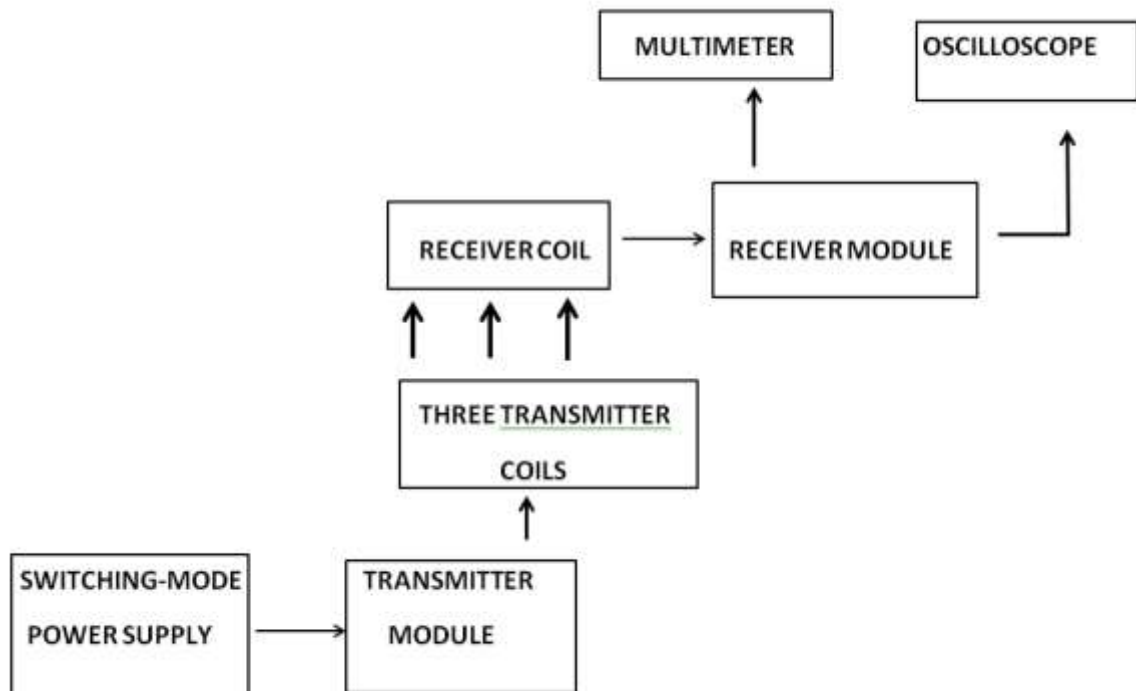


Fig 45: Spatial diagram of the measurement Set-up to observe the effect of lift-off distance on induced voltage and current

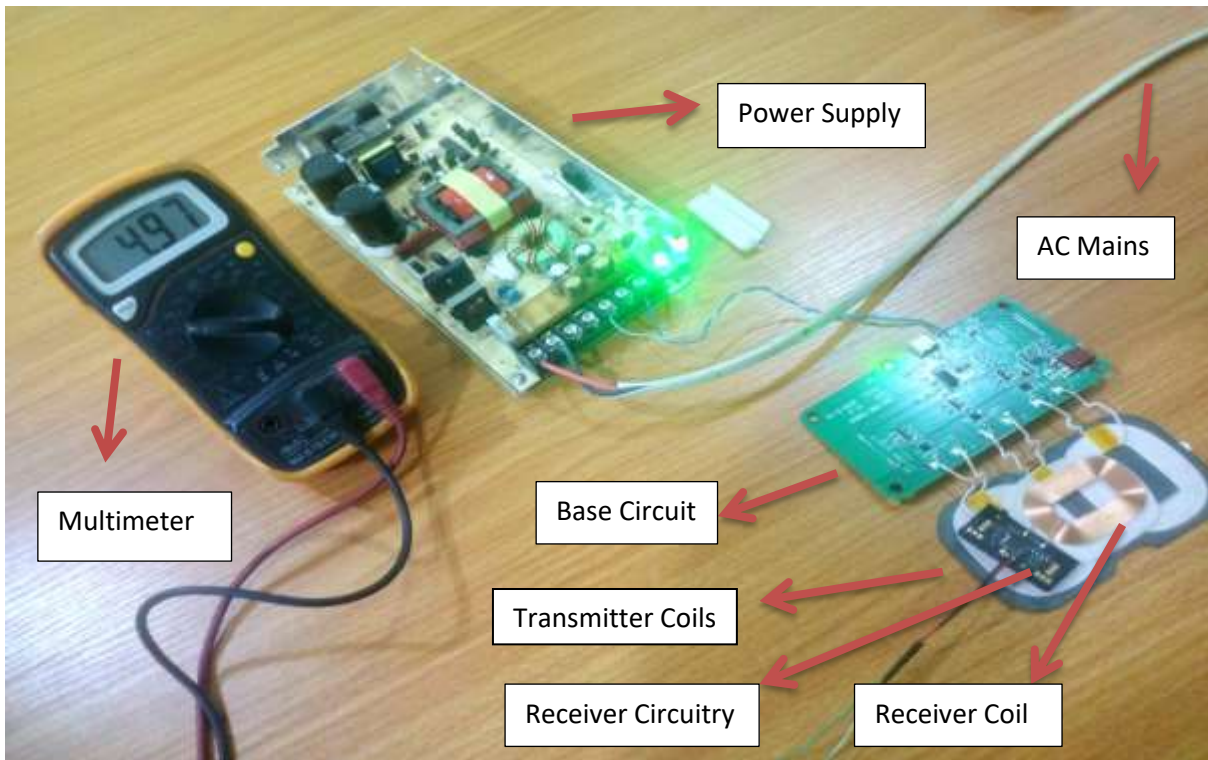


Fig 46: Set-up for measurement of distance of coverage.

Table 10: Receiver output reading in relation to the lift-off.

Lift-off	Receiver Voltage (fixed Regulated)	Receiver Current
1mm	4.97V	600 mA
2mm	4.97V	450 mA
3mm	4.97V	360 mA
4mm	4.97V	310 mA
5mm	4.97V	240 mA
6mm	4.97V	210 mA
7mm	4.97V	162 mA
8mm	4.97V	150 mA
9mm	4.97V	132 mA

10mm	4.97V	120 mA
11mm	4.96V	110 mA
12mm	4.96V	70 mA
13mm	4.96V	54 mA
14mm	4.96V	41 mA
15mm	4.96V	28 mA
16mm	4.96V	19 mA
17mm	4.95V	17 mA
18mm	4.95V	10 mA

Table (10) shows the measured receiver output reading. It depicts that the minimum voltage output from the receiver is 4.95 volts and this is due to the fact that the bq51013 IC regulates the output. Beyond 18mm lift-off distance, no output is recorded from the receiver. It also shows that the maximum operating distance of the coil is 18mm.



Fig 47: Measurement of the Receiver voltage at 2mm lift off.

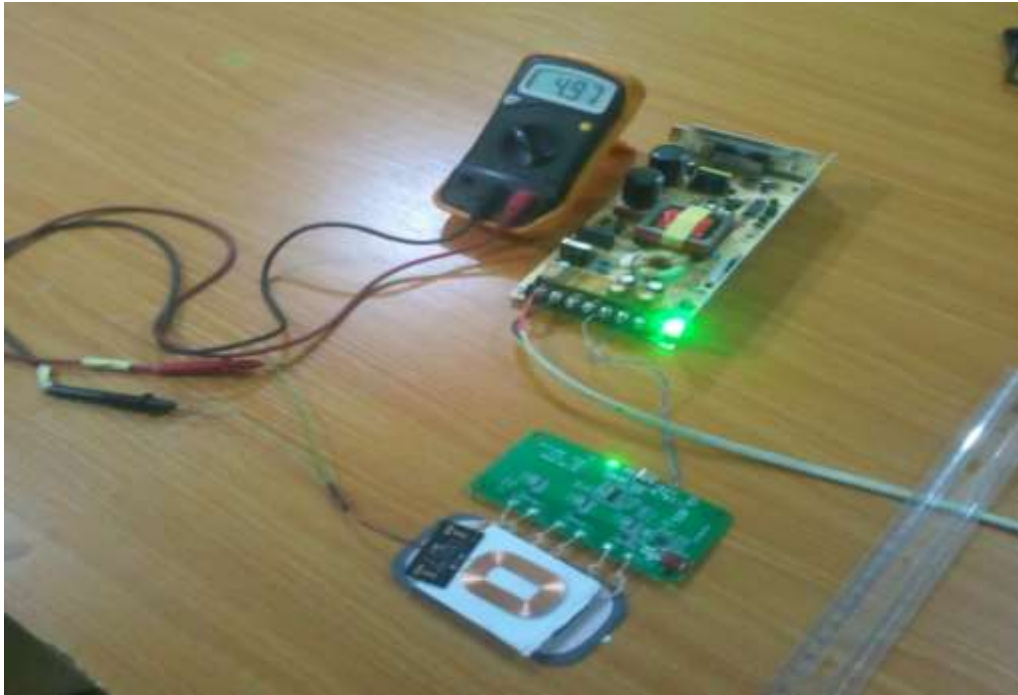


Fig 48: Measurement of the Receiver voltage at 8mm lift off.

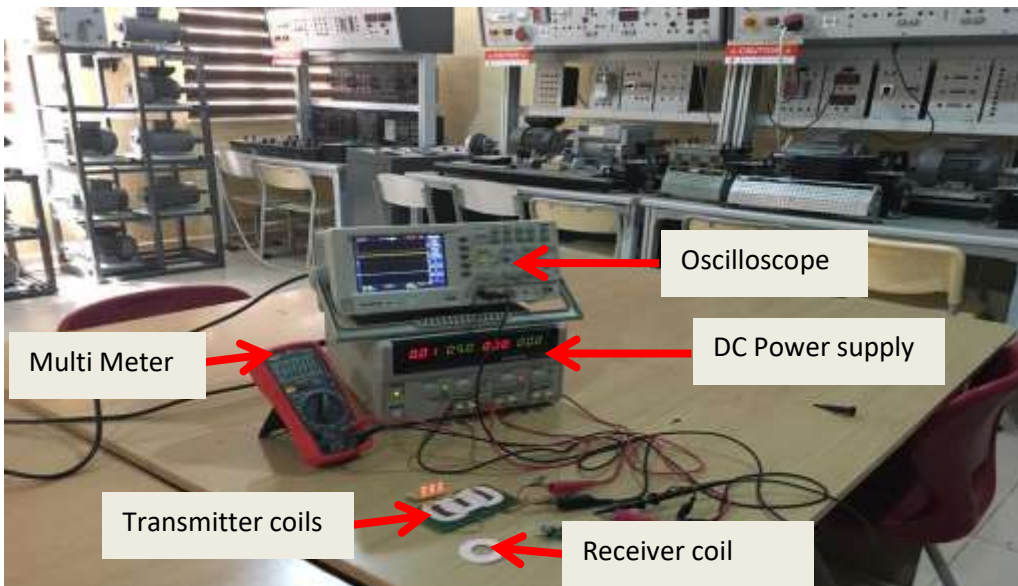


Fig 49: Measurement of coil direct mutual inductance.

8.7 Section Summary

One of the goals of this project is to design a system with a high efficiency value. The efficiency of the system depends of quality factors of the primary and secondary coils used

and the coupling coefficient. For high efficiency values, the values of these two quantities must be high too.

The coupling coefficient shows how tightly coupled the two coils are. The value varies proportionally with the distance between the two coils. It also varies proportionally with the number of coil turns. This is because with increasing coil turns, the magnetic field strength increases and thereby reducing the effect of increased lift-off distance. This implies that with greater coil turns or larger coils, the operating distance is improved which improves the coupling coefficient and as such increases the mutual inductance between the coils. Consequentially, the efficiency of the system is improved.

The quality factor depends on high switching frequency values as well as coil inductance values. With more coil turns, the coil inductance can be increased though this increases the I^2R resistive losses of this coil. Higher excitation current has been shown to reduce coil inductance. Hence, increasing the excitation current and the number of coil turns will slightly increase the coil inductance value while greatly increasing the resistive losses. The coil designed has an inductance value that minimizes the resistive loss and has an acceptable Q factor value.

The power output, output voltage and current to the receiver coil is within the required range even at the maximum possible efficiency of 98%. This is desirable and implies that the receiver coil or module will not receive power above its absolute ratings.

The experimental validation or testing showed that due to the A6 TRT coil system used, the magnetic field strength of the transmitter coil was stronger and removed the issue of coil misalignment which is a disadvantage of dead-zone. And since the TRT coil configuration eliminates the occurrence of dead-zone in WPT system, misalignment issue is reduced and free positioning of charging device is possible.

9.0 CONCLUSION

The basis of this project is to design a wireless power transfer (WPT) system that is efficient enough and allows for multiple simultaneous charging of mobile devices or usage by consumer premise equipment (CPEs) with emphasis on mobile phone.

In designing the system several considerations were made in terms of power supply, Transmission Circuit, Receiver Circuit, coil design and the components used. The power supply is a switching-mode power configuration and has several advantages over the regular linear mode power supply. These advantages include efficiency, control, less space and continuous conduction mode if needed. The only drawback is the noise introduced but at high switching frequencies this noise is pushed down.

A robust design was implemented in the Transmitter and Receiver Circuit Design which made use of passive component to minimise power consumption in the circuits.

A novel transmitter coils was investigated using Comsol Multiphysics, The study visualised and compared the Magnetic field generated by Three sets of coil configuration (SRT coil configuration, DRT coil configuration and the Novel TRT coil configuration). It was observed that the Novel TRT configuration under the same condition with other coil configuration gave wider region of conduction, and a higher amplitude of magnetic field Strength. This gives rise to improved efficiency and mitigates to problems associated due to dead-zone which is inherent in a single coil transmitter system. The Novel TRT transmitter coil configuration also allows for free positioning of mobile device to be charged on the Transmission coil.

Consideration for voltage tolerance levels was a major factor in the design of the input voltage into any section system. The voltage is kept within the absolute ratings of the

integrated circuits or component as specified in the various datasheets. And for each module designed, tests were conducted to ensure that the working was as intended within an acceptable error margin. The overall system was evaluated by testing individual modules or section, thereafter modules are coupled together and the final testing was done to ascertain the viability and functionality of the system.

A robust design and implementation of a wireless power Transmission system employing induction coupling was carried out in this body of research. The research established that the power transfer efficiency of the system is greater than 90%, the maximum coverage distance of the system is about 18mm and also a novel transmitter coil configuration that eliminates the problem of dead zone in the system was proposed and implemented. Furthermore, experiments were carried to validate and evaluate the overall system.

10.0 PUBLICATION(S)

10.1 Journal Paper(s)

E.C. Ashigwuike, B.S Emmanuel, P.C. Udeh, S. Thomas, W.Oloyombo, P.Okpe. “Mitigation of Dead Zone in Wireless Power Transmission Systems used for Charging Small CPEs”, *AEU- International Journal of Electronics and Communication*. (Under Review).

10.2 Conference Paper(s)

E.C. Ashigwuike, B.S Emmanuel, P.C. Udeh, S. Thomas, W.Oloyombo, P.Okpe, “Modelling and Simulation of Wireless Power Transmitter Coil Configurations for Mitigation of Dead Zone in Wireless Power Transmission System. *1st International Conference on Multi-Disciplinary Engineering and Applied Sciencies (ICMEAS) 2021*. Nile University Nigeria.

11.0 ACKNOWLEDGEMENTS

The Authors will like to acknowledge The Nigerian Communication Commission (NCC) for funding this research and all members of the NCC research and Development Team for their valuable advice during the course of this project. Our deep gratitude goes to Prof. O. Nnodu and her team at the Centred for Sponsored Project, University of Abuja for their prompt response and valuable advice on the management of the Grant.

12.0 REFERENCES

- [1] M. Etemadrezaei, "Wireless power transfer," *Elsevier*, 2018
- [2] W. C. Brown, "The history of power transmission by radio waves," *IEEE Trans. Microwave Theory Tech.*, vol. 32, pp. 1230-1242, September 1984.
- [3] C. G. Kim, D. H. Seo, J. S. You, J. H. Park, and B. H. Cho, "Design of a contactless battery charger for cellular phone," *IEEE Trans. Ind. Electron.*, vol. 48, pp. 1238-1247, December 2001.
- [4] G. B. Joung and B. H. Cho, "An energy transmission system for an artificial heart using leakage inductance compensation of transcutaneous transformer," *IEEE Trans. Power Electron.*, vol. 13, pp. 1013-1022, November 1998.
- [5] T. Sekitani, M. Takamiya, Y. Noguchi, S. Nakano, Y. Kato, T. Sakurai, and T. Someya, "A large-area wireless power-transmission sheet using printed organic transistors and plastic MEMS switches," *Nature Mater*, vol. 6, pp. 413-417, June 2007.
- [6] O. Knecht and J. W. Kolar, "Comparative evaluation of IPT resonant circuit topologies for wireless power supplies of implantable mechanical circulatory support systems," *Proceedings of Applied Power Electronics Conference and Exposition*, 2017, pp. 3271-3278.
- [7] M. P. Kazmierkowski, A. J. Moradewicz, "Unplugged but Connected: Review of Contactless Energy Transfer Systems," *IEEE Industrial Electronics Magazine*, vol. 6, no. 4, 2012, pp. 47-55.
- [8] D. Patil, M. K. McDonough, J. M. Miller, B. Fahimi, P. T. Balsara, "Wireless Power Transfer for Vehicular Applications: Overview and Challenges," *IEEE Transactions on Transportation Electrification*, vol. 4, no. 1, 2018, pp. 3-37.

- [9] X. Mou, O. Groling, H. Sun, "Energy-Efficient and Adaptive Design for Wireless Power Transfer in Electric Vehicles," *IEEE Transactions on Industrial Electronics*, vol. 64, no. 9, 2017, pp. 7250-7260.
- [10] A. S. Mohamed, C. R. Lashway, O. Mohammed, "Modeling and Feasibility Analysis of Quasi-Dynamic WPT System for EV Applications," *IEEE Transactions on Transportation Electrification*, vol. 3, no. 2, 2017, pp. 343-353.
- [11] S. Li, C. Mi, "Wireless Power Transfer for Electric Vehicle Applications," *IEEE Journal of Emerging and Selected Topics in Power Electronics*, vol. 3, no. 1, 2015, pp. 4-17.
- [12] I. Graurs, A. Vizulis, A. Rubenis, A. Laizans, "Wireless energy supply to public transport units with hybrid drive – trends and challenges," *Transport and Telecommunication*, vol. 15, no 1, 2014, pp. 67-76.
- [13] R. Saltanovs, A. Krivchenkov, A. Krainyukov, "Analysis of effective wireless communications for V2G applications and mobile objects," *Proceedings of 58th International Scientific Conference on Power and Electrical Engineering of Riga Technical University*, 2017, pp. 1-5.
- [14] R. Saltanovs, I. Galkin, "Method of adjustment and stabilization of parameters for wireless energy transfer system," *Proceedings of 9th European Conference on Power Electronics and Applications (EPE'17 ECCE Europe)*, 2017, pp 1 - 6.
- [15] W. Xu, W. Liang, J. Peng, Y. Liu, Y. Wang, "Maximizing Charging Satisfaction of Smartphone Users via Wireless Energy Transfer," *IEEE Transactions on Mobile Computing*, vol. 16, no. 4, 2017 pp. 990-1004.
- [16] O. Knecht, R. Bosshard, J. Kolar, C. Starck, "Optimization of Transcutaneous Energy Transfer coils for high power medical applications," *Proceedings of 15th Workshop on Control and Modeling for Power Electronics (COMPEL)*, 2014, pp.1-10.

- [17] Y. Liu, R. Mai, D. Liu, Y. Li, Z. He, "Efficiency Optimization for Wireless Dynamic Charging System with Overlapped DD Coil Arrays," *IEEE Transactions on Power Electronics*, vol. PP, no. 99, 2017, pp. 1-1
- [18] R. Bosshard, J. W. Kolar, "All-SiC 9.5 kW/dm³ On-Board Power Electronics for 50 kW/85 kHz Automotive IPT System," *IEEE Journal of Emerging and Selected Topics in Power Electronics*, vol. 5, no. 1, 2017, pp. 419-431.
- [19] D. Panfilov, O. Husev, F. Blaabjerg, J. Zakis, K. Khandakji, "Comparison of three-phase three-level voltage source inverter with intermediate dc-dc boost converter and quasi-Z-source inverter," *IET Power Electronics*, vol. 9, no. 6, 2016, pp. 1238-1248.
- [20] D. Vinnikov, J. Zakis, O. Husev, R. Strzelecki, "New high-gain step-up DC/DC converter with high frequency isolation. Proceedings of "Twenty-Seventh Annual," *IEEE Applied Power Electronics Conference and Exposition (APEC)*, 2012, pp. 1204-1209.
- [21] K. Kroics, U. Sirmelis, L. Grigans, V. Brazis, "Digitally controlled 4-phase interleaved DC-DC converter with coupled inductors for storage application in microgrid," *Proceedings of 9th International Conference on Compatibility and Power Electronics (CPE)*, 2015, pp. 504-509.
- [22] S. Kim, S. Lee and S. Lim, "Magnetic resonant coupled band wireless power transfer system with in-band communication," *Journal of Semiconductor Technology and Science*, Vol. 13, No. 6, December 2013, pp 562 – 568.
- [23] Y. Chen, D. B. da Costa and H. Ding, "Interference analysis in wireless power transfer," *IEEE Communication Letters*, 2017.
- [24] Y. Bu, T. Mizuno and H. Fujisawa, "proposal of a wireless power transfer technique for low-power multireceiver applications," *IEEE Transactions on Magnetics*, vol. 51, no. 11, November 2015

- [25] L. Wu and B. Zhang, "reconfigurable transmitter coil structure for highly efficient and misalignment-insensitive wireless power transfer systems in megahertz range," *Chinese Journal of Electrical Engineering*, vol. 5, no. 3, June 2, pp 56 – 62
- [26] J. H. Kim, B. Lee, J. Lee, S. Lee, C. Park, S. Jung, S. Lee, K. Yi and J. Baek, "Development of 1 MW inductive power transfer system for a high speed train," *IEEE transactions on Industrial Electronics*, 2015
- [27] Y. G. Kim and S. Nam, "Determination of the impedance parameters of antennas and the maximum power transfer efficiency of the wireless power transfer," *IEEE Transactions on Antennas and Propagation*, vol. 67, No. 8, August 2019
- [28] C. A. Baguley, S. G. Jayasinghe and U. K. Madawala, "Theory and control of wireless power transfer systems," *Elsevier Control of Power Electronic Converters and Systems*, 2018
- [29] D. Brizi, J. P. Stang, Agostino Monorchio and G. Iazzi, "A compact magnetically dispersive surface for low frequency wireless power transfer applications," *IEEE*, 2020
- [30] D. Belo, D. C. Ribeiro, P. Pinho and N. B. Carvalho, "A selective, tracking and power adaptive far-field wireless power transfer system," *IEEE Transactions on Microwave Theory and Technique*, vol. 67, No. 9, September 2019
- [31] S. Li, Z. Liu, H. Zhao, L. Zhu, C. Shuai, Z. Chen, "Wireless Power Transfer by Electric Field Resonance and its Application in Dynamic Charging," *IEEE Transactions on Industrial Electronics*, vol. 63, no. 10, 2016, pp. 6602-6612.
- [32] J. Zakis, D. Vinnikov, L. Bisenieks, "Some design considerations for coupled inductors for integrated buck-boost converters," *Proceedings of "International Conference on Power Engineering, Energy and Electrical Drives*, 2011, pp. 1-6.
- [33] I. G. Sirbu, L. Mandache, "Comparative analysis of different topologies for wireless power transfer systems," *Proceedings of International Conference on Environment and*

Electrical Engineering and 2017 IEEE Industrial and Commercial Power Systems Europe, 2017, pp. 1-6.

- [34] L. Liivik, A. Chub, D. Vinnikov, J. Zakis, "Experimental study of high step-up quasi-Z-source DC-DC converter with synchronous rectification," *Proceedings of International Conference on Compatibility and Power Electronics(CPE)*, 2015, pp. 409-414.
- [35] J. Dai, D. C. Ludois, "A Survey of Wireless Power Transfer and a Critical Comparison of Inductive and Capacitive Coupling for Small Gap Applications," *IEEE Transactions on Power Electronics*, vol. 30, no. 11, 2015, pp. 6017-6029.
- [36] F. Lu, H. Zhang, C. Mi, "A Two-Plate Capacitive Wireless Power Transfer System for Electric Vehicle Charging Applications," *IEEE Transactions on Power Electronics*, vol. 33, no. 2, 2018, pp. 964-969.
- [37] B. Regensburger, S. Sinha, A. Kumar, J. Vance, Z. Popovic, K. Afridi, "Kilowatt-scale large air-gap multi-modular capacitive wireless power transfer system for electric vehicle charging," *Proceedings of Applied Power Electronics Conference and Exposition (APEC)*, 2018, pp. 666-671.
- [38] K. Kroics, J. Zakis, "Electronic ballast for gas discharge lamp based on input - series output- series resonant converter," *Proceedings of International Exhibition and Conference for Power Electronics, Intelligent Motion, Renewable Energy and Energy Management (PCIM Europe)* 2017, pp. 1186-1192.
- [39] D. Roserio, N. Azeez, S. Williamson, "A modified resonant converter for wireless capacitive power transfer systems used in battery charging application," *Proceedings of IEEE Transportation Electrification Conference and Expo (ITEC)*, 2016, pp. 1-6.
- [40] R. L. Steigerwald, "A comparison of half-bridge resonant converter topologies," *IEEE Transactions on Power Electronics*, vol. 3, no. 2, 1988, pp. 174-182.
- [41] C. T. Rim, "Wireless charging of electric vehicles," *Elsevier*, 2018, pp 1113 – 1137.

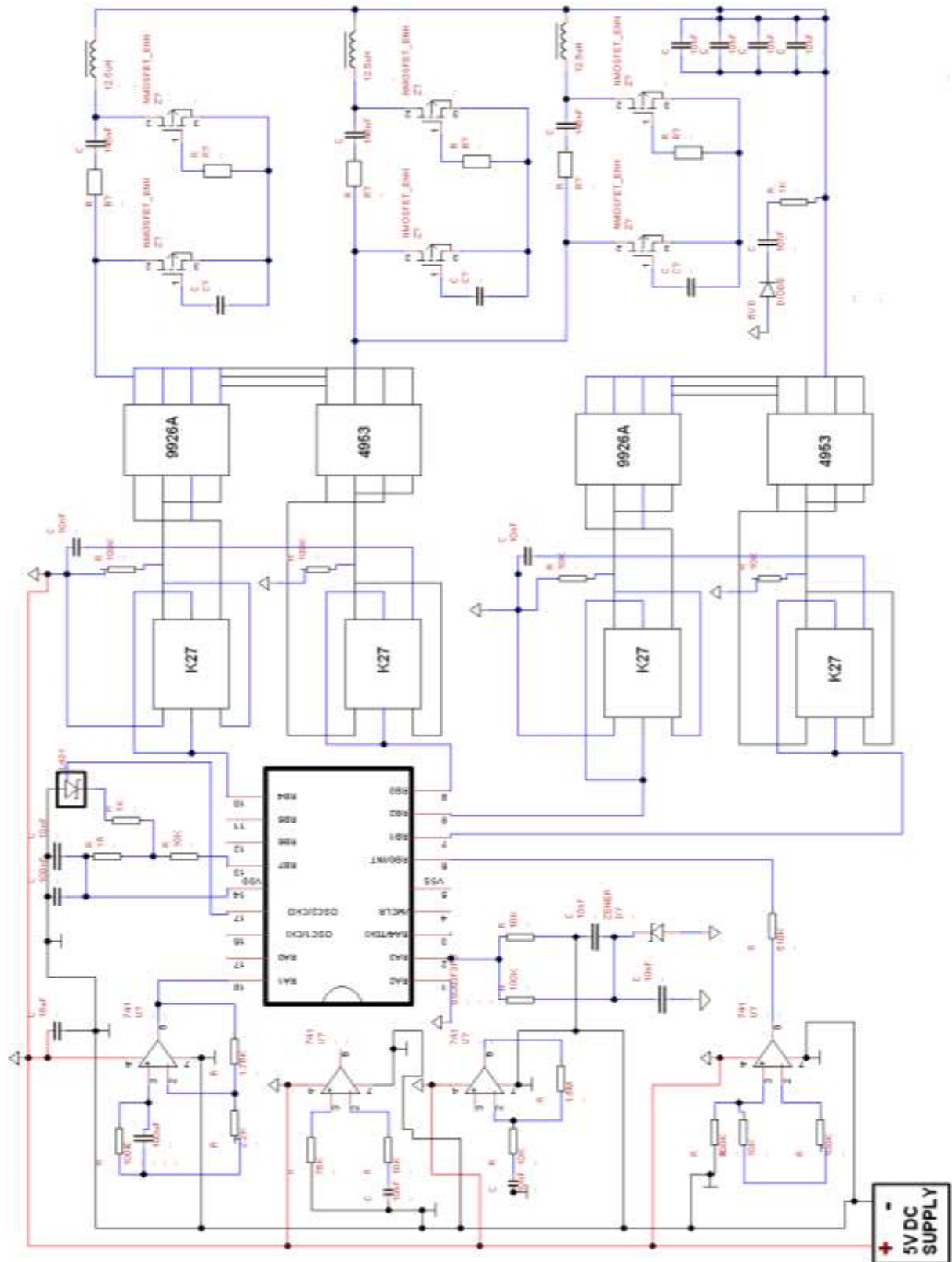
- [42] Y. Li, J. Zhao, Q. yang, L. Liu, J. Ma and X. Zhang,"a novel coil with high misalignment tolerance for wireless power transfer," *IEEE Transactions on Magnetics*, 2019
- [43] Z. Yan, B. Song, Y. Zhang, K. Zhang, Z. Mao and Y. Hu,"A rotation-free wireless power transfer system with stable output power and efficiency for autonomous underwater vehicles," *IEEE Transactions on Power Electronics*, 2018
- [44] S. Huang, J. Zhang, W. Wu and L. Xia," Impact of non-ideal waveforms on gaN power FET in magnetic resonant wireless power transfer system," *Chinese Journal of Electrical Engineering*, vol. 5, No. 3, September 2019.
- [45] S. D. Barman, A. W. Reza, N. Kumar, M. E. Karimi and A. B. munir,"Wireless powering by magnetic resonant coupling: recent trends in wireless power transfer system and its applications," *Elsevier Renewable and Sustainable Energy Reviews*, 2015, pp 1525 – 1552.
- [46] A. T. L. Lee, W. Jin, S. Tan and S. Y. Hui,"Buck-boost single-inductor multiple-output (SIMO) high-frequency inverters for medium-power wireless power transfer," *IEEE Transactions on Power Electronics*, 2018
- [47] K. Lee, C. Jeong and S. H. Chue,"Analysis of factors effecting on optimal configuration of two receivers for a three-coil wireless power transfer system," *IEEE Systems Journals*, 2018.
- [48] Y. Zhang, T. Lu, Z. Zhao, F. He, K. Chen and L. Yuan," Selective wireless power transfer to multiple loads using receivers of different resonant frequencies," *IEEE Transactions on Power Electronics*, 2014
- [49] X. Chen, S. Yu and Z. Zhang," A receiver-controlled coupler for multiple output wireless power transfer applications," *IEEE Transactions on Circuits and Systems*, Vol. 66, No.11, November 2019, pp 4542 - 4552

- [50] W. Jin, A. T. L. Lee, S. Tan and S. Y. Rui, "A Gallium Nitride (GaN)-based single inductor multiple-output (SIMO) inverter with multi-frequency AC outputs," *IEEE Transactions on Power Electronics*, 2019
- [51] S. Ashok and M. Muruganandam, "Power optimisation for wearable heart rate measurement device with wireless charging," in *Journal of Medical Engineering and Technology*, March 2017.
- [52] S. Chatterjee, A. Iyer, C. Bharatiraja, I. Vaghasia and V. Rajesh, "Design optimisation for an efficient wireless power transfer system for electric vehicles," in *Elsevier, 1st international conference on Power Engineering, Computing and Control, PECCON-2017*, 2-4 March, 2017, VIT University, Chennai Campus, pp 1015 – 1023.
- [53] J. Zhang and E. Wang, "Efficient analysis of multiple-transmitter wireless power transfer systems," in *Hindawi International Journal of Antennas and Propagation*, vol. 2018, Article ID 341523, pp 1 – 11.
- [54] W. B. Zimmerman, "Multiphysics Modeling With Finite Element Methods (Series On Stability, Vibration And Control Of Systems, Serie)(Series," 2006.
- [55] R. J. Shapoorabadi, A. Konrad and A. Sinclair, "Computation of current densities in the receiving mode of electromagnetic acoustic transducers," *J. Appl. Phys.*, vol. 97, pp. 10Q106, 2005.
- [56] S. Thomas, S. Obayya, R. Taneja and W. Balachandran, "A Coupled Electromagnetic and Mechanical Analysis of Electromagnetic Acoustic Transducers," *International Journal for Computational Methods in Engineering Science and Mechanics*, vol. 10, pp. 124-133, 2009.
- [57] R. Jafari-Shapoorabadi, A. Sinclair and A. Konrad, "Finite element determination of the absolute magnitude of an ultrasonic pulse produced by an EMAT," in *Ultrasonics Symposium*, 2000 IEEE, 2000, pp. 737-741.

- [58] M. A. Houran, X. Yang, and W. Chen, "Magnetically Coupled Resonance WPT : Review of Compensation Topologies, Resonator Structures with Misalignment, and EMI Diagnostics" , MDPI Journal, 2018.
- [59] A. M. Jawad, R. Nordin, and S. K. Gharghan, "Opportunities and Challenges for Near-Field Wireless Power Transfer : A Review" , MDPI Journal , 2017, pp. 1–28.
- [60] A. Massa, G. Oliveri, F. Viani, and P. Rocca, "Array designs for long-distance wireless power transmission: State-of-the-art and innovative solutions," Proc. IEEE, vol. 101, no. 6, pp. 1464–1481, 2013.
- [61] X. Lu, P. Wang, D. Niyato, D. I. Kim, Z. Han, and C. Engineering, "Wireless Charging Technologies: Fundamentals, Standards, and Network Applications," EEE Communications Surveys and Tutorials, 2016, pp. 1–40.
- [62] Sang Wook Han, "Wireless Interconnect using Inductive Coupling in 3D-ICs " https://deepblue.lib.umich.edu/bitstream/handle/2027.42/94034/swhanpns_1.pdf?sequence=1 2012.
- [63] Anonymous, "Zhuzhou Insulation material Co. Ltd; transformer coil coating - technical manual," 2011.
- [64] J. Zhao,"A new calculation for designing multilayer planar spiral inductors," *Pulse*, pp 37 – 40
- [65] <http://www.upsbatterycenter.com/blog/methods-charging-sli-battery> (accessed 21st August, 2021)
- [66] <http://www.quora.com/what-is-trickle-charge-and-how-does-it-help-the-cellphone-battery> (accessed 21st August, 2021)
- [67] <http://www.reviewgeek.com/64478/which-iphones-have-wireless-charging> (accessed 21st August, 2021)

13.0 APPENDIX

13.1 Appendix A – COMPLETE CIRCUIT DIAGRAM



13.2 Appendix B

13.2.1 8s003f3p6 Pin Descriptions

PIN	MAIN FUNCTION	DEFAULT FUNCTION	ALTERNATE FUNCTION	ALTERNATE FUNCTION AFTER REMAP
PD4	Port D4	Timer 2 – Channel 1/BEEP/Output/UART1 Clock		
PD5	Port D5	Analog Input 5/UART1 data transmit		
PD6	Port D6	Analog Input 6/UART1 data receive		
VCAP	1.8 V regulator capacitor			
VDD	Digital Power Supply			
PB5	Port B5	I ² C data		Timer 1 – Break Input
PC3	Port C3	Timer 1 – Channel 3		Timer1 – Inverted Channel 1
PC4	Port C3	Configurable Clock Output/Timer 1 – Channel 4		Timer 1 – Inverted channel 2
PC5	Port C5	SPI Clock		Timer 2 – Channel 1
PC6	Port C6	SPI Master Out/Slave in		Timer 1 – Channel 1
PC7	Port C7	SPI Master In/Slave out		Timer 1 – Channel 2
PD2	Port D2	Analog Input 3		Timer 2 – Channel 3
PD3	Port D3	Analog Input 4/Timer 2 – Channel 2/ADC External Trigger		

13.3 Appendix C

13.3.1 Assembly Program Listing

```
;This program is used to configure the pins of the microcontroller to provide oscillations to
;the K27 ICs
;*****
;equates section
tmr0 equ 1
porta equ 5
portb equ 6
portc equ 7
status equ 3
trisa equ 85h
trisb equ 86h
trisc equ 87h
trisd equ 88h
option_R equ 81h
zerobit equ 2
count equ 0ch
;*****
list p=16f84
org 0
goto start
;*****
;configuration bits
_config h'3ff0
;*****
;subroutine section
;0.1ms delay
del1 clrf count
again decfsz count
                goto again
                return
;*****
;initialization of ports and timers
bsf                TRISB,FAULT_BIT                ;Fault input from driver

movlw                0x0C

movwf                CCP1CON                ;CCP1 and CCP2 configured to PWM

movwf                CCP2CON
```

```

bsf          T2CON,2          ;Timer2 ON

movlw       PR2_VALUE          ;Load PR2 value to PR2 register

movwf      PR2

movlw       0x90

movwf      CCPR1L

movwf      CCPR2L

movlw       0x81

;*****
;
CALCULATE_FREQUENCY

movff      FREQUENCY,PORTD
clrf      TEMP

clrf      TEMP1
movlw     HIGH(FREQUENCY_SCALE)
;FREQUENCY_SCALE/Frequency

movwf     TEMP_LOCATION          ;16 bit by 8 bit division

movlw     LOW(FREQUENCY_SCALE)  ;

movwf     TEMP_LOCATION+1

continue_subtraction

bsf       STATUS,C

movf      FREQUENCY,W

subwfb   TEMP_LOCATION+1,F

clrf     WREG

subwfb   TEMP_LOCATION,F

btfss    STATUS,C

```

```

goto            keep_result_in_rpm

incf           TEMP,F

btfsc         STATUS,C ;Result of the division is stored in TEMP&TEMP1

incf           TEMP1,F

goto          continue_subtraction
keep_result_in_rpm
;Timer0 value = FFFF-Timer0

bsf           STATUS,C

movlw         0xFF

subfwb        TEMP,F

subfwb        TEMP1,F           ;The Timer0 reload value stored in

movff         TEMP1,FREQ_REF_H  ;FREQ_REF_H & FREQ_REF_L

movff         TEMP,FREQ_REF_L   ;These values will be loaded to
return        ;Timer0 in Timer0 overflow interrupt

;*****
;configuration section
start         bsf status, 5
              movlw b'11111111'
              movwf trisa
              movlw b'00000000'
              movwf trisb
              movlw b'01101100'
              movwf trisc
              movwf option_R
              bcf status, 5
              clrf PortA
              clrf PortB
              clrf PortC
              clrf count

;*****
;Main program
ANALOG3      btfss PortC, 2
              goto ANALOG3

```

```

ANALOG4      btfss PortC, 3
              goto ANALOG4
ANALOG5      btfss PortC, 5
              goto ANALOG5
ANALOG6      btfss PortC, 6
              goto ANALOG6
PAIR         movlw b'11000000'
              movwf PortB           ;send pulse to base of K1 and K4
              call del1
              btfsc PortA, 5
              jmp ANALOG3
              movlw b'11100111'
              movwf PortB
              call del1
              btfsc PortA, 5
              jmp ANALOG3
              goto PAIR           ;continuously repeat

```

13.4 Appendix D

13.4.1 Prototype Testing



Fig 49: An Energised four (4) Compartment Transmitter prototype



Fig 50: An Energised four (4) Compartment Transmitter prototype charging a phone with an inbuilt wireless receiver (iphone 11 promax) .

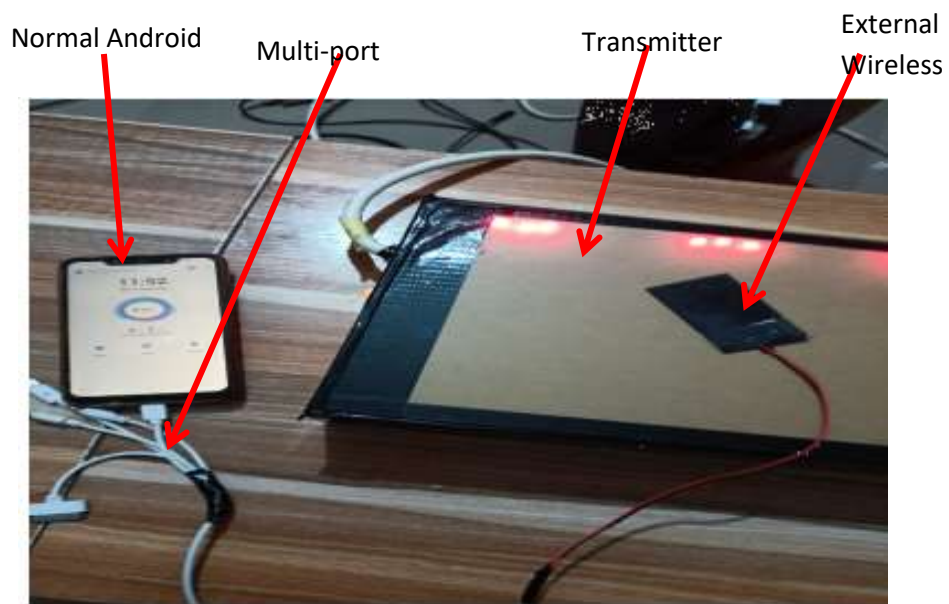


Fig 51: An Energised four (4) Compartment Transmitter prototype charging a phone with external wireless receiver (Normal Android phone).